Application of machine learning techniques to predict the unconfined compressive strength of sustainable cementitious materials used in the mining industry

by

Balasooriya Arachchilage Chathuranga Sanjaya Jayathilake

A thesis submitted in partial fulfillment of the requirements for the degree of

Master of Science

in

MINING ENGINEERING

Department of Civil and Environmental Engineering
University of Alberta

© Balasooriya Arachchilage Chathuranga Sanjaya Jayathilake, 2023

Abstract

Various forms of cementitious materials, including shotcrete, grouts, and cemented paste backfill (CPB), are made with ordinary Portland cement (OPC). They are widely used for both underground and surface mining applications. However, due to the high carbon footprint of OPC production, the mining industry has shown a significant interest in using sustainable cementitious materials. Alkali-activated slag (AAS)-based CPB and calcium sulfoaluminate cement (CSA)-based mixtures have emerged as promising sustainable cementitious materials for different mining applications, owing to their reduced carbon footprint and other advantages (i.e., high early age strength, improved durability, and reduced energy requirements) over OPC-based mixtures. For mining applications, it is required to ensure that the unconfined compressive strength (UCS) of these cementitious materials meets the strength requirements. The UCS of both AAS-based CPB and CSA cement-based mixtures are influenced by multiple features related to cement composition, material proportioning, curing conditions, and admixtures. Currently, those mixture designs depend heavily on the experimental approach, which is usually limited to a limited number of influential features at a given time. This has resulted in an insufficient understanding of the non-linear relationships between multiple input features and UCS of the aforementioned sustainable cementitious materials. The insufficient understanding poses challenges in designing mixtures that can meet the specific strength requirement for mining applications. Compared with the experimental approach, machine learning (ML) methods can consider multiple input features simultaneously to build prediction models. ML is a promising alternative approach that can assist the mixture designs of cementitious materials efficiently by improving the understanding of complex non-linear relationships and by providing accurate and rapid UCS predictions. Despite its significance, to the best of the author's knowledge, no studies in the current literature have

reported the use of ML techniques for predicting the UCS of AAS-based CPB and CSA cement-based mixtures.

Therefore, this study aimed to utilize ML methods to build complex relationships between multiple input features and the UCS, to predict the UCS of AAS-based CPB and CSA cement-based mixtures, and to help spread the applications of low-carbon cementitious materials in our mining industry. For these purposes, accurate strength prediction models were developed based on meaningful datasets collected from experimental literature. All ML models were evaluated for their performances on testing data using commonly used performance evaluation metrics. Results showed that the extreme gradient boosting regression (XGBR) model constructed on the optimal dataset suggested by the least absolute shrinkage and selection operator (LASSO) method produces the best results with a prediction accuracy of 95% for CSA cement-based mixtures. In addition, the feature importance ranking results revealed curing time, water-to-cement ratio (w/c), belite content, and ye'elimite content as the most influential features on the UCS of CSA cement-based mixtures. Furthermore, the Shapely-Additive exPlanations (SHAP) method could describe the non-linear relationships between input features and UCS, both qualitatively and quantitatively. For AAS-based CPB, gradient boosting regression (GBR) outperformed the other ML models with a prediction accuracy of 96.7 %. The curing time, w/c ratio, and aggregate-to-cement ratio were ranked as the most important input features for the AAS-based CPB mixture designs. Overall, this study will improve the understanding of complex non-linear relationships between input features and the UCS of AAS-based CPB and CSA cement-based mixtures and will guide future mixture designs through rapid UCS predictions. Ultimately, this work will help spread the application of sustainable cementitious materials in the mining industry and contribute to the goal of net-zero mining by facilitating more efficient mixture design processes.

Preface

This thesis is an original work by Chathuranga Balasooriya Arachchilage, which employed machine learning techniques to predict the unconfined compressive strength of sustainable cementitious materials used in the mining industry, namely, alkali-activated slag-based cemented paste backfill and calcium sulfoaluminate cement. This thesis is based on two journal papers that are published or submitted for consideration for publication.

Chapter 2 of this thesis has been published as **C.B. Arachchilage**, C. Fan, J. Zhao, G. Huang, W.V. Liu, A machine learning model to predict unconfined compressive strength of alkali-activated slag-based cemented paste backfill. Journal of Rock Mechanics and Geotechnical Engineering. © Elsevier. (2023).

Chapter 3 of this thesis has been submitted for consideration for publication as **C.B. Arachchilage**, G. Huang, C. Fan, W.V. Liu, Forecasting unconfined compressive strength of calcium sulfoaluminate cement mixtures using ensemble machine learning techniques integrated with shapely-additive explanations. Construction and Building Materials. © Elsevier. (With Editor).

In this thesis, I was responsible for conceptualization, data collection, data analysis, python programming, writing, review, and editing. Dr. Wei Victor Liu was my academic supervisor, who provided me with resources and was involved with conceptualization, supervision, review, and editing. In Chapters 2 and 3, Dr. Guangping Huang and Chengkai Fan assisted me with investigating, analyzing, reviewing, and editing. In Chapter 3, Jian Zhao contributed to collecting data.

Acknowledgment

First and foremost, I would like to express my sincere gratitude to my supervisor, Dr. Wei Victor Liu, for providing me with the invaluable opportunity to pursue my graduate studies at the esteemed University of Alberta. I am profoundly grateful for his exceptional guidance, unwavering support, constant motivation, care and trust that he bestowed upon me during this life-changing journey. His mentorship has been instrumental in overcoming obstacles and passing through difficult situations along the way.

I am utterly grateful to my previous mentors, Mrs. Maheshwari Wickrama, Dr. Anjula Dassanayake, Dr. G.V.I. Samaradivakara, Dr. Saman Illankoon, and Nimila Dushyantha, for encouraging me to pursue higher studies and laying the groundwork for my journey in academia.

I would like to thank the colleagues in my research group, Dr. Guangping Huang, Dr. Linping Wu, Chengkai Fan, Jian Zhao, Yunting Guo, Dr. Huawei Xu, Dr. Ömer Uğurlu, Zhiqiang Feng, and Kourosh Gholami for their kind assistance, encouragement, and support on my studies and day to day life. I am fortunate to have such great friends by my side who have made me feel at home, despite being far away from my home country.

Lastly, my sincere gratitude goes to my wife Veenavi Pemachandra, for her understanding, unwavering support, encouragement, and love. I am forever grateful to my loving mother, Indrani Mathota, and my dear father, Balasooriya Jayathilake, for their selfless sacrifices in shaping me into the person I am today. Even though they are thousands of miles away, their unconditional love and blessings always helped me to achieve more in this endeavor.

Table of contents

List of figures

List of tables

Chapter 1. Introduction

1.1. Research background

Cementitious materials (e.g., concrete, shotcrete, grout, and cemented paste backfill (CPB)) play a crucial role in the mining industry. In Canada, around 10% of the total cement (about 1.35 million tonnes) produced is consumed by the mining industry (Arcila and Beland 2023). Cementitious materials are widely used for both underground and surface mining applications. For example, concrete is commonly used for mine infrastructure construction (i.e., buildings) (Brescia-Norambuena et al. 2021), underground support pillars (Cao et al. 2021) and underground mining pavements (Brescia-Norambuena et al. 2021). In addition, shotcrete and grout materials are used for a wide range of mining applications, including linings of tunnels and ground and rock supports (Chen et al. 2022). Furthermore, CPB is adopted by the mining industry to backfill mine voids, as it facilitates safe mining environments and effective management of mine waste (i.e., tailings) (Đurđevac Ignjatović et al. 2022). Overall, the continuous production of cementitious materials is imperative to ensure smooth mining operations.

Ordinary Portland cement (OPC) is the most widely used cementitious material in the mining industry (Qi and Fourie 2019; Tao et al. 2023). However, the production of OPC is inherently unsustainable as it generates about 900 kg of carbon dioxide (CO_2) per every tonne of OPC produced (Naqi and Jang 2019). To achieve the net-zero emissions goal by 2050 (Bouckaert et al. 2021), the mining industry is facing a great challenge to reduce the CO_2 emissions related to OPC consumption. To address this challenge, one promising solution is to use sustainable cementitious materials instead of OPC-based cementitious materials. Sustainable cementitious materials include but are not limited to mixtures based on alkali-activated slag (AAS) cement, calcium sulfoaluminate (CSA) cement, magnesium based-cement, carbonatable calcium silicate cement

(CCSC), and calcium hydro silicate-based cement (Naqi and Jang 2019). Among the list, the scope of this thesis is limited to AAS-based CPB and CSA cement-based mixtures, based on the industry need, research significance, and the author's previous experience. AAS-based CPB contributes to 80-90% less CO_2 generation during its production when compared with OPC-based CPB (Rashad 2013). Consequently, the global warming potential (i.e., the impact of CO_2 emissions on the absorption of heat radiation in the atmosphere) of AAS-based CPB production is around 70% lower when compared with OPC-based CPB production (Weil et al. 2009). Likewise, CSA cement generates about 40% less CO_2 during its production (Huang et al. 2020). This reduction is attributed to several factors, including the low limestone requirement, the lower calcination temperature requirement (i.e., around 1200 °C), and the porous nature of the CSA clinker (i.e., less energy required to grind) (Coppola et al. 2018). Therefore, both AAS-based CPB and CSA cement-based mixtures have a significant potential to contribute toward the net-zero emissions goal with their applications in the mining industry.

Despite the potential of AAS-based CPB and CSA cement-based mixtures, their mixture designs confront substantive challenges. The mixture design should satisfy the strength requirement of a particular mining application to ensure safe mining operations (Cihangir et al. 2012; Moreira and Silva 2020). The unconfined compressive strength (UCS) of those mixtures is influenced by multiple features related to curing conditions, material proportioning, use of admixtures (i.e., retarders, superplasticizers, and activators), and particle size distributions of aggregate material (Cihangir et al. 2012; Tao et al. 2023). Currently, the mixture designs of AAS-based CPB and CSA cement-based mixtures depend heavily on the resource-intensive (i.e., material, cost, and time) experimental approach (Tran et al. 2022). Consequently, most of the previous experimental studies have been able to consider only a limited number of influencing features at a time in the

mixture designs. This limitation of experimental methods hampers the ability to capture non-linear relationships and subtle variations between input features and UCS, leading to an insufficient understanding of the relationships, which impedes the wide application of these low-carbon sustainable cementitious materials in the mining industry.

Beyond experimental methods, data-driven machine learning (ML) methods have emerged as an invaluable tool, aiding the design of cementitious materials in the recent past (Adel et al. 2022; Ekanayake et al. 2022; Minaz Hossain et al. 2023; Nguyen et al. 2022; Qi et al. 2018b; Qi et al. 2018c; Qi et al. 2019b; Zhao et al. 2023). ML refers to a collection of algorithms that can acquire knowledge by observing data while being able to extend itself by gathering new knowledge autonomously without being programmed (Woolf 2009). ML methods possess significant advantages over conventional experimental approaches. First, ML can provide rapid and accurate predictions without the need for physical testing, which can save time, cost, and material (Tran et al. 2022). Second, ML can build complex non-linear relationships between multiple input features and the output feature, which would otherwise be difficult to achieve using experimental methods alone (Nguyen et al. 2022). Third, some non-linear models (i.e., tree-based models) and statistical tools can be used alongside ML algorithms (i.e., mutual information (Liu et al. 2022)) to provide valuable insights into the importance of individual features for predictions (Qiu et al. 2020). Fourth, sophisticated tools such as the SHapely Additive exPlanations (SHAP) (Lundberg and Lee 2017) can be integrated into the ML models to interpret complex non-linear relationships both qualitatively and quantitatively (Ekanayake et al. 2022). The advantages of ML methods make them promising candidates for providing rapid and accurate UCS predictions by establishing complex non-linear relationships between multiple input features and the UCS of sustainable cementitious materials. ML can ultimately help spread the application of sustainable cementitious

materials and contribute to the emission reduction of our mining industry as it allows for reduced costs and time, informed decision-making, and a better understanding of the overall mixture designs. Despite its significance and potential, no studies have been conducted to apply ML techniques to predict the UCS of AAS-based CPB and CSA cement-based mixtures. Therefore, it is of great interest to extract readily available published experimental results to compile meaningful databases and to construct ML models to understand the complex non-linear relationships while predicting the UCS of AAS-based CPB and CSA cement-based mixtures.

1.2. Literature review

1.2.1. Introduction to artificial intelligence and machine learning

Artificial intelligence (AI) is a broad topic in the field of computer science. In AI applications, machines perform intelligent tasks by mimicking human cognitive processes (Russell 2010). ML is an important branch of AI, which was originally introduced by Arthur Samuel in 1959 (Kazemi 2023). ML has the ability to utilize various algorithms to unearth complex patterns in data, with mathematical or statistical techniques (Mitchell 2007). Furthermore, ML can learn automatically and improve the knowledge without being explicitly programmed (Kazemi 2023).

ML techniques follow a set of key steps during their application. These steps can be listed as (1) extracting datapoints from published documents or generating data through experimental techniques to compile datasets (2) applying data cleaning, data visualization, and data pre-processing techniques (3) employing feature engineering techniques (4) selecting suitable ML algorithms and constructing them on the compiled datasets (5) configuring and optimizing the constructed models (6) testing and validating the models on test data (7) selecting the most suitable model (Kazemi 2023). In addition to the above, additional steps, such as ranking the features based on importance, and interpreting the models can also be performed (Lundberg et al. 2020).

1.2.2. Categories of machine learning

ML can be categorized based on two main aspects: (1) by the process it uses to learn (2) type of the problem or output of interest (Edgar and Manz 2017). From the point of the first aspect, ML can be classified into three categories: (1) unsupervised learning; (2) supervised learning; (3) reinforcement learning (Bonetto and Latzko 2020). Using the second aspect, ML can further be categorized into four fields: (1) regression; (2) classification; (3) clustering; (4) anomaly detection (Edgar and Manz 2017).

In supervised learning, labeled data are available (i.e., the outcome of a particular combination of values for input features is known and labeled) (Edgar and Manz 2017). The collection of multidimensional data can be referred to as the data set, whereas each element is a datapoint (Bonetto and Latzko 2020). Supervised learning deals with the construction of ML models for a set of data which includes input and output pairs (Bonetto and Latzko 2020). Some of the most popular supervised learning algorithms are multiple linear regression (MLR), artificial neural network (ANN), support vector machine (SVR), decision tree (DT), and ensemble learning (boosting and bagging methods) (Russell 2010). In contrast to supervised learning, unsupervised learning deals with unlabeled data to extract information and identify relationships between variables (Mitchell 2007). Popular unsupervised methods include but are not limited to, K-means clustering, self-organizing maps (SOMs), hierarchical clustering, and principal component analysis (PCA) (Edgar and Manz 2017). Reinforcement learning is different from both supervised and unsupervised learning methods, as it teaches an agent to make decisions and take actions in an environment by observing the environment's current condition (Edgar and Manz 2017). Some of the reinforced learning models are the transductive support vector machine and the Markov decision process (Bonetto and Latzko 2020).

In classification problems, the ML algorithms learn from labeled data (i.e., discrete values) and classify new observations into the labels already learned. In contrast, the regression models learn from labeled data to predict continuous values for new observations. Clustering methods can detect similarities between data to define clusters of like observations. In anomaly detection, a dataset containing normal observations is used to train the model to identify if the new data are anomalous (i.e., deviated from normal) (Bonetto and Latzko 2020).

1.2.3. Applications of machine learning in cementitious materials

The engineering community has identified ML as a vital tool that can be used for the advancement of cementitious materials. According to a review by Kazemi (2023), over 450 studies have applied ML techniques on cementitious materials in the past decade alone (i.e., from 2013 to 2023). Moreover, this trend has been observed globally, with multiple studies originating from countries such as China, Iran, India, the United States, Australia, and Canada (Kazemi 2023). An increasing trend in the application of ML techniques has been noticed, as the number of publications in 2021 and 2022 almost equaled the total number of publications from the year 2023 to 2020 (Kazemi 2023). The increased usage of ML techniques can be attributed to the benefits such as better time management and reduction of cost and resources (Tran et al. 2022).

Among many different ML applications on cementitious materials, supervised learning regression models have been the most commonly used ML algorithms (Kazemi 2023). To efficiently develop mixtures that meet the strength requirements for engineering applications, many scholars have focused their research efforts on using regression ML models for predicting the UCS of different cementitious materials (Kazemi 2023). For example, Nazari and Sanjayan (2015) built support vector regression (SVR) models to predict the UCS of geopolymer pastes, using a dataset comprising 12 different input features collected from the literature. The best performing SVR

model could achieve a high prediction of 89% for testing data. Likewise, the ensemble models constructed by Chou and Pham (2013) could achieve accuracies over 93% when predicting the UCS of high-performance concrete (HPC) made with OPC and other additives (i.e., blast furnace slag, fly ash, and silica fume). In this study, all the ML models were constructed on a dataset collected from the literature which considered a total of eight input features. Similarly, Choudhary et al. (2021) used an experimental results-based dataset to build artificial neural network (ANN) models for predicting the UCS of ultra-high-performance concrete. In this study, eight input features were simultaneously considered, and the best performing ANN model reportedly achieved a very high prediction accuracy of 99% for testing data. Furthermore, an ensemble model built on an experimental results-based dataset comprising six input features performed excellently with an accuracy of 99% when predicting the UCS of calcined sludge-based cementitious materials (Zhang et al. 2022a). In addition, another ensemble model with an accuracy of 93% has been used to predict the UCS of carbon nanotube-reinforced cementitious materials (Li et al. 2022). This study reportedly used a dataset collected from literature comprising 11 different input features. Moreover, various ML models, including random forest (RF), ANN, and ensemble learning have been used to build models to predict the UCS of OPC-based CPB (Qi et al. 2019a; Qi et al. 2018b; Qi et al. 2018c; Qi et al. 2021). In these studies, the prediction models could achieve very high accuracies of over 90%. In addition to providing accurate and rapid UCS predictions by constructing complex relationships between multiple input features and UCS, the majority of the aforementioned studies also offer insights into feature ranking importance and provide detailed interpretations of the prediction results. Therefore, ML has a significant potential to guide the mixture designs of cementitious materials more efficiently while saving time, cost, and material. Despite its potential, no research efforts have been taken to employ ML techniques on AAS-based

CPB and CSA cement-based mixtures to guide their mixture designs through accurate UCS predictions. To address this research gap, an organized study should be conducted to extract datapoints from contemporary literature pertaining to experimental results of AAS-based CPB and CSA cement-based mixtures and to construct and evaluate the performance of different UCS prediction models.

1.3. Research objective

The overall objective of this study is to apply machine learning (ML) techniques to forecast the unconfined compressive strength (UCS) of sustainable cementitious materials that can be used in the mining industry.

In pursuit of the overall objective, two sub-objectives have been identified as follows:

(1) To build ML models on a dataset collected from literature to predict the UCS of alkali-activated slag-based cemented paste backfill (AAS-based CPB).
(2) To build ML models on a dataset collected from literature to predict the UCS of calcium sulfoaluminate (CSA) cement-based mixtures.

1.4. Thesis structure

The thesis is structured to include detailed information about the two investigations mentioned in the main objective of this study and is presented in four chapters. **Chapter 1** introduces the background of this research while elucidating the research problem. It further defines the main and sub-objectives of this study.

Chapter 2 presents the first investigation: the application of ML techniques to forecast the UCS of AAS-based CPB mixtures. This chapter includes background information on AAS-based CPB and the research problem of its challenging mixture design. In addition, this chapter includes the

detailed methodology followed to achieve the objectives of this investigation and a comprehensive discussion of the results obtained. At the end of this chapter, the major findings of this investigation are listed, followed by the advantages and limitations of the study, and directions for future research.

Chapter 3 presents the second investigation: the application of ML techniques to forecast the UCS of CSA cement mixtures. This chapter includes a more detailed introduction to the research background and research problem, descriptions of methodologies followed, and results obtained for feature selection, ML model performance evaluation, and feature importance ranking. The chapter further concludes the major findings of this investigation. Moreover, the advantages and limitations of the study, and directions for future research are listed at the end.

Chapter 4 concludes the major findings of this work related to the two investigations. In addition, the key contributions of this study are listed in this chapter.

Chapter 5 summarizes the limitations of this work while discussing the recommendations for future work in this area of research.

Chapter 2. A machine learning model to predict unconfined compressive strength of alkali-activated slag-based cemented paste backfill

This chapter has been published as **C.B. Arachchilage**, C. Fan, J. Zhao, G. Huang, W.V. Liu, A machine learning model to predict unconfined compressive strength of alkali-activated slag-based cemented paste backfill. Journal of Rock Mechanics and Geotechnical Engineering. © Elsevier. (2023).

2.1. Introduction

Cemented paste backfill (CPB) is a sustainable mine backfill technology that improves the safety and efficiency of mining operations (Qi and Fourie 2019). CPB usually consists of mixing water, dewatered mine tailings, and hydraulic binder (Hewitt et al. 2009). Typical binders include but are not limited to, ordinary Portland cement (OPC), natural pozzolans (e.g., volcanic tuff and pumice), fly ash, and alkali-activated slag (AAS) (i.e., blast furnace slag activated with an alkali solution, such as sodium hydroxide (SH) or sodium silicate (SS)) (Tariq and Yanful 2013). Of these, AAS has shown advantages, such as increased early-stage strengths (Cihangir et al. 2015), enhanced durability (i.e., resistance against acid and sulfide attacks) (Cihangir et al. 2012), reduced heat discharge (Benzaazoua et al. 2004), and improved flowability (Ercikdi et al. 2009) of CPB. In addition, the overall cost of AAS is relatively low (i.e., 50% of the cost of OPC) because it reuses slag (i.e., a waste product) as the binder (Cihangir et al. 2012). Therefore, AAS-based CPB has a great potential to be the leading technology for mine backfill.

Despite its great potential, the mixture design of AAS-based CPB confronts substantive challenges. The mixture design is required to ensure that the unconfined compressive strength (UCS) of AAS-based CPB satisfies the demands for safe underground mining operations (Cihangir et al. 2012). To understand the mixture design, scholars have investigated the influence of various design parameters (e.g., physical and chemical properties of tailings, binder, and alkali-activator) on the UCS of AAS-based CPB. Parameters considered in these investigations include but are not limited to, particle size distribution (PSD) of tailings (Zhang et al. 2021), binder dosage, water-to-binder ratio, liquid-to-solid ratio (Cihangir et al. 2015; Cihangir et al. 2018; Cihangir et al. 2012), silicate modulus and Na_2O content of the activator (Cihangir and Akyol 2018; Cihangir et al. 2012; Jiang et al. 2019; Jiang et al. 2022b), and curing age (Cihangir et al. 2015; Cihangir et al. 2018;

Jiang et al. 2020; Jiang et al. 2019). Although a multitude of experimental studies have been conducted to investigate various design parameters, most of the experimental studies are limited to understanding the relationship between only one design parameter and the UCS of the AAS-based CPB. It is crucial to consider multiple design parameters simultaneously to understand their relationships with the UCS and to improve the mixture design of AAS-based CPB.

Having the ability to build complex relationships between multiple input parameters and outputs, machine learning (ML) has attracted much attention in the last decade (Liang et al. 2020). ML can be identified as a collection of algorithms that can derive outputs automatically for a given set of input data (El Naqa and Murphy 2015). Prominent ML methods include but are not limited to, gradient boosting regression (GBR) (Jerome 2001), random forest (RF) (Breiman 2001) support vector regression (SVR) (Pisner and Schnyer 2020), and artificial neural network (ANN) (Sajda 2002). These methods have previously been employed to forecast the UCS of different OPC-CPB mixtures. For example, Qi et al. (2018a) trained a GBR model on a dataset that included 13 different design parameters to predict the UCS of OPC-CPB. The model achieved a prediction accuracy of 96.3%, while being able to investigate the effects of multiple parameters (e.g., solids content, cement-tailings ratio (c/t), curing time and chemical properties of tailings) on UCS. Likewise, Sun et al. (2020b) studied the effects of solids content, fine tailings percentage, and curing time on the UCS of OPC-CPB mixtures using an SVR model with a prediction accuracy of 97.3%. Their model indicated contrasting results in strength gain rates (i.e., increasing and decreasing) when increasing the fine tailings content at two different solids contents in the mixture. Qi et al. (2018b) used an ANN model trained on a dataset comprising four different design parameters and reported a prediction accuracy of 97.9%. They identified a combined effect of curing time and tailings type on UCS, as a significant difference in the strength development trends

was noted for different tailings types at various curing intervals. In addition, the literature review reports the usage of an RF model with an accuracy of 98.9% to predict the UCS of OPC-CPB. The trained model described the relationships between multiple design parameters, including c/t ratio, solids content, and curing time and UCS of OPC-CPB. These ML models accurately predicted the UCS of OPC-based CPB by constructing relationships between multiple input parameters and the UCS of the OPC-based CPB. However, despite the existing applications for OPC-based CPB, there is a lack of research of using ML methods on AAS-based CPB in both the literature and engineering applications.

To this end, the objective of this study was to build prediction models based on a dataset of experimental results from the contemporary literature to forecast UCS of AAS-based CPB mixtures. First, a generalized dataset comprising 307 data points was collected from publications of nine different experimental studies. Then, the dataset was pre-processed and divided into training (80%) and test (20%) sets. The training set was used to construct four different ML models: GBR, RF, SVR, and ANN. In the next step, comparisons were made among the trained models based on their performances on the test set to select the best model. After that, the relative importance of each mixture design parameter for the prediction model was investigated based on the best model. This study is the first application of the ML models to forecast the UCS of AAS-based CPB, which can be used to replace the demanding and costly experimental approach.

2.2. Methodology

2.2.1. Overall workflow

The overall workflow of the study is depicted in Figure 2.1. A dataset comprising experimental results related to AAS-based CPB research was collected from the previous literature. Then, the collected dataset was pre-processed (normalized to be in the value range of 0 to 1). Afterward, the whole dataset was split into a training set (80%) and a testing set (20%) to train and evaluate the ML models. Next, four ML models (GBR, RF, SVR, and ANN) were built on the training set. A random search hyperparameter tuning method was used to tune the most critical hyperparameters of each model to improve the performances of the models. The performance of each preliminary and tuned model on the training set was evaluated using three statistical parameters: coefficient of determination (R^2), root mean squared error (RMSE), and mean absolute error (MAE). In addition, each tuned model's prediction accuracy was evaluated on the test set by using the same metrics to select the best model. After that, a relative importance test was carried out based on the best model. Relative importance can be used to interpret the data and rank the parameters based on the degree of influence on the prediction model (Fan et al. 2022). Finally, the ability of the model to understand complex relationships between multiple inputs and the UCS was investigated. The above ML modeling work was implemented on Jupyter Notebook using the Python language (version 3.8.8).

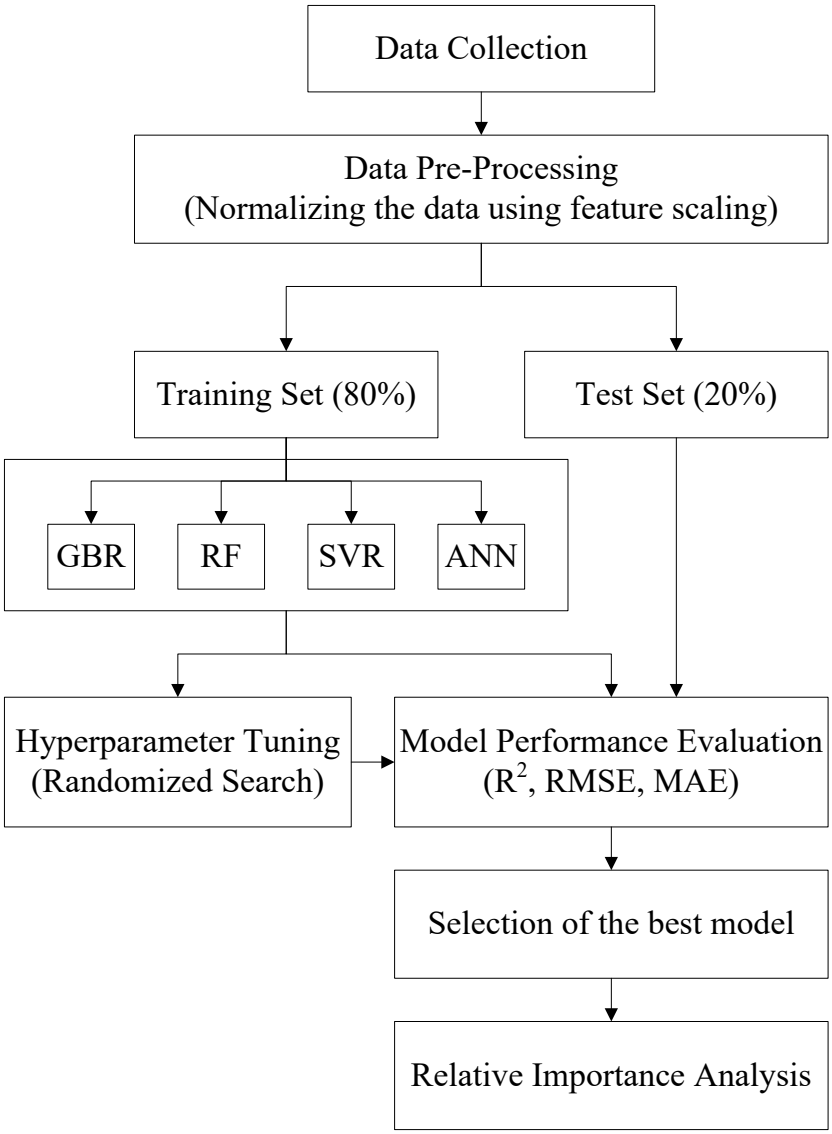

Figure 2.1 Overall workflow of the study.

2.2.2. Data preparation

2.2.2.1. Data collection

A systematic bibliographic survey (Figure 2.2) was conducted to extract experimental results as data points. Alkali-activated slag cemented paste backfill, uniaxial compressive strength, and mechanical strength were used as the keywords on Web of Science and Compendex science databases to search for literature related to AAS-based CPB research. First, a total of 19

publications indexed from the year 1900-2022 had been solicited. The selected literature covered the studies that have been conducted in multiple countries, including China, Turkey, Canada, and the United States. Next, they were filtered based on the usability of the data in this study. A total of nine publications were found suitable for data extraction. Others were not chosen due to missing data, different mixture designs (i.e., use of additives), and different activators (except for different blends of SS and SH). Therefore, this study was limited to experimental studies conducted in China (five studies) and Turkey (four studies). A database was created of experimental results containing 307 data points extracted from the above-selected literature.

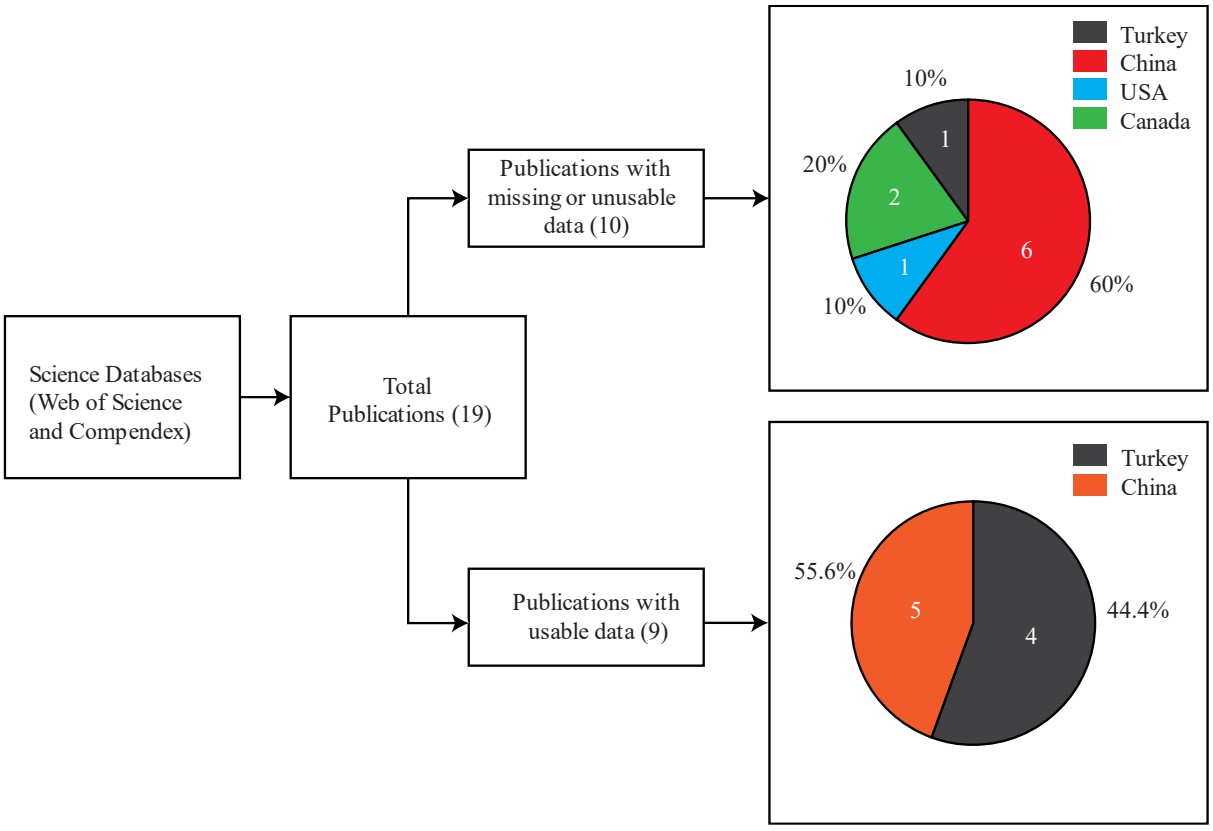

Figure 2.2 Bibliographic analysis of the publications related to AAS-based CPB research.

It is worth mentioning the availability of accurate UCS prediction models for OPC-based CPB built using much fewer data points. Two different ML models, which have been trained

respectively, with only 136 data points (Qi et al. 2018c) and 132 data points (Qi et al. 2020b), an ANN model which uses only 51 data points (Hu et al. 2022), and an RF model built only with 144 data points (Qiu et al. 2020) can be presented as examples. However, each of the above models has been built using the results of single experimental schemes. In contrast, the database used in this study was based on nine different experimental studies and was much larger when compared with the above examples. Table 2.1 summarizes the sources of data used in this study alongside primary information referring to the type of tailings, slag, and activators.

The dataset represents a wide variety of tailing types, such as copper, zinc, gold, iron, and stone waste. In addition, blast furnace slag with variations in its chemical composition (acidic and neutral slags, or combinations of various proportions of silica fume) has been used as the binder in the cited articles. Therefore, this study was not limited to a single experimental scheme and was successful in collecting a more generalized data set. It was expected that the diversity of the data set would have a positive effect on the establishment of robust ML models.

Table 2.1 Sources of collected data for the ML model

Source	Type of tailings	Type of slag	Type of activator	Source
1	Cu/Zn tailings	Blast furnace slag	$NaOH/Na_2SiO_3$	(Cihangir et al. 2018)
2	Cu/Zn tailings	Blast furnace slag (acidic/neutral)	$NaOH/Na_2SiO_3$	(Cihangir et al. 2012)
3	Cu/Zn tailings	Blast furnace slag	$NaOH/Na_2SiO_3$	(Cihangir et al. 2015)
4	Cu/Zn tailings (deslimed)	Blast furnace slag	$NaOH/Na_2SiO_3$	(Cihangir and Akyol 2018)
5	Au tailings	Blast furnace slag	$NaOH/Na_2SiO_3$	(Ercikdi et al. 2009)

Source	Type of tailings	Type of slag	Type of activator	Source
6	Au tailings	Blast furnace slag	$NaOH/Na_2SiO_3$	(Jiang et al. 2020)
7	Stone waste	Blast furnace slag	$NaOH/Na_2SiO_3$	(Zhang et al. 2021)
8	Fe tailings	Blast furnace slag and silica fume	$NaOH/Na_2SiO_3$	(Sun et al. 2020a)
9	Au tailings	Blast furnace slag	$NaOH/Na_2SiO_3$	(Jiang et al. 2022a)

2.2.2.2. Data description

The input features were selected under five main categories, including the PSD characteristics of tailings, characteristics of the mixture design, chemical composition of the activator, tailings, and slag. A statistical summary of the input variables is presented in Table 2.2. PSD has a direct effect on the strength development of AAS-based CPB as the overall porosity of the CPB mixtures is influenced by the size gradation of tailings (Cihangir and Akyol 2020). The coefficient of uniformity (C_u) and coefficient of curvature (C_c) were selected as input parameters in the model, since they are good indicators of particle gradation (Keaton 2018). According to the extracted value range of C_u (3.62-43.33) and C_c (0.341-41.13), the tailings material can be classified and graded in the database. In practice, PSD of tailings can be measured using the laser particle size analyzer (Jiang et al. 2022a), and C_u and C_c can be calculated using the formulae mentioned in Table 2.2.

Table 2.2 Description of the dataset

Category	Parameter	Description	Minimum	Maximum
PSD characteristics of tailings	Coefficient of uniformity	D_{60}/D_{10}	3.62	43.33
	Coefficient of curvature	$D_{30}^2/(D_{60\times}D_{10})$	0.341	41.13
Characteristics of mixture design	Binder dosage (%)	Mass of dry binder (g)/ (mass of dry binder (g) + mass of dry tailings (g))	5	30
	Liquid-to-solid ratio (%)	Mass of total liquids (g)/mass of total solids (g)	0.204	0.445
	Water-to-binder ratio (%)	Mass of water (g)/mass of binder (g)	1.23	5.8
Chemical composition of activator	Silicate modulus of the activator	Mass of SiO_2 (g)/mass of Na_2O (g)	0	2
	Na_2O content of the activator (%)	As a percent of the dry weight of the slag	3.1	22.55
Chemical composition of tailings	Mass percent of SiO_2 (%)	As a percent of the dry weight of the tailings	4.47	62.5
	Mass percent of Al_2O_3 (%)	As a percent of the dry weight of the tailings	0.29	18.1
	Mass percent of CaO (%)	As a percent of the dry weight of the tailings	1.24	63.56
Chemical composition of slag	Mass percent of SiO_2 (%)	As a percent of the dry weight of the slag	24.36	41.1

Category	Parameter	Description	Minimum	Maximum
	Mass percent of Al_2O_3 (%)	As a percent of the dry weight of the slag	8.06	16.2
	Mass percent of CaO (%)	As a percent of the dry weight of the slag	0.83	57.7
Others	Curing age (d)	Curing time before subjecting to UCS tests	7	224

Binder dosage, liquid-to-solid ratio (l/s), and water-to-binder ratio (w/b) can be identified as the most influential mixture design parameters for the strength development of AAS-based CPB mixtures (Cihangir et al. 2015; Cihangir et al. 2018; Cihangir et al. 2012; Jiang et al. 2020; Jiang et al. 2019; Jiang et al. 2022a). Consequently, these parameters were selected as input parameters of the ML model to represent information on the mixture proportion (i.e., content of water, binder and solids). Liquid-to-solid ratio values were always less than 1, indicating solid content is higher than liquids in the mixture. Its range was limited when compared with other mixture design parameters. Binder dosage had a larger range of values between 5-30, representing a various number of trials by scholars. Values for these parameters can be obtained by measuring the individual masses of water, solids and binder contents used in a particular mixture and by using relevant formulas mentioned in Table 2.2.

The selection of silicate modulus (M_s) and Na_2O content of the activator as input parameters for the model was based on the fact that these parameters control the amount of hydration products formed and determine the strength of AAS-based CPB mixtures (Jiang et al. 2020). M_s was calculated based on the ratio of the mass of SiO_2 (g)/mass of Na_2O (g). M_s becomes zero when SH

alone is used as the activator, as SH does not contribute to the SiO_2 content. In contrast, the Na_2O content obtains non-zero values, even when SH alone is used. Based on different blends of SS and SH, Na_2O content had a large range of values.

Although aluminosilicate minerals are less reactive due to their crystalline form in mine tailings, alkali activation has been able to dissolve the above mineral compounds providing reactive aluminum and silica to the cement mixtures (Tian et al. 2020). In addition, many scholars have investigated the effect of chemical parameters of tailings on the strength development of OPC-based CPB mixtures and have identified that the strength is dependent upon the chemical characteristics of tailings (e.g., content of SiO_2) (Benzaazoua et al. 2002; Kesimal et al. 2005). In contrast, the same effect on UCS of AAS-based CPB has been barely assessed in experimental studies. In this study, the inclusion of data from different types of tailings material permitted the investigation of this effect on the UCS of AAS-based CPB. Contents of SiO_2, Al_2O_3 and CaO in tailings were selected as the chemical indices of importance for hydration reactions and included in the model as input parameters. All of these parameters had significant value spans, representing different types of tailings. Next, SiO_2, Al_2O_3 and CaO contents of slag material were included as input parameters in the model, as they can be considered as the most prominent constituents of slag material which determines the quality of the hydration reactions of AAS-based CPB, after being alkali-activated and mixed with tailings and water (Jiang et al. 2020). As the quality of cement hydration is indicative of the strength, contents of the above chemical constituents have a direct influence on the UCS of AAS-based CPB. All chemical composition parameters of tailings, binder and activator can be determined using X-ray fluorescence (XRF) (Jiang et al. 2020) test in practice.

The number of curing days was selected as the last input, as the UCS is reported to be highly dependent on the curing time of the mixture (Cihangir et al. 2015). Data were extracted for a wide range (7-224) of curing days, as the UCS has shown drastically different values when moving from short to long term. Finally, the UCS values extracted from experimental results were defined as the output. They also had a wide range of values, from 0.139 MPa to 7.965 MPa, with a mean value of 2.678 MPa. The data distribution characteristics of the input variables are illustrated in Figure 2.3, which represents the frequency of each value in each input parameter using histogram plots. Parameters on the categories of PSD characteristics of tailings, the chemical composition of tailings, and slag did not show a wide data distribution. This was because this study was limited to only a few different types of tailings and slags. In contrast, all other parameters had good data distributions between their corresponding minimum and maximum values.

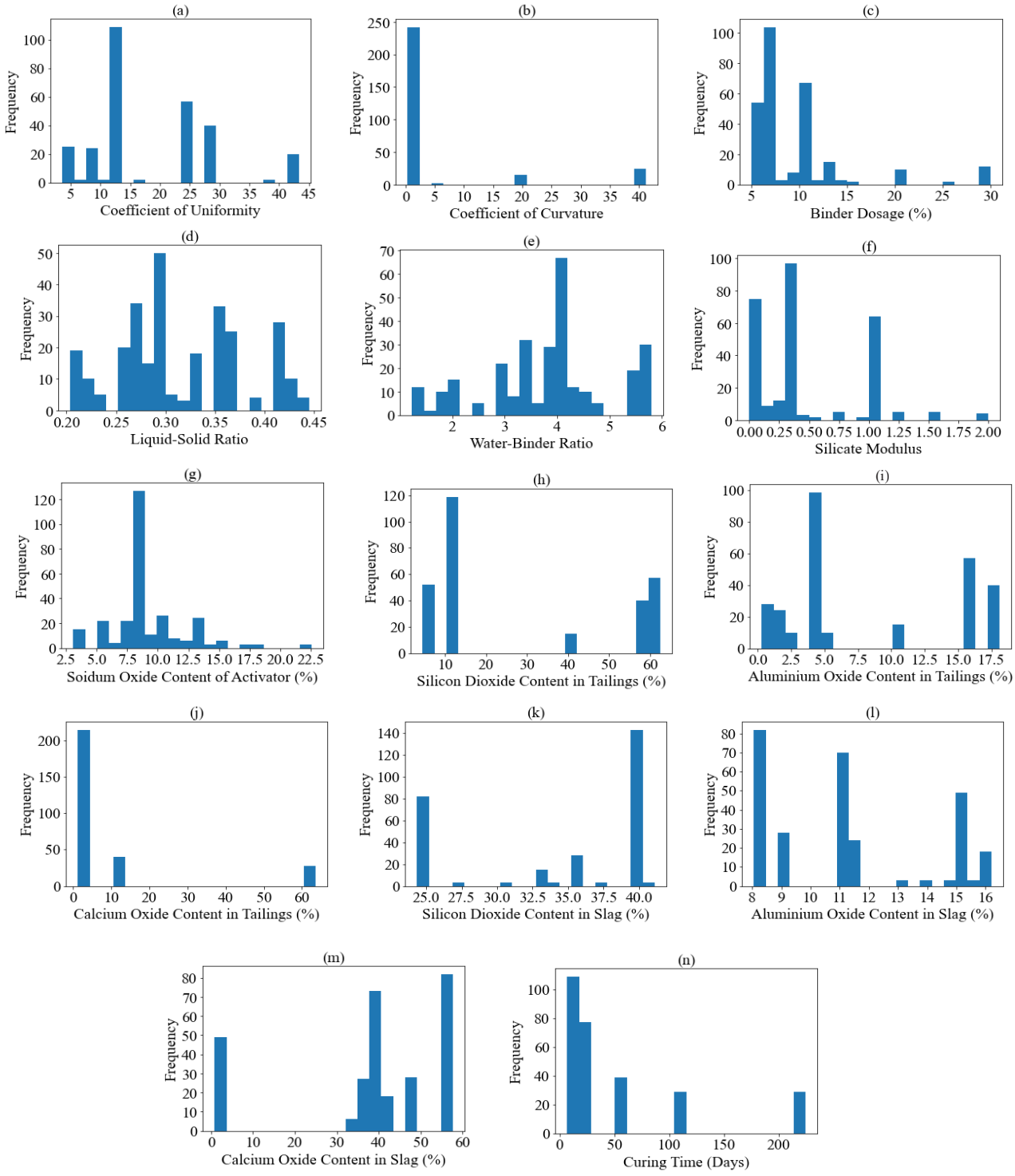

Figure 2.3 Data distribution plots for input variables: (a-m) Histogram plots of input variables related to physical and chemical characteristics of CPB mixture, and (n) Histogram plot for curing days.

2.2.2.3. Data preprocessing

The range of data distribution of each feature varied significantly in the selected data set for this study. For example, the value range of the liquid-to-solid ratio is between 0.204 and 0.445, whereas the curing age had a larger range of 7-224. If feature scaling is ignored, the vast differences in ranges will make the ML algorithm misjudge the superiority of the features (Juszczak et al. 2002). Therefore, before training the ML models, feature scaling was conducted to normalize the data distribution in each feature. Normalization was adopted in this study where the values were shifted and rescaled to be in the range of 0-1. The formula for normalization is written as

$$X' = \frac{X - X_{\min}}{X_{\max} - X_{\min}} \tag{2-1}$$

where X' is the normalized value, X is the actual value, $X_{\min}$ is the minimum value of the selected feature distribution, and $X_{\max}$ is the maximum value of the selected feature distribution. Data normalization was followed by data split into two sets: the training set (80%) and test set (20%). All the models were built on the training set, and their performances were evaluated on the test set.

2.2.3. ML methods

Four powerful ML models were used to address the regression problem in this study. GBR and RF models were selected from the tree-based ensemble learning methods category. Another two single learning methods, SVR and ANN, were selected for comparison purposes. All ML models were trained using the Scikit-learn Python package. Brief descriptions of each algorithm and the base of their selections in this study are presented below.

2.2.3.1. GBR algorithm

The GBR algorithm has been successfully applied in previous studies related to mechanical strength predictions of CPB materials (Qi et al. 2020b) and OPC-based cement mixtures (Eyo and Abbey 2021). Their results have shown that the performance of the GBR model is superior to that of conventional models. Therefore, the GBR model was selected as one of the ML models in this study. In boosting ML algorithms, the weak learners which fail to predict the output accurately are given the priority and converted to strong learners. Among the available boosting methods, the gradient boosting method applies an additive sequential theorem. The residual errors are calculated in the initial step (first of many trees that are built) to identify the weak learners and can be defined as the observations with large residual errors. Their predictions are improved by building a second tree to address the residuals. The sequence is continued by building a third tree, based on the error calculations of the first two. This iterative process (Figure 2.4) will continue until the stopping criterion is fulfilled. The weighted sum of predictions will be calculated based on the results obtained from all the previous tree models (Jerome 2001). Although the squared error loss function is considered to be the simplest of the loss functions, Huber loss and absolute error functions can also be used whenever the usage of squared error is limited (Hastie et al. 2009).

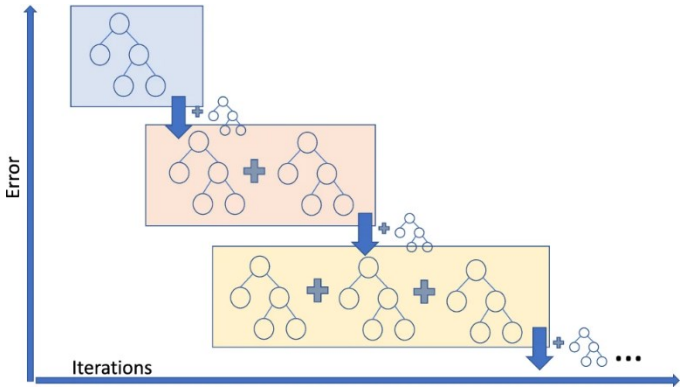

Figure 2.4 GBR model training iterative process (modified from (Baturynska and Martinsen 2021)).

2.2.3.2. RF algorithm

A validated RF model with very high accuracy has been used for UCS prediction of OPC-based CPB mixture by (Qi et al. 2019a). Due to similarities in the application between the two studies, the RF algorithm was selected as the second ML model in this study. RF is also an ensemble learning technique that obtains better performance by assembling the outputs of many different regression trees. In the RF algorithm, the feature space is segmented using different types of partitioning criteria. First, the corresponding region of an observed data point is selected. Then the prediction is executed based on the mean or the mode of all the data present in that region. RF eliminates the high variance issue involved with the decision trees algorithm, by using a bootstrap method to extract samples from the training set (Fan et al. 2023a). Therefore, many independent decision trees are built using bootstrap samples Figure 2.5. At the final stage, all the trees are bagged, and the predicted values are averaged (Breiman 2001).

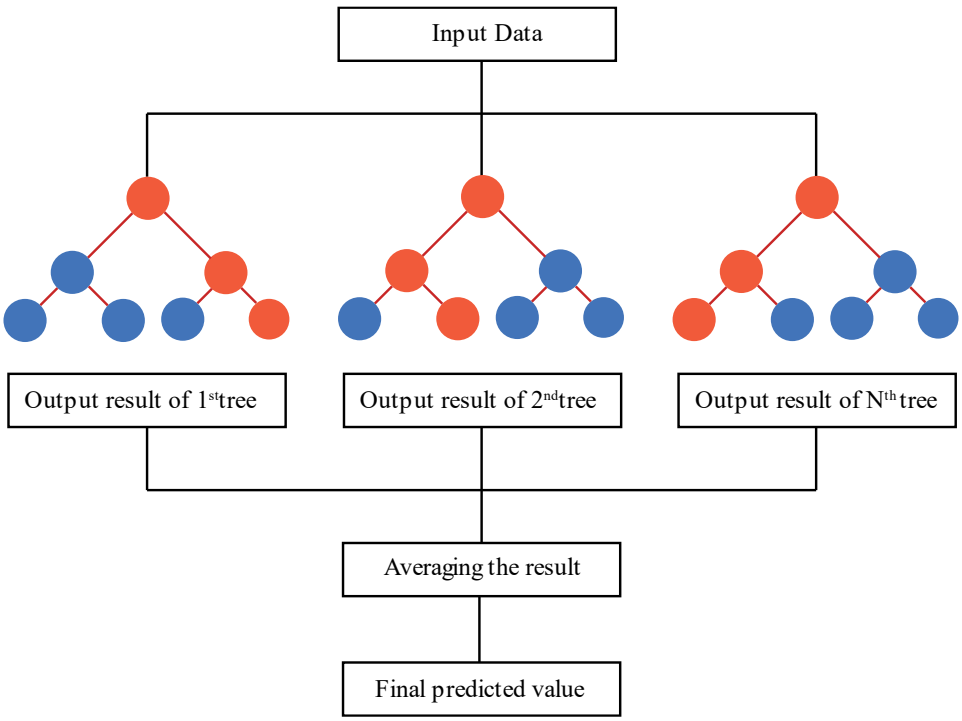

Figure 2.5 Illustration of RF algorithm (modified from (Kwak et al. 2022)).

2.2.3.3. SVR algorithm

SVR models have been used to build accurate prediction models in various research themes, such as rockburst intensity monitoring, fly-rock distance modeling, and UCS estimations in cementitious materials (Yu et al. 2021). Therefore, SVR was chosen as an ML model to be used in this study due to its robustness in the application. In the SVR algorithm, the input feature space is split using optimum boundaries. The boundaries are defined as hyperplanes, and their simplest format is a line when the feature space is limited to two dimensions. However, in three-dimensional space, the hyperplane is a two-dimensional plane that divides the data set. The optimum hyperplane is constructed by the algorithm by maximizing the margin. In other terms, the optimum hyperplane has the smallest perpendicular distances from the data points Figure 2.6. The data points which are closest to the margin are called support vectors. Higher dimensional spaces are

used to map the data points, whenever the data are inseparable. The mapping functions are termed kernel functions, i.e., radial bias, sigmoid, and polynomial functions (Boser et al. 1992).

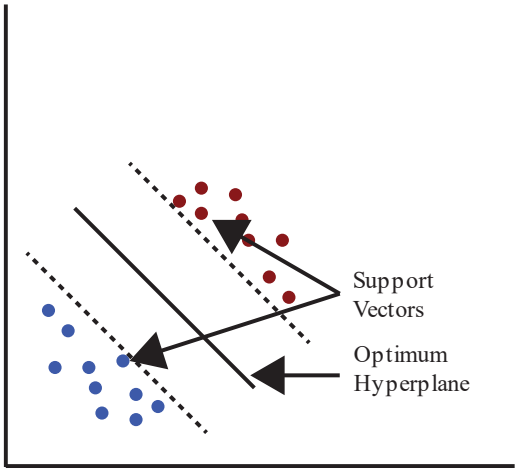

Figure 2.6 Optimum hyperplane in support vector machines (modified from (Tinoco et al. 2014)).

2.2.3.4. ANN algorithm

The ANN method has been used to predict the UCS of CPB mixtures successfully in previous research (Yu et al. 2021). Therefore, it was used as an ML model in this study to have a wide variety of algorithms for comparison purposes. ANN is a computer program designed to mimic the human brain function, with a special relation to neurons. The architecture of ANN models consists of three main parts: the input layer, hidden layers, and output layer. In addition, each of the hidden layers has a pre-defined number of neurons. A network of connections between the neurons in different layers is initiated using a feed-forward algorithm (Figure 2.7).

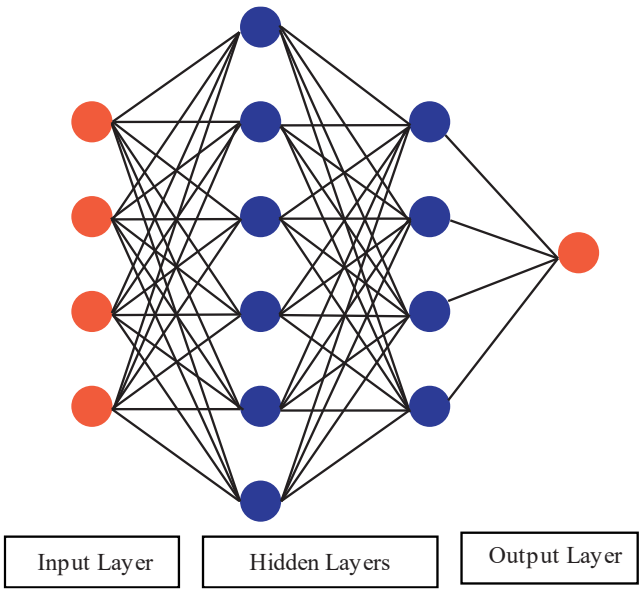

Figure 2.7 Schematic representation of the ANN algorithm with input, hidden, and output layers (modified from (Noorani and Mehrdoust 2022)).

However, no connections will be formed between neurons in a layer. For each connection, a weight will be assigned. In the training process, both input and output data will be introduced to the model, and the values of the hidden layer neurons will be calculated using the assigned weights. The algorithm uses a linear sum function followed by a nonlinear activation function to calculate these values. The most used activation functions are the identity, logistic, tanh, and relu functions. In the final step, a back-propagation algorithm will be employed, and the weights will be adjusted in an iterative process until the errors between the calculated and the predicted output values are minimized.

2.2.4. Hyperparameter tuning of the ML models

The main objective of hyperparameter tuning in this study was to improve the prediction performance of preliminary models. Hyperparameters can be defined as the set of parameters not directly learned inside the estimating algorithms. They must be passed as arguments to the training

models. The performance of the prediction models is highly dependent upon the selection of these hyperparameters. For example, the C value in the Support Vector Regressor contributes to the bias and variance trade-offs of the model. Accordingly, optimum parameters must be determined and used in the models to improve prediction accuracies. However, a manual approach would not be feasible for this purpose due to the infinite combinations (due to continuous space of the values) of different parameters within one estimator. Consequently, the Randomized Search method in the Scikit-learn model selection library was used to obtain the optimum hyperparameters of each model in this study. This method randomizes the search over the parameters, which reduces computation time. In the application of this method, an iterative *k*-fold cross-validation process was executed, and the RMSE metric was defined as the decisive parameter for the selection of the optimum model. The *k* value was set to 5, based on the recommendations by (Wu et al. 2020) and (Liang et al. 2020). Table 2.3 summarizes the critical hyperparameters that needed to be tuned in each model, and their optimum values.

Table 2.3 Hyperparameters of the ML model

Model	Hyperparameter	Optimum value
GBR	learning rate	0.1
	min_samples_leaf	1
	min_samples_split	4
	n_estimators	938
	max_depth	4
	subsample	0.3323
SVR	C	615.69
	gamma	0.457
	epsilon	0.052
RF	min_samples_leaf	1
	min_samples_split	2
	n_estimators	89
	max_depth	13
ANN	alpha	0.0001
	hidden_layers	2
	number of neurons in a layer	200

2.2.5. Performance evaluation metrics for the ML models

The study used three performance evaluation metrics available for regression problems. Scikit-learn python package's metrics module was used for this purpose. The test set portion of the

original data was used as the input to obtain the predictions using the trained model. The predicted values were compared with the actual target values in the test set to measure the prediction accuracies using the following metrics.

The first metric, the R^2 score, can be used to verify the degree of match between the predicted and true values. The best fit between the two sets corresponds to an R^2 value of 1. Accordingly, the R^2 value should be close to 1 for the models to be accepted as accurate. The following formula (Equation 2-2) is used for the R^2 calculations:

$$R^2 = 1 - \frac{\sum_{i=1}^{n}(y_i - \hat{y}_i)^2}{\sum_{i=1}^{n}(y_i - \overline{y_i})^2} \qquad (2\text{-}2)$$

where y_i is the actual target value, $\hat{y}_i$ is the predicted value of the output, and $\overline{y_i}$ is the average value of the actual target values.

RMSE can be used to determine the degree of dispersion between the original target value and the predicted value, and it is simply the squared version of the calculated value of mean squared error (MSE). Equation 2-3 represents the formula for the calculation of RMSE:

$$RMSE = \sqrt{\frac{\sum_{i=1}^{n}(y_i - \hat{y}_i)^2}{N}} \qquad (2\text{-}3)$$

where N is the number of samples available in the test set. When the MSE and RMSE are low, the prediction models are accurate. The RMSE can be used as an indicator of the average distance between a data point and the fitted line.

MAE is also an indication of the degree of fit between the actual target data and the predicted data since it outputs the absolute error values. MAE can be calculated by

$$MAE = \frac{\sum_{i=1}^{n}|(y_i - \hat{y}_i)|}{N} \qquad (2\text{-}4)$$

It is accepted that models with R^2 scores close to 1 with very low RMSE and MAE values can yield better results with higher accuracy (Wu et al. 2020). After hyperparameter tuning, the selection of the best-performing model can be a concern since the performance results might fall close to each other. Therefore, a ranking system developed by Zorlu et al. (2008) was used to rank the ML models based on R^2, RMSE and MAE values on the test set predictions. The highest obtainable score was 4 for each metric (because there were 4 models), where the highest R^2 value and lowest error metric values were given equal scores of 4. Decremental scores (3, 2 and 1 for the next best performing models) were assigned for other low-performing models.

2.3. Results and discussion

2.3.1. Comparison between preliminary and tuned ML models

Preliminary ML models were constructed using the default hyperparameter values for each ML model. It was observed that all preliminary models (before tuning) exhibited overfitting problems because their prediction accuracies were comparatively low for new data (test set). Among all four preliminary models, the GBR model displayed the best performance, with an R^2 score over 0.92 for the test set (Table 2.4). Contrastingly, SVR performed poorly on both training and test data sets, achieving R^2 scores of only 0.712 and 0.694, respectively. However, the performances of preliminary ANN and RF models were acceptable, obtaining R^2 scores over 0.85 on the test set predictions.

Table 2.4 Performance results of preliminary and tuned ML models

Model	Type	Training set			Test set		
		R^2 score	RMSE	MAE	R^2 score	RMSE	MAE
GBR	Tuned	0.999	0.055	0.045	0.969	0.237	0.162
	Preliminary	0.966	0.272	0.199	0.928	0.361	0.296
SVR	Tuned	0.998	0.064	0.052	0.889	0.446	0.289
	Preliminary	0.712	0.793	0.498	0.694	0.741	0.542
RF	Tuned	0.979	0.213	0.144	0.907	0.408	0.335
	Preliminary	0.979	0.215	0.144	0.904	0.414	0.335
ANN	Tuned	0.983	0.19	0.126	0.887	0.449	0.342
	Preliminary	0.965	0.276	0.198	0.864	0.495	0.37

In the next step, critical hyperparameters of each model were tuned to improve the prediction performances. The resulting optimum hyperparameter values from the randomized search tuning method are presented in Table 2.3. Updated hyperparameters reduced the overfitting issues of GBR, SVR and ANN models by generalizing them for new data sets. The effect was highest on the SVR model, as the R^2 score could be improved by 28% for the test data set predictions. In addition, the RMSE and MAE errors could be reduced by 40% and 47%, respectively. In contrast, hyperparameter tuning had a minimal effect on the RF model, with no significant improvements noted. This insensitivity of the RF model to its hyperparameters has been previously reported in the literature. For example, the R^2 value could only be increased by 0.01% after tuning the hyperparameters of an RF model, which was used to predict the UCS of OPC-based CPB (Qi et al. 2019a). The overall comparison between preliminary models and tuned models is illustrated in Figure 2.8, which shows that the hyperparameter tuning improved the prediction accuracies of GBR, SVR and ANN models by improving R^2 score and by reducing RMSE and MAE. The

importance of having tuned ML models for accurate predictions in regression algorithms has been previously pointed out in the literature. For example, in the study by Qi et al. (2020b) to predict UCS of OPC-based CPB, the hyperparameter tuning improved the R^2 value of the GBR model from 97.9% to 98.9%. Similarly, Sun et al. (2020b) reported a decrease in RMSE value of an SVR model (which was used to predict UCS of OPC-based CPB) from 0.259 to 0.082, when optimum hyperparameters were used.

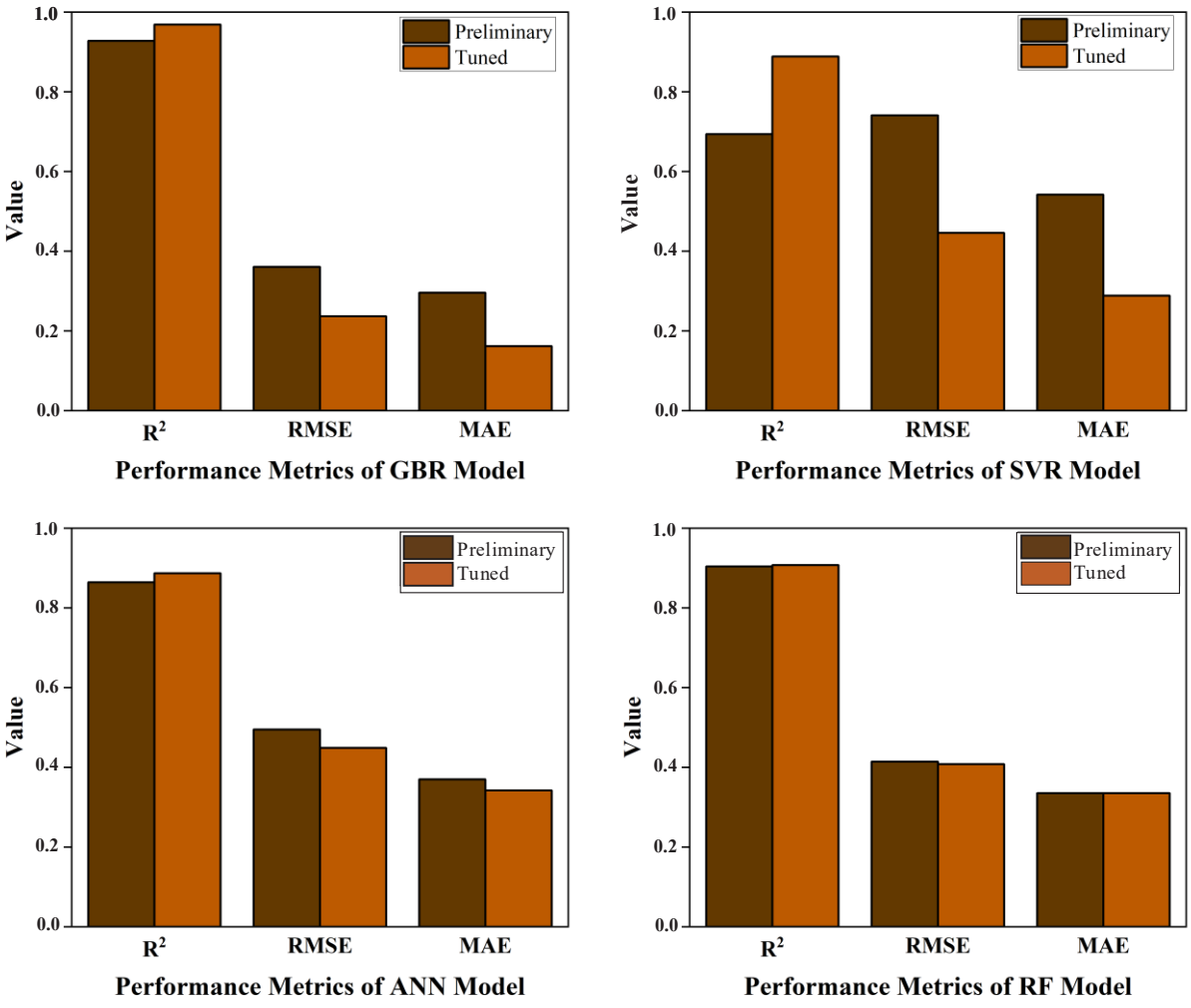

Figure 2.8 Performance comparison between preliminary and tuned ML models.

2.3.2. Selection of the best ML model

Table 2.5 shows the scores (based on the ranking system by Zorlu et al. (2008)) that the ML models obtained depending on their prediction performances on the test set. The total score for each model was calculated by adding the scores obtained for each performance metric. Based on the total scores in Table 2.5, the reliability of models to predict the UCS of AAS-based CPB materials can be ranked as GBR > RF > SVR > ANN. The ensemble models (i.e., GBR and RF) outperformed the other two models by obtaining the highest scores of 12 and 8, respectively. In addition, the superior performance of GBR over the other ensemble ML technique of RF can be ascribed to the ability of the GBR algorithm to convert weak learners into strong learners in successive steps. Similar results can be found where GBR and RF models were used for UCS prediction of cement-based mixtures. For example, Lu et al. (2019) reported a higher accuracy of 98% by the GBR model than the RF model, which had an accuracy of only 95% in predicting the UCS of OPC-based CPB. Likewise, Qi et al. (2020a) reported a better accuracy of 0.98 for a GBR model over a accuracy of 0.95 for a RF model, which were constructed to predict pressure drop of pipe flow in OPC-based CPB. In summary, the GBR model is the best suited model for UCS predictions of AAS-based CPB, based on the model evaluation results in this study.

Table 2.5 Model ranks based on the performance metrics

Model	R^2		RMSE		MAE		Total score	Rank
	Value	Score	Value	Score	Value	Score		
GBR	0.969	4	0.237	4	0.162	4	12	1
SVR	0.889	2	0.446	2	0.289	3	7	3
RF	0.907	3	0.408	3	0.335	2	8	2
ANN	0.887	1	0.449	1	0.342	1	3	4

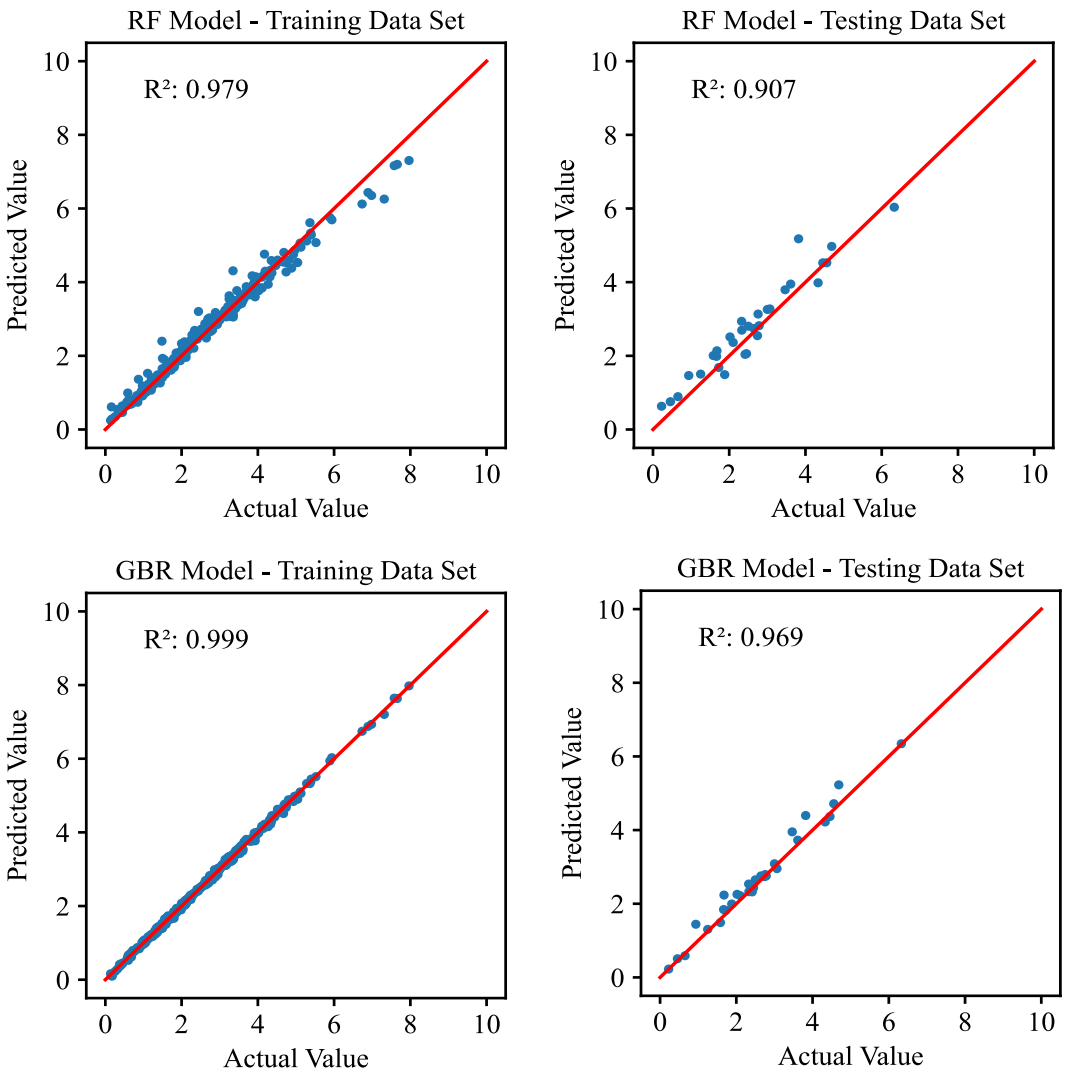

Figure 2.9 Actual vs. predicted UCS values of GBR and RF ML models

Scatter plots were created to visualize the agreement between actual and predicted UCS values of the ML models. A scatter point represents an actual value (i.e., an experimental result extracted from literature) of UCS in *X* axis and its corresponding predicted value in *Y* axis. It could be observed that scatter points of GBR and RF models in the test set predictions were closer to the best-fit line, indicating an excellent agreement (Figure 2.9). Comparably, multiple points were located far from the best-fit lines in the scatter plots of the SVR and ANN models (Figure 2.10). This confirmed the ability of ensemble ML techniques to outperform the single learning

techniques. Similar results can be found in the literature where a higher prediction performance (R^2 of 0.99) of a RF model over an SVR model (R^2 of 0.98) has been reported, when predicting the UCS of OPC-based CPB (Liu et al. 2020).

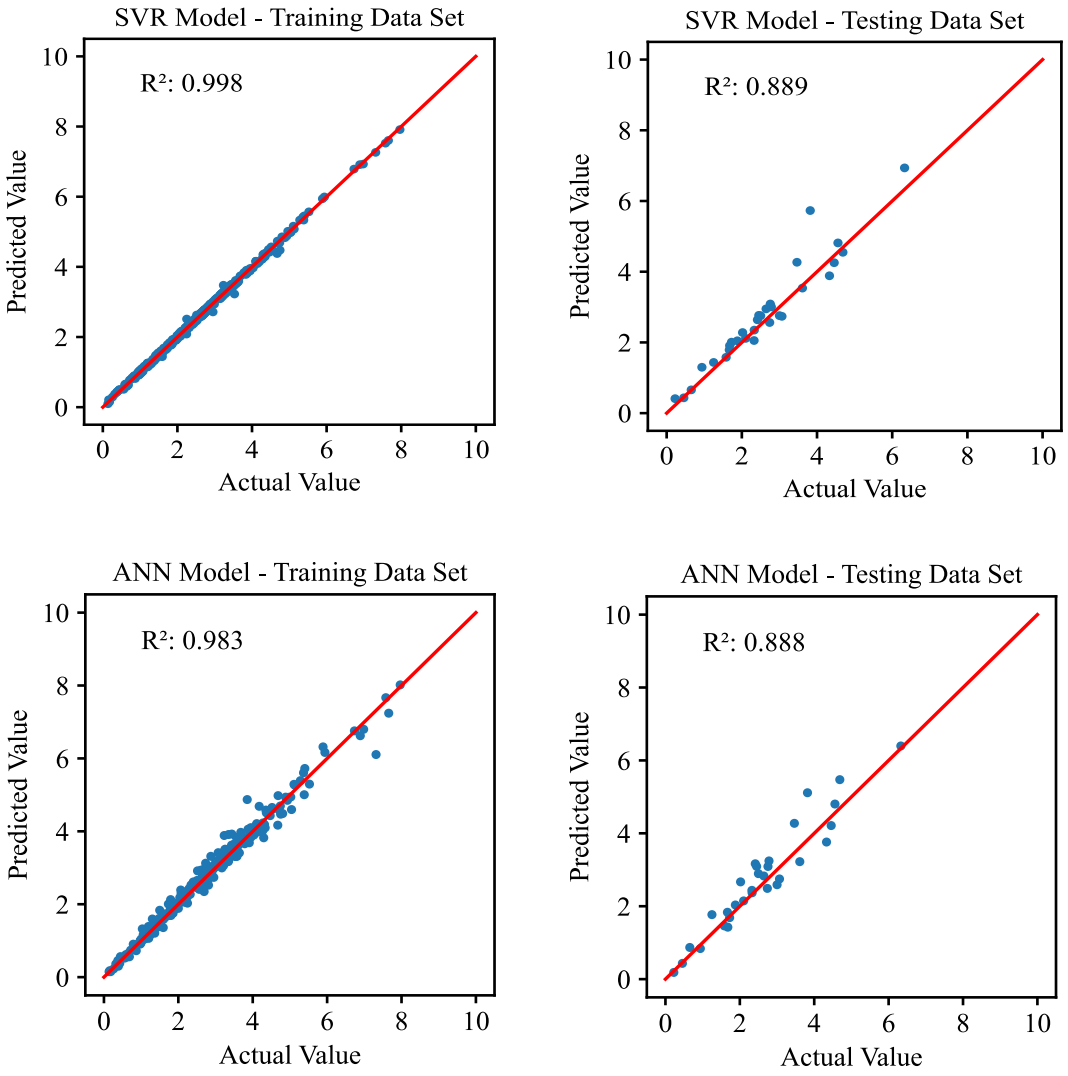

Figure 2.10 Actual vs. predicted UCS values of SVR and ANN models

2.3.3. The relative importance (RI) of input parameters

Figure 2.11 illustrates the ranking of the importance of features in this study. It provides crucial information on each input parameter's degree of impact on the UCS of AAS- based CPB mixtures.

A higher RI indicates a greater impact on the UCS Qiu et al. (2020). This information is highly useful for engineers to make decisions in the mixture design process, as it permits to focus only on the most influential parameters, when trying to achieve the desired strength in a mixture.

2.3.3.1. Curing time

RI results show that curing time has the highest RI (19.98%), indicating that it is the most influential parameter for UCS prediction of AAS-based CPB. Cihangir et al. (2018) reported that UCS is greatly influenced by the number of curing days, since hydration products increase with time. For example, when the number of curing days changed from 14 to 112, the UCS increased by 318% (Cihangir et al. 2018). The inclusion of curing time as a parameter in the prediction model provides valuable information on the required number of days to achieve the desired strength (i.e., UCS required to match the stability requirement of a certain mine site). It will assist engineers in planning production cycles (i.e., when to end the production and when to resume production after backfilling) to avoid ore loss and to reduce costs (Bloss 2014).

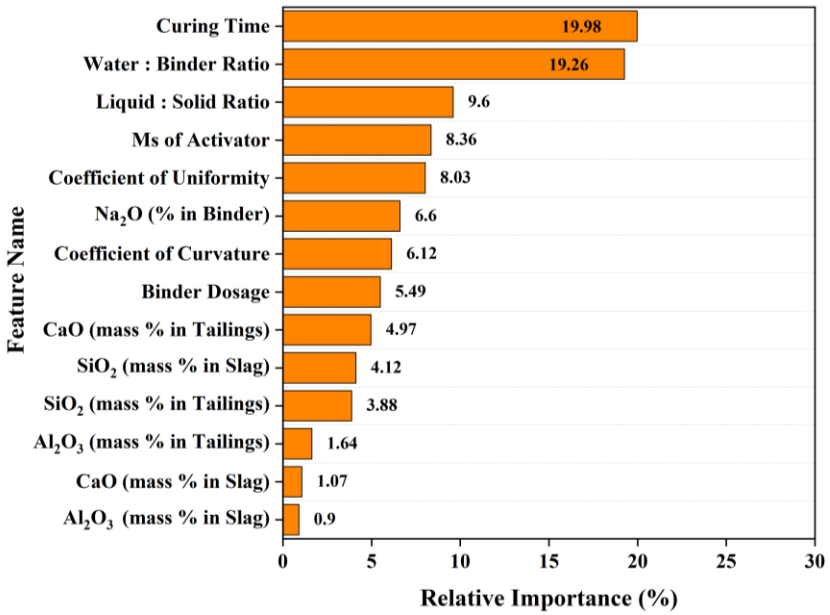

Figure 2.11 Relative importance of features based on the GBR model.

2.3.3.2. Water-binder (w/b) ratio, liquid-to-solid ratio (l/s) and binder dosage

The w/b ratio, l/s ratio and binder dosage are the most common physical parameters considered by researchers in the mixture designs of AAS-based CPB (Cihangir and Akyol 2018; Cihangir et al. 2015). In this study, w/b ratio was the feature with the second highest overall importance (19.26%) for the prediction model. Jiang et al. (2020) investigated the influence of the w/b ratio on UCS and found that UCS dropped by 20% when the w/b ratio was increased from 3.8 to 4.4. This has been attributed to the increased void spaces, resulting in weaker bonding between solid particles (Jiang et al. 2020). Next, l/s ratio, with an importance score of 9.6%, had the third highest important score. Jiang et al. (2019) pointed out that decreasing the l/s ratio from 0.369 to 0.316 increased the 28-d UCS by 31%. This can be ascribed to the lower initial porosity and ease of ability of the hydration products to fill the pore spaces when the solids content is high (i.e., at lower l/s ratios) (Pacheco-Torgal et al. 2008). Design engineers can initiate the mixture design process using the proposed ML model by manipulating these two parameters first. This is because the w/b ratio and l/s ratio are the physical mixture design parameters with the strongest influence on the prediction model. On the other hand, it is interesting to note that the importance of binder dosage to the model is relatively low (5.49%). Jiang et al. (2019) reported an increase in UCS by 79% when the binder dosage was increased from 8% to 12%. The same increment in binder dosage could be represented by a relatively lower decrement of 1.46 (i.e., from 4.39 to 2.93) in the w/b ratio. Similar to the above reports, RI results indicated that the w/b ratio is much more effective than the binder dosage to be used as a parameter in the model. Therefore, binder dosage as an input parameter can be removed from the model to improve the efficiency of the model and to avoid repetitiveness of the same parameter. This assists design engineers with considering the water content and binder

content simultaneously in the mixture design, instead of controlling them as two different parameters.

2.3.3.3. Silicate modulus (M_s) and Na_2O content of the alkali-activator

From the literature, it is noted that the M_s and Na_2O concentration are the two main chemical mixture design parameters that represent the characteristics of the alkali-activator (Cihangir et al. 2015; Cihangir et al. 2012; Jiang et al. 2022a). M_s and Na_2O have close and medium rankings in the RI results, with importance scores of 8.36% and 6.6%, respectively. In accordance with the RI results, literature reports that the silicate polymerization due to increased soluble Si ion concentration (with increasing M_s) in liquid SS-activated cement mixtures has produced higher compressive strengths (Duxson et al. 2005; Pacheco-Torgal 2015; Shi and Fernández-Jiménez 2006). Furthermore, when increasing the Na_2O up to 10%, an increase followed by a decrease in UCS has been noticed in an AAS-based CPB (Zhang et al. 2021). In addition, excess Na_2O has resulted in undesirable amounts of Na^+ cations, leading to stresses during polymerization (Xu and Van Deventer 2000). The UCS of a particular AAS-based CPB mixture at different M_s and Na_2O contents can easily be determined with the inclusion of M_s and Na_2O contents as parameters in the prediction model. This allows the design engineers to identify optimum values of the above parameters (i.e., M_s and Na_2O values at maximum UCS) for a particular mixture which will avoid excess usage of chemicals.

2.3.3.4. PSD of the tailing material

C_u and C_c represent the PSD of the tailing material by relating to the fines content. The RI results proved that C_u and C_c are critical input variables in the prediction model with RI of 8.03% and 6.12%, respectively. However, the effect of PSD of tailings on the UCS has seldom been investigated in experimental studies. Scholars have used the direct tailings output from processing

plants at mine sites without processing them further to test at different particle sizes (Cihangir et al. 2015; Cihangir et al. 2012; Jiang et al. 2020; Jiang et al. 2019; Jiang et al. 2022a; Xu and Van Deventer 2000). However, the trained model permits engineers to consider different PSDs of a particular tailings type to decide on further processing of the tailings.

2.3.3.5. Chemical composition parameters of tailings and slag

Chemical composition parameters of tailings and slag can be identified as the least influencing features (RI below 5%) for the prediction of UCS. Between the above, mass percentages of the constituents of slag had a minimal effect and can be attributed to the low mass proportion of slag when compared with tailings and water in the final mixture. However, the mass percent of SiO_2 in both slag and tailings can still have an influence based on their rankings in RI results. Reports that the reactive SiO_2 content is significant in determining the UCS of AAS-based CPBs support the above RI results (Papadakis et al. 2002; Walker and Pavía 2011). In addition, the RI results indicated that the CaO content in tailings has a similar effect on the model performance. Cihangir et al. (2012) reported higher compressive strengths when materials with relatively low contents of CaO were used. Therefore, it is advisable to include the CaO content of tailings in the ML model as a parameter for accurate predictions of UCS. However, the influence of Al_2O_3 content in tailings and the slag is negligible according to the RI results. This can be attributed to the comparatively very low mass percent of Al_2O_3 in the used materials. Therefore, removing the least affected features can improve the performance and efficiency of the ML model. In practice, this means that engineers can use the above information to select only the valid input parameters to predict the UCS of AAS-based CPB.

2.4. Conclusions

This work is the first study that used advanced machine learning (ML) techniques to predict the unconfined compressive strength (UCS) of alkali-activated slag (AAS) based cemented paste backfill (CPB). The main conclusions drawn from this study are as follows:

(1) Tree-based ensemble machine learning (ML) models (gradient boosting regression (GBR) and random forest (RF)) outperformed the single learning models (support vector regression (SVR) and artificial neural network (ANN)) in predicting the UCS of AAS-based CPB mixtures. SVR and ANN could only achieve prediction accuracies of 88.9% and 88.7%, respectively, on the test set. In contrast, both GBR and RF models obtained prediction accuracies of over 90%.

(2) Curing time was the most important parameter (19.98%) for the prediction model. Engineers will benefit from the information regarding the curing time needed to obtain desired strength levels of a particular AAS-based CPB mixture. It will assist them in scheduling the ore production cycles in underground mines.

(3) The importance of binder dosage (5.49%) for the prediction model was relatively low when compared with the other common physical mixture design parameters (i.e., water-to-binder ratio (w/b) (19.26%) and liquid-to-solid ratio (l/s) (9.6%)). This permits engineers to consider the water content and binder content in a single parameter, without having to control them as two different parameters.

(4) Silicate modulus and the Na_2O content of the alkali-activator had a significant influence on the prediction model, with respective importance scores of 8.36% and 6.6%. Design engineers would be able to determine the optimum activator content for different AAS-based CPB mixtures using the proposed ML model. The importance of the coefficient of uniformity (C_u) (8.03%) and coefficient of curvature (C_c) (6.12%) on the prediction model was equally notable.

The inclusion of C_u and C_c in the prediction model will provide valuable insights for engineers to decide on further processing of tailings to change the particle size to achieve AAS-based CPB mixtures with higher UCS.

(5) Chemical composition parameters of tailings and slag had a relatively low (i.e., below 5%) influence on the model. Among the oxide compounds, Al_2O_3 had the least influence on the prediction model (i.e., less than 2%). Therefore, the most critical oxide compounds in both the tailings and slag could be identified as SiO_2 and CaO.

(6) The GBR model was proposed as the final model for UCS predictions due to its superior performance over the others. It showed a prediction accuracy of 96.7% (R^2) on the test set, indicating that it has the potential to accurately predict the UCS of AAS-based CPB mixtures.

Chapter 3. Forecasting unconfined compressive strength of calcium sulfoaluminate cement mixtures using ensemble machine learning techniques integrated with shapely-additive explanations

This chapter has been submitted for peer review as **C.B. Arachchilage**, G. Huang, C. Fan, W.V. Liu, Forecasting unconfined compressive strength of calcium sulfoaluminate cement mixtures using ensemble machine learning techniques integrated with shapely-additive explanations. Cement and concrete composites. © Elsevier. (Under Review).

3.1. Introduction

Calcium sulfoaluminate (CSA) cement is a sustainable cement that possesses many advantages over ordinary Portland cement (OPC) (Shi et al. 2011), such as high early age strength (Huang et al. 2019), rapid setting time (Huang et al. 2019), shrinkage compensation (Yu et al. 2018), and low carbon footprint (Shi et al. 2011). The design of a CSA cement mixture for achieving the desired unconfined compressive strength (UCS) is challenging due to the influence of multiple features, such as the composition of the cement, curing conditions, material proportioning, and the use of admixtures (Tao et al. 2023). Currently, the CSA cement mixture design depends heavily on the traditional experimental approach, which is resource-intensive, demanding large quantities of materials, substantial financial investment, and significant time commitment (Tran et al. 2022). According to a thorough literature review, until now, most of the previous experimental studies have focused on assessing the influence of only a limited number of features at a time, leading to a less comprehensive understanding of the relationships. For example, in the study by García Maté et al. (2016), the primary focus was on the influence of the type of retarder on the UCS, while keeping the dosage of the retarders constant. Similarly, Huang et al. (2020) investigated the influence of retarder dosage by varying the dosage from 0% to 1%, but only for one specific type of retarder, namely molasses. Another study by Burris and Kurtis (2018) solely investigated the influence of citric acid as a retarder at varying dosages (i.e., 0% to 3%). Furthermore, Xu et al. (2018) studied the influence of curing temperature at different ages, but the analysis was only limited to a narrow range of levels (5 °C, 20 °C, and 40 °C). In addition, it is worth mentioning that most of the reported experimental studies, including those mentioned above, were carried out using fixed cement compositions, material proportions, and curing conditions. The limitations

associated with the experimental approach make it difficult to observe subtle variations and potential non-linear relationships between input features and the UCS of CSA cement.

Based on existing experimental results, machine learning (ML) methods may be considered to learn the current knowledge domain of CSA mixture design. As an emerging trend, many ML methods, such as artificial neural network (ANN) (Mohamed et al. 2021), support vector regression (SVR) (Dahish et al. 2023), decision tree (DT) (Khan et al. 2023), and ensemble learning (Nguyen et al. 2022; Shah et al. 2022) have been documented in the literature for assisting the mixture design of novel cementitious materials. Of these, ensemble learning, a well-known category of machine learning (ML), has been paid much attention in the current literature as it involves the principle of combining multiple base models to create an ensemble model that can outperform a single base model (Erdal 2013). Ensemble models usually include but are not limited to, gradient boosting regression (GBR) (Friedman 2001), extreme gradient boosting regression (XGBR) (Chen and Guestrin 2016), light gradient boosting regression (LGBR) (Ke et al. 2017), and random forest (RF) (Breiman 2001). These ensemble ML methods have been frequently used to build accurate non-linear strength prediction models for novel cementitious mixtures, which typically involve multiple input features. For example, Shah et al. (2022) trained an XGBR model to predict the UCS of one-part alkali-activated material that could obtain a very high accuracy of 96%. In comparison, the reported performance of the single learning ridge regression model was 43% lower in this study. In addition, Nguyen et al. (2022) built an RF model that could produce excellent results for testing data, with a 94% prediction accuracy while outperforming a single learning k-nearest neighbors regression model by a margin of 11%. Furthermore, another XGBR model achieved a high accuracy of 93% on testing data when predicting the UCS of carbon nanotube-inserted cement paste (Li et al. 2022). In contrast, the performance of tested single-

learning linear regression and support vector regression models was much lower, achieving only 69% and 81% accuracies. Therefore, ensemble learning is a promising approach that can be used to build accurate non-linear strength prediction models involving multiple input features in the cement and concrete industry. However, to the best of our knowledge, no studies in the current literature have reported the use of ensemble learning models for predicting the UCS of CSA cement mixtures.

To fill this gap, the objective of this study was to build accurate ensemble ML models using a dataset of experimental results extracted from literature to predict the UCS of CSA cement mixtures. Initially, a total of 723 unique data points could be assembled from 24 different publications reported worldwide. After removing irrelevant or redundant features through feature selection methods, the modified datasets were used to build four different ensemble ML models: GBR, XGBR, LGBR, and RF. Next, each ML model was evaluated on the testing data to select the model with the best prediction performance. Finally, to address the lack of interpretability of the prediction results, the SHapely Additive exPlanations (SHAP) method developed by Lundberg and Lee (2017) was integrated as a tool for the best-performing ML. The SHAP method was preferably used as it not only provides feature importance information but also elucidates the underlying rationale behind each prediction (Ekanayake et al. 2022).

The novelty of this study can be expressed in three key aspects. First, a comprehensive literature review of the experimental studies of CSA cements was conducted to compile a diversified and meaningful dataset that has not been previously assembled. Second, this study is the first to develop ensemble ML models that enable rapid UCS predictions of CSA cement by incorporating multiple input features simultaneously. Third, the SHAP analysis allowed for a comprehensive evaluation of feature importance in the context of the strength of CSA cement, which has not been

previously explored. This assists engineers to make informed decisions on CSA cement mixture designs when aiming to achieve the desired strength for a particular application. Overall, this study may function as the groundwork for the efficient design and development of CSA cement mixtures with the application of ML modeling and its interpretations.

3.2. Methodology

3.2.1. Overall workflow of the study

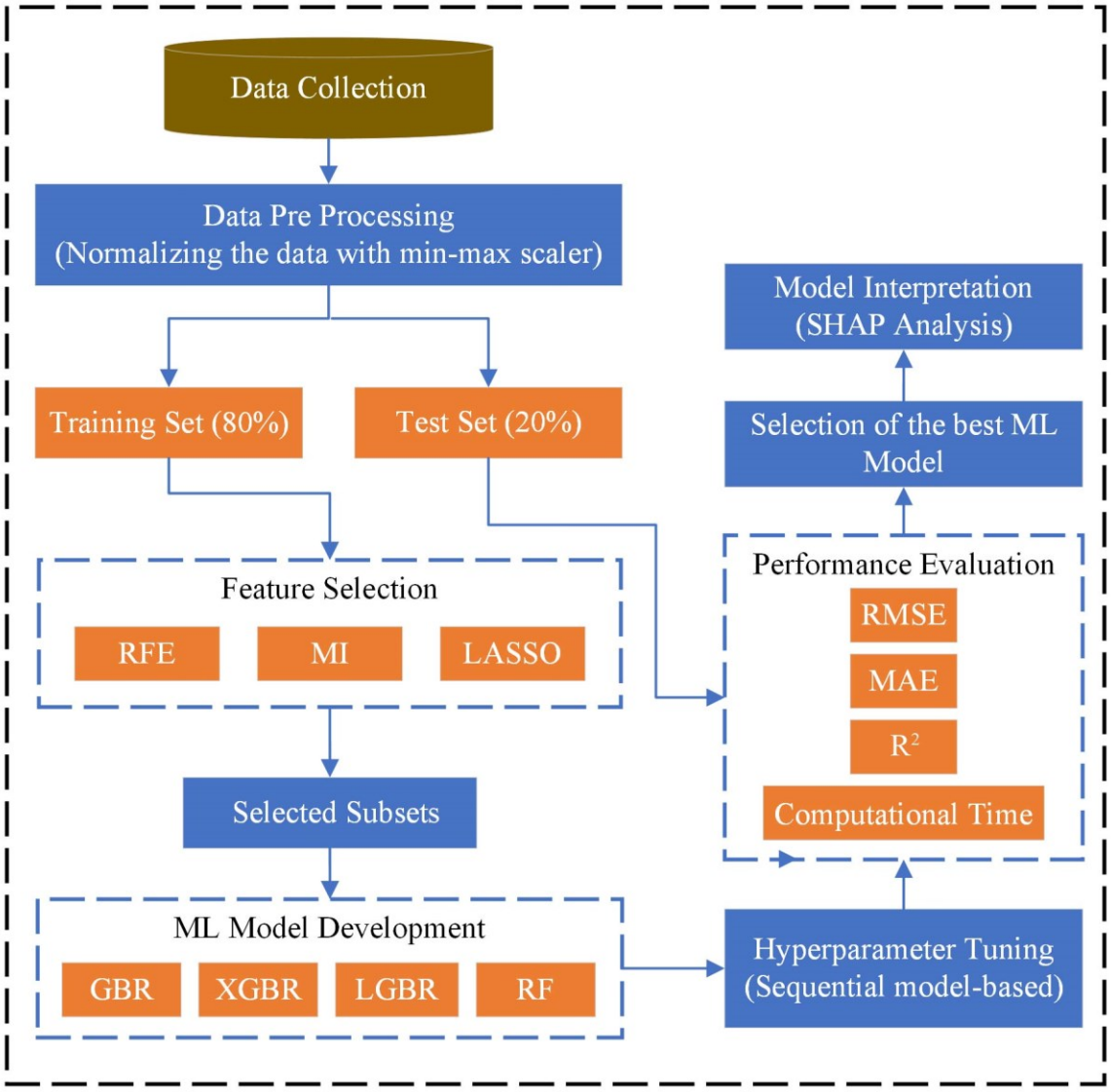

Figure 3.1 Schematic diagram of the overall methodology followed in the study

The overall methodology followed in this study is illustrated in Figure 3.1. Initially, experimental results related to the determination of UCS of CSA cement were extracted from the previous literature to create a dataset including multiple input features and a single output (i.e., UCS). Next, the collected data were normalized using a min-max scalar to convert the data values to be in the range of 0 to 1. Then, the pre-processed dataset was split into two separate sets: a training set (for model training) and a test set (for model evaluation). Afterward, three different feature selection methods: recursive feature elimination (RFE), mutual information (MI), and least absolute shrinkage and selection operator (LASSO) regression were employed on the training set to extract the features with the most influence to be included as input features in the ML models. Next, four different ML models: GBR, XGBR, LGBR, and RF were built on the modified training dataset (i.e., dataset constituent of only the optimum subset of input features). In addition, the performance of each ML model was improved by tuning the most critical hyperparameters, using a sequential model-based optimization method. After that, the performances of the trained models were evaluated on the test set using three statistical parameters: coefficient of determination (R^2), root mean squared error (RMSE), and mean absolute error (MAE). Moreover, each ML model was evaluated based on the computational time as an additional metric. Finally, the ML model with the best prediction performance was selected as the most accurate model for the prediction of UCS of CSA cement and its results were interpreted using the SHAP analysis. It is important to note that the above methodology was carried out using the sci-kit learn package (version 1.0.2) on Jupyter Notebook (python programming with version 3.9.13) installed in a desktop computer (configurations: Intel Core i7 3.6 GHz processor, 16 GB of RAM).

3.2.2. Data preparation

3.2.2.1. Data collection

A comprehensive bibliographic survey was conducted to compile an organized dataset of published experimental results. Calcium sulfoaluminate cement, CSA cement, compressive strength, retarder, and plasticizer were applied as keywords in renowned scientific databases of the Web of Science and Compendex to identify articles that were compatible with data extraction. A total of 24 publications cataloged from the year 1900-2023 could be identified from the bibliographic survey. Finally, a dataset comprising 723 unique data points could be assembled from the extracted literature to build the prediction models. It is noteworthy to mention the availability of many other accurate ML models built on smaller datasets used to predict UCS of similar cementitious materials. An XGBR model built with only 173 data points (Shah et al. 2022), a GBR model constructed based on a dataset of 328 data points (Shen et al. 2022), and two RF models that use only 424 (Nguyen et al. 2022) and 616 data points (Zhang et al. 2023), respectively, can be introduced as examples. In comparison, the dataset used in this study is much larger and can be used to establish more generalized models.

Table 3.1 provides a summary of the articles used in this study, including information on the source and country of origin. The data points originate from 10 different countries across three major continents: North America, Europe, and Asia. Despite the dominant representation of data originating from China, the reported usage of several types of CSA cement in their studies adds diversity to the dataset. This wide-ranging data collection ensures that the developed ML model is not biased toward a particular region or a specific type of CSA cement.

Table 3.1 Summary of the sources of data used in the study

	Country	Source
1	Canada	(Huang et al. 2020)
2	Canada	(Huang et al. 2022a)
3	China	(Hu et al. 2017)
4	Germany	(Skocek et al. 2015)
5	United States	(Burris and Kurtis 2018)
6	China	(Chen et al. 2021)
7	China	(Zou et al. 2020)
8	China	(Shen et al. 2023)
9	China	(Jing et al. 2022)
10	China	(Zhang et al. 2016)
11	Spain	(García Maté et al. 2016)
12	China	(Ke and Zhang 2020)
13	China	(Chen et al. 2018)
14	Finland	(Nguyen et al. 2019)
15	China	(Li et al. 2018b)
16	United States	(Burris and Kurtis 2022)
17	Canada	(Huang et al. 2022b)
18	Belgium	(Mohan et al. 2021)
19	India	(Shenbagam and Chaunsali 2022)

	Country	Source
20	Thailand	(Rungchet et al. 2016)
21	Germany	(Zajac et al. 2019)
22	France	(Morin et al. 2017)
23	China	(Xu et al. 2018)
24	China	(Wang et al. 2017)

3.2.2.2. Data description

The collected dataset consists of nine numerical and three categorical input features, with the UCS serving as the output feature. The selected input features were chosen to represent distinct types of cement, experimental conditions, and curing conditions that were reported in the extracted articles. Out of the common mineralogical constituents available in CSA cement, ye'elimite, belite, and calcium sulfate can be identified as the most prominent components that contribute to cement hydration and consequent ultimate strength (Huang et al. 2020). Therefore, the content of these mineralogical constituents was chosen as input features in the dataset to represent the type of CSA cement used in each experiment. It is important to note that an adapted Bogue's Equation (Equations 3-1 to 3-3) (Chen and Juenger 2011) was used to estimate the mineralogical compositions from oxide compositions, whenever the mineralogical compositions were not directly reported in the sources.

$$ye'elimite\ \% = 1.995(Al_2O_3\%) - 1.273(Fe_2O_3\%) \quad (3\text{-}1)$$

$$belite\ \% = 2.867(SiO_2\%) \quad (3\text{-}2)$$

$$calcium\ sulfate\ \% = 1.700(SO_3\%) - 0.445(Al_2O_3\%) + 0.284(Fe_2O_3\%) \quad (3\text{-}3)$$

The w/c and a/c were also selected as input features as they provide information about the quantities of added water and fine aggregates, concerning the quantity of cement. The type of retarder, type of superplasticizer (categorical variables), and dosages of retarder and superplasticizer (numerical variables) were chosen as input features in the dataset as they can be used to represent the type and dosage of the most commonly used admixtures in CSA cement. Curing temperature and time were added to the dataset as input features to include information about the curing conditions of the cement. An additional categorical feature, namely the type of test was included in the dataset to investigate the impact of the standard used to determine the UCS in the reported experiments.

A statistical summary of the numerical input features and the UCS is presented in Table 3.2. The wide distribution of values observed in all three mineralogical compositions is due to the inclusion of data from a diverse range of experiments that utilized several types of CSA cement. In addition, the dataset included a substantial range of w/c ratio values, ranging from 0.26-0.80. This attests to the advantage of using data-driven methods over experimental approaches, as it allows for the incorporation of significant value spans that would otherwise be difficult to achieve inside a single experimental scheme. In contrast to the w/c ratio, the range of values of the a/c ratio was limited as most of the studies have used common cement preparation standards. It is important to note the inclusion of results from cement pastes, where the a/c ratio is 0 as a result of no aggregate usage. Furthermore, despite the fact that the majority of data points correspond to samples cured at room

temperature, data obtained from samples cured across a broad temperature range of 20°C to 80°C could also be included in the dataset. Similarly, both retarder and superplasticizer dosages exhibited significant value spans, with a value of 0 indicating pure CSA mixtures without any admixtures. Moreover, the dataset included data points representative of both long-term and short-term strengths, with minimum and maximum curing times of 1 hr and 2160 hr, respectively. Additionally, Figure 3.2 illustrates histograms representing the dataset concerning various input features, which are in agreement with the statistical analysis of data, represented by Table 3.2. Finally, a significant distribution of values could be seen in the output feature: UCS, with a minimum of 0 MPa (i.e., early age strength of mixtures with higher dosages of retarders) and a maximum of 105.7 MPa.

Table 3.2 Statistical summary of the dataset about numerical input features

Input feature	**Mean**	**Standard deviation**	**Minimum**	**Maximum**
Ye'elimite content % (w/w)	38.13	15.92	21.8	76.2
Belite content % (w/w)	30.34	12.66	9.7	52.4
Calcium sulfate content % (w/w)	14.63	10.02	0	45.2
Water-to-cement ratio	0.41	0.10	0.26	0.8
Aggregate-to-cement ratio	1.23	1.29	0	3.125
Curing temperature (°C)	28.47	14.92	20	80
Retarder dosage (% cement mass)	0.42	0.58	0	3
Superplasticizer dosage (% cement mass)	0.37	0.58	0	1.75

Input feature	Mean	Standard deviation	Minimum	Maximum
Curing time (hr)	239.26	326.26	1	2160
UCS (MPa)	44.88	20.30	0	105.7

Besides the numerical input features, categorical data on the type of retarder, superplasticizer, and test were transformed into vectors using the label encoding method (i.e., assigning a numerical value to represent each category). One-hot encoding, which is another popular method, was not chosen because it can significantly increase the dimensionality of the features and consequently increase the computational cost of ML modeling (Rashid et al. 2022). For the type of retarder and superplasticizer, the number 0 was assigned to indicate the absence of any admixture. Within the retarder category, the numbers 1-7 were assigned to represent the usage of molasses, sodium gluconate, a mixture of citric acid and borax, tartaric acid, borax, citric acid, and vitamin C respectively. Similarly, the numbers 1-4 were used to represent polycarboxylate acid, β-naphthalenelfonic acid, aminosulfonic acid, and powder naphthalene as superplasticizers. According to Figure 3.2, the data points were well distributed among different admixture types, which further improves the generalization of ML models built on the dataset. Additionally, within the category of test type, values 1-3 were assigned to indicate the different standards of UCS testing. Specifically, value 1 represented the ASTM C39/C39M-18 (ASTM) standard for testing cylindrical specimens, value 2 represented the testing of cubic specimens (with varying specimen sizes between experiments), and value 3 represented the GB/T 17671-2021 (ISO 2021) standard or the ISO 679: 2009 (ISO 2009) standard for testing using triple test molds. As shown in Figure

3.2, the final dataset included well-distributed data points that correspond to UCS results obtained using different testing standards.

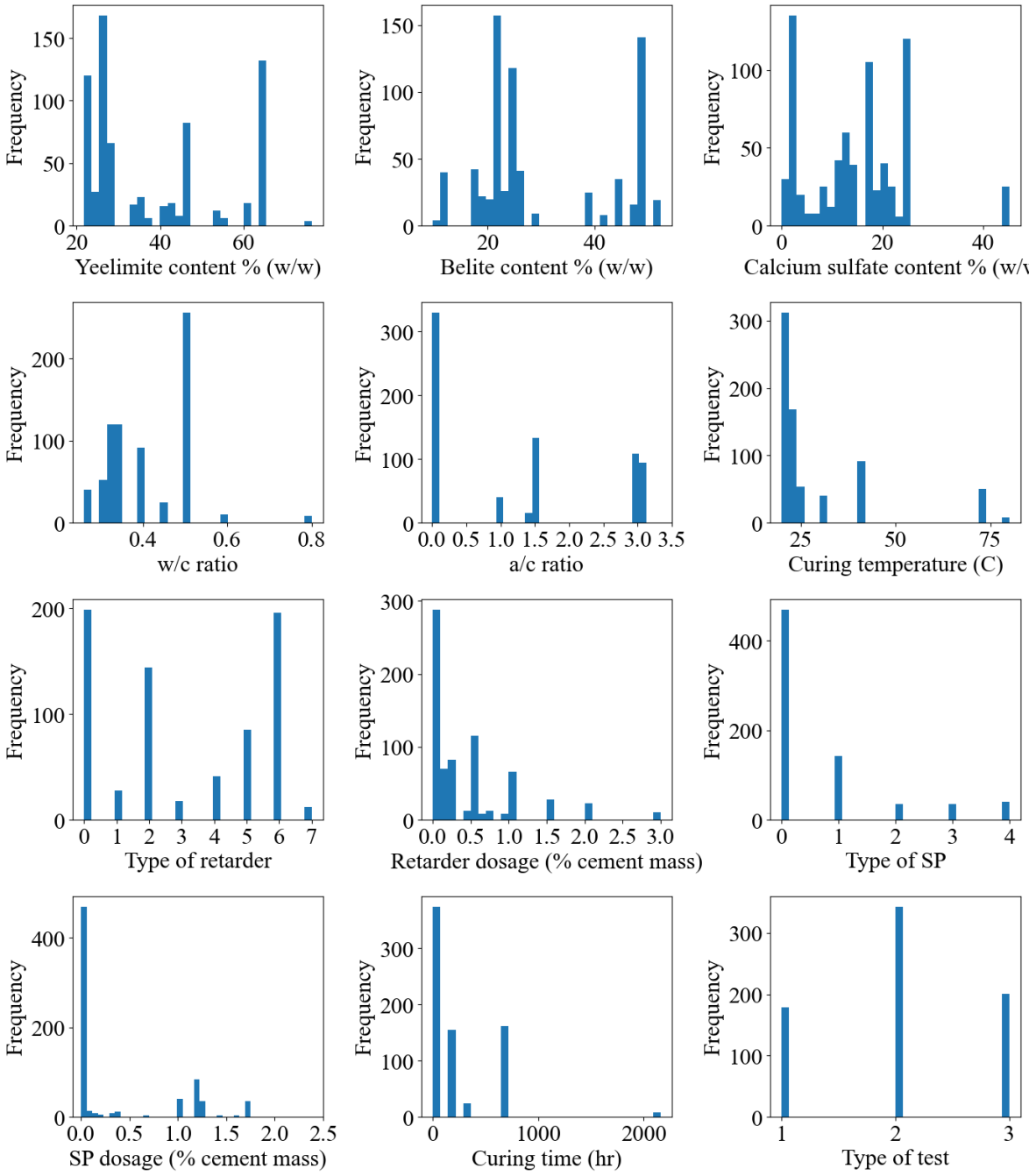

Figure 3.2 Distribution of data of input features

3.2.2.3. Data pre-processing

According to Table 3.2, the range of data distribution varied across different input features. For example, the value range of curing time was 1-2160 hr, whereas the w/c ratio was limited to a value range of 0.26-0.8. In such instances, ML models could misjudge the superiority of input features (Arachchilage et al. 2023). Therefore, each input data value in the dataset was scaled and normalized to be in the range of 0 to 1, using the min-max scaling method represented by Equation 3-4.

$$X_{scaled} = \frac{X - X_{min}}{X_{max} - X_{min}} \tag{3-4}$$

where X_{scaled} is the normalized value, X is the original input value, X_{min} is the minimum value of the input feature and X_{max} is the maximum value of the input feature. The normalized dataset was then split into two portions: the training data set (80%) and the testing data set (20%). It is worth mentioning that this particular split proportion has been frequently used in studies involving a similar number of data points in the field of ML applications on cementitious materials (Huo et al. 2022; Liang et al. 2022; Rahman et al. 2021) . The training data were used to build the ML models whereas the testing data were used to evaluate the performances of the models.

3.2.3. Feature selection methods

Feature selection is an essential step in ML applications that aids in the identification of input features that may contain redundant or irrelevant information (Li et al. 2017). This study employed three prominent feature selection methods to perform a comparative study to select the optimal subset of input features that yield the best performance in ML models. Filter methods, such as (mutual information) MI, employ statistical methods to score the relationship between each input feature and output. MI method measures the mutual dependence between two features based on

the amount of information acquired about a feature by observing the other (Liu et al. 2022). Features that exhibit a lower association with the output, as indicated by lower MI values, are eliminated from the datasets. In contrast to filter methods, wrapper methods integrate an ML model to find the optimal subset of input features, such as in RFE (Bahl et al. 2019). RFE starts with the full set of input features and removes the least prominent features recursively several times which equals the length of the original set of features. Ultimately, the subset which yields the best results according to the selected performance evaluation criteria is selected as the optimal subset of features. Embedded feature selection techniques, such as LASSO regression, conduct the feature selection inside the model training step, and it is less complex when compared with wrapper methods (Liu et al. 2022). The LASSO method introduces a penalty term to its cost function by setting the coefficients of redundant and irrelevant features to zero (Tibshirani 2011). The penalty term can be controlled to determine the number of coefficients set to zero.

3.2.4. Machine learning models

Ensemble learning techniques have reportedly been able to build accurate prediction models by establishing complex non-linear relationships between multiple input features and the strength of cementitious materials as output (Adel et al. 2022; Li et al. 2022; Min et al. 2023). Based on the learning technique, ensemble methods can be categorized into two types: boosting and bagging. Boosting methods involve a sequential training process, whereas the bagging methods build parallel models. In this study, three boosting methods (i.e., GBR, XGBR, and LGBR) and one bagging method (i.e., RF) were chosen, which are known to produce prediction results with high accuracy.

3.2.4.1. Gradient boosting regression

The GBR method minimizes a loss function in an iterative process until the defined stopping criteria are fulfilled. In each iteration of sequential trees, the loss is minimized by identifying the weak learners in previous steps and assigning higher weights to those learners (Friedman 2001). As a result, the final output would be optimal, as the weak learners were continuously updated.

3.2.4.2. Extreme gradient boosting regression

XGBR algorithm, which was originally introduced by (Chen and Guestrin 2016), integrates the concepts of basis function and weights into the principle of gradient boosting. It is an advanced version of the GBR algorithm which is equipped with an additional regularization term to help reduce overfitting problems. In addition, the accuracy of the XGBR method is enhanced by applying a second-order Taylor expansion to the loss function.

3.2.4.3. Light gradient boosting regression

LGBR has been introduced by Microsoft in 2016, subjecting it to open-source development (Ke et al. 2017). LGBR can be considered an improvement of XGBR as it can address the scalability and efficiency issues of XGBR when handling datasets that are either large or highly dimensional (Li et al. 2018a). In addition, LGBR models require lesser computational time for training and are less prone to overfitting.

3.2.4.4. Random forest

RF uses a bootstrapping technique to add randomness to the sample extraction process when building independent decision trees (Fan et al. 2023a). This randomness contributes to better performances of RF when compared with the conventional decision tree method, by reducing

overfitting. In the final stage, all individual trees that were built are bagged and the predictions are averaged (Breiman 2001).

3.2.5. Hyperparameter tuning

A sequential-model-based optimization method named Scikit-Optimize (Head et al. 2018) was employed in this study to tune the hyperparameters due to its reported ability to enhance the performance of ensemble ML models (Nguyen et al. 2022). Sequential-model-based optimization efficient method that requires less computational time for identifying the optimal configuration of hyperparameters (Lacoste et al. 2014).

This method is based on Gaussian process estimators where the objective function is defined in Equation 3-5.

$$f(\theta) = \sqrt{\frac{1}{N}\sum_{j=1}^{N}\left(y_j - y(x_j)\right)^2} \tag{3-5}$$

where, y_j is the output, $y(x_j)$ is the predicted value and N is the number of samples.

3.2.6. Performance evaluation metrics

Three commonly used statistical metrics were chosen in this study to evaluate the prediction performance of ensemble ML models. The selected metrics: R^2, RMSE and MAE values are calculated using Equation 3-6, Equation 3-7, and Equation 3-8, respectively (Fan et al. 2022, 2023b, c).

$$R^2 = 1 - \frac{\sum_{i=1}^{N}\left(y_j - y_i\right)^2}{\sum_{i=1}^{N}\left(y_j - \bar{y}\right)^2} \tag{3-6}$$

$$RMSE = \sqrt{\frac{\sum_{i=1}^{N}(y_j - y_i)^2}{N}} \quad (3\text{-}7)$$

$$MAE = \frac{\sum_{i=1}^{N}|y_j - y_i|}{N} \quad (3\text{-}8)$$

where, N is the number of samples, y_j is the actual value, y_i is the predicted value, and $\bar{y}$ is the mean of the predicted values. A model with a higher R^2 and lower RMSE and MAE error values is considered to be accurate when compared with ML models with higher errors and lower R^2 (Min et al. 2023).

3.2.7. Interpretation of the model by SHAP analysis

The SHAP analysis was originally developed by Lundberg and Lee (2017). It utilizes a game theory approach where each input feature is considered a player in a game and the prediction is the result of that game. The SHAP analysis computes the effect of including an individual feature on the model prediction as its marginal contribution to the model. This value is determined by comparing the prediction difference of two models: one built with the relevant feature included and another built without it. Since the effect of excluding a feature i is dependent upon other features of the model, the marginal contribution of i is calculated for all possible subsets $S \subseteq F \backslash \{i\}$, where F is the set of all input features. The final SHAP values are calculated as weighted averages of all the marginal contributions, according to Equation 3-9.

$$\emptyset_i = \sum_{S \subseteq F \backslash \{i\}} \frac{|S|!\,(|F| - |S| - 1)!}{|F|!} \left[f_{S \cup \{i\}}(x_{s \cup \{i\}}) - f_s(x_s) \right] \quad (3\text{-}9)$$

where, $\emptyset_i$ is the SHAP value of i^{th} feature, S is all feature subsets, F is the set of all input features, $f_{S \cup \{i\}}$ is the model trained excluding the i^{th} feature, f_s is the model trained including the i^{th} feature,

x_s is the value of input features in the set S, and $x_{s\cup\{i\}}$ is the value of input features without the i^{th} feature.

Although some feature selection methods (i.e., MI and LASSO) and the ensemble models employed in this study can be used for establishing feature ranking, SHAP analysis was preferably used due to several reasons. First, it offers consistency compared to other methods, meaning that if two different models produce identical predictions for a given instance, the SHAP method assigns the same feature importance ranking for the two models (Zhao et al. 2023). Second, the SHAP method calculates the impact of each feature on the prediction for every instance in the dataset (Feng et al. 2021). This high-level granularity improves the accuracy of results as it allows for a more detailed understanding of the relationships between input features and output. The SHAP values computed for each individual prediction can be subjected to an absolute value transformation, followed by averaging across corresponding input features. The resulting mean absolute SHAP value attributed to each input feature serves as the basis to establish feature importance ranking (Feng et al. 2021).

3.3. Results and discussion

3.3.1. Feature selection results

Three feature selection methods: RFE, MI and LASSO were employed on the same training dataset to identify the optimal subset of input features to construct the ML models. Compared to other feature selection methods (i.e., MI and LASSO) that provide a fixed subset of selected features, the results of the RFE algorithm depend on the selected estimator (i.e., type of regression algorithm) (Liu et al. 2022). Consequently, the optimal subset selected by the RFE method can be different from model to model.

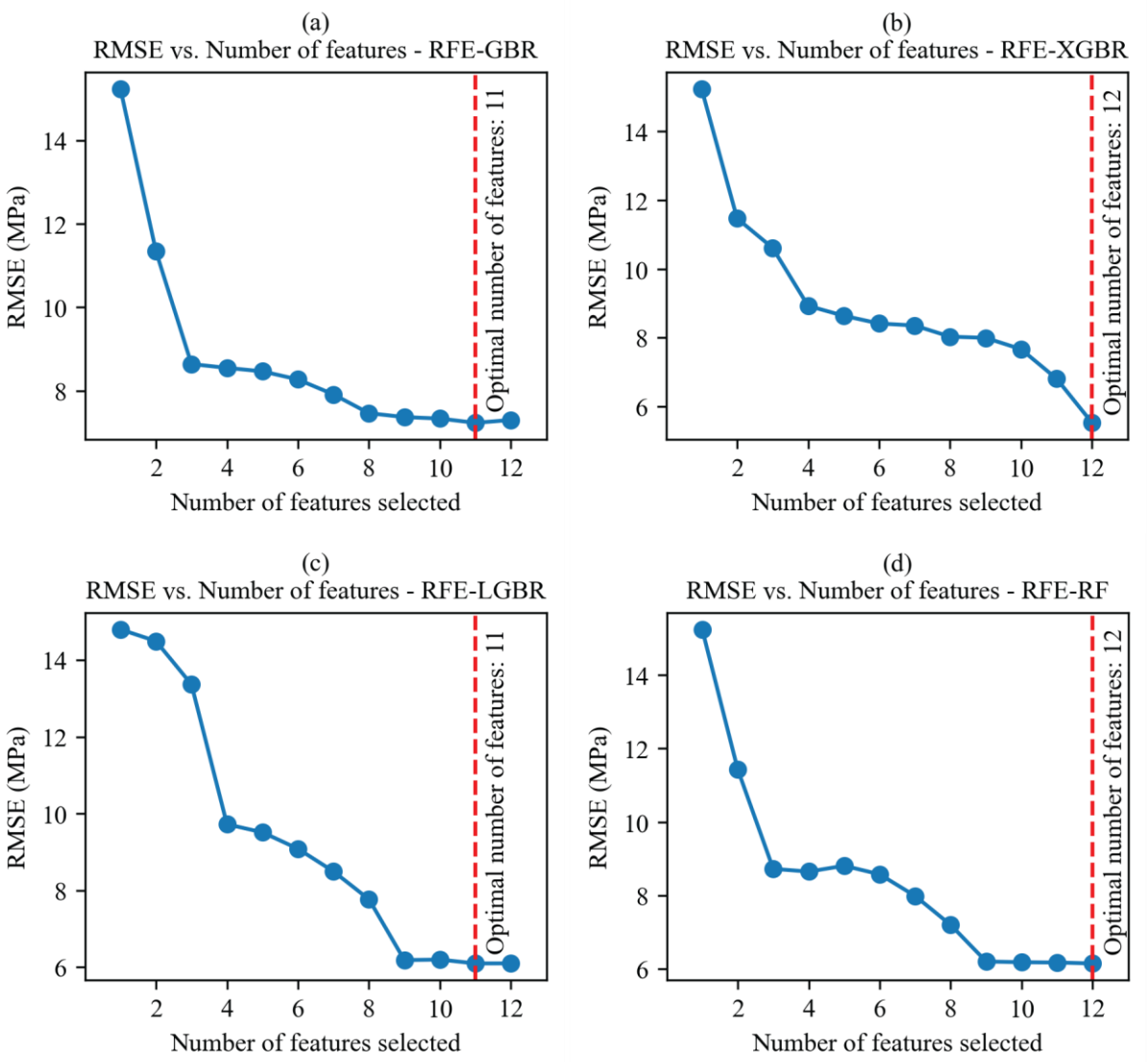

Figure 3.3 Selection of the optimum number of input features by RFE

Figure 3.3 illustrates the behavior of the average RMSE value based on a 10-fold CV (represented as blue dots), with the number of input features based on the RFE method. The optimal number of input features could be determined by locating the point in the plot where the RMSE was a minimum. This point was marked on the graph with a red dashed line. The ideal number of features selected by the RFE method was 11 when using GBR and LGBR as estimators. The only excluded feature was the type of superplasticizer. In contrast, when using XGBR and RF as estimators, the

RMSE value increased with the removal of input features. This observation suggests that the original set of input features remains optimal if XGBR and RF are used as estimators.

In the MI method, the input features: type of test, and retarder dosage were assigned with notably lower MI scores of 0.1 and 0.06, respectively, when compared with the other input features Figure 3.4. Therefore, the optimal subset derived from the MI method included only 10 input features. Liu et al. (2022) adopted the same strategy when using MI to identify the optimal number of features to estimate the energy consumption of buildings.

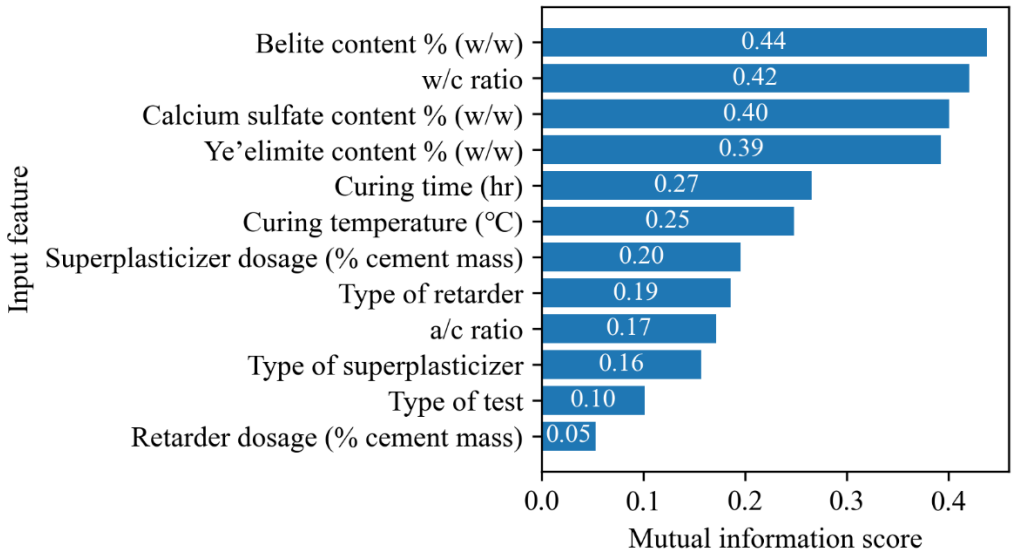

Figure 3.4 MI scores of input features

Unlike the MI method, the LASSO method assigns a value of zero to the absolute regression coefficient for insignificant features, making it a straightforward process to identify important features (Liu et al. 2022). Superplasticizer dosage was the only input feature discarded by the LASSO method, with an absolute regression coefficient of zero (Figure 3.5). Consequently, the optimal number of input features selected by the LASSO algorithm was 11.

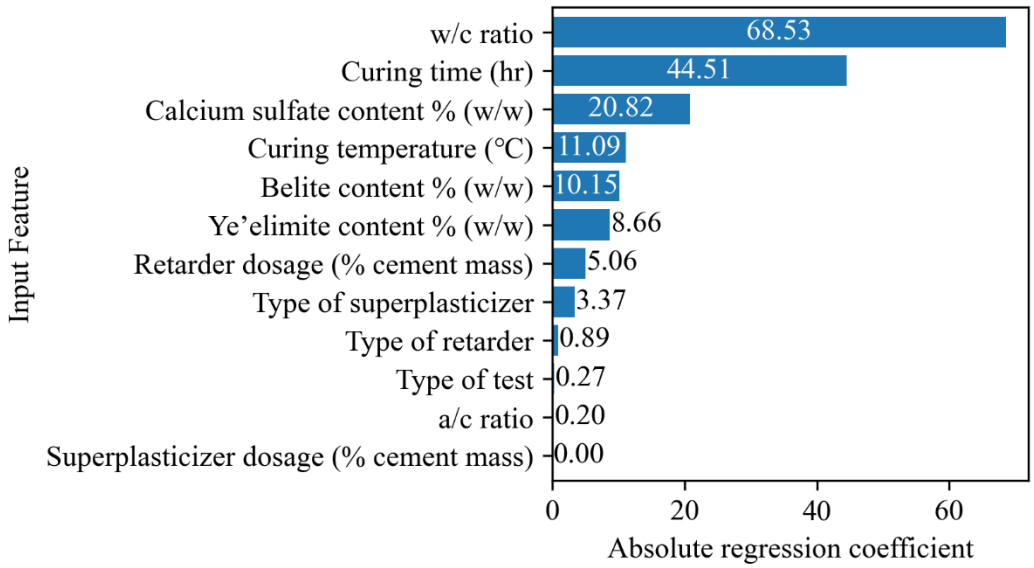

Figure 3.5 Absolute regression coefficients of the LASSO method

3.3.2. Selection of the best ML model based on feature selection

Four different ML models: GBR, XGBR, LGBR, and RF were constructed using the original training dataset as well as additional datasets modified based on the findings in Section 3.3.1. In addition, each model was optimized for prediction performance using the sequential-model-based optimization hyperparameter tuning method (Head et al. 2018). The prediction performance of each ML model on the testing data in terms of performance evaluation metrics and computational time are summarized in Table 3.3. The term Null is used to denote the absence usage of any feature selection method.

Table 3.3 Performance of ML models on test data based on different feature selection methods

Algorithm	Feature selection method	Number of selected features	R^2	RMSE (MPa)	MAE (MPa)	Computational Time (s)
GBR	Null	12	0.93	5.011	3.289	14.55
	MI	10	0.90	6.169	4.286	11.32
	RFE	11	0.93	4.963	3.376	13.98
	LASSO	11	**0.94**	**4.858**	**3.204**	**11.87**
XGBR	Null	12	0.95	4.538	2.954	22.87
	MI	10	0.90	6.292	4.309	18.39
	RFE	12	0.95	4.538	2.954	22.87
	LASSO	11	**0.95**	**4.365**	**3.087**	**18.18**
LGBR	Null	12	0.94	4.908	3.616	16.19
	MI	10	0.90	6.258	4.382	11.70
	RFE	11	0.93	5.100	3.462	12.91
	LASSO	11	**0.94**	**4.878**	**3.437**	**12.80**
RF	Null	12	0.89	6.578	4.832	18.40
	MI	10	0.88	6.681	4.745	16.67
	RFE	12	0.89	6.578	4.832	18.40
	LASSO	11	**0.92**	**5.581**	**3.886**	**18.10**

According to Table 3.3, the LASSO-GBR model obtained the highest R^2 of 0.94, and the smallest error values of 4.858 MPa and 3.204 MPa for RMSE and MAE, respectively, by outperforming the Null-GBR (0.93, 5.011 MPa, 3.289 MPa), the MI-GBR (0.90, 6.169 MPa, 4.286 MPa) and RFE-GBR (0.93, 4.963 MPa, 3.376 MPa) models. Furthermore, the computational time of the LASSO-GBR model was 2.68 s and 2.11 s lower than the Null-GBR model and RFE-GBR model, respectively, although it was 0.55 higher than the MI-GBR model. Similar observations can be made for LASSO-XGBR, LASSO-LGBR, and LASSO-RF models, as they exhibited superior prediction performances compared to the other models that utilize the same respective algorithm on different datasets. In summary, the results indicate that the optimal dataset suggested by the LASSO method contributes to the best performance in all ML algorithms selected in this study. The superior performance of the LASSO method can be ascribed to its regularization capability which selectively removes only the least important input features by assigning them zero coefficients (Otchere et al. 2022). Similar results can be found in the study conducted by Otchere et al. (Otchere et al. 2022) to predict the water saturation level of petroleum reservoirs. In their study, the ensemble model built on the dataset selected by the LASSO method achieved the lowest errors of 0.0034 and 0.012 for MAE and RMSE, respectively, by outperforming the other models built based on the results of filter and wrapper feature selection methods.

It is important to note that the sequential-model-based optimization method was employed to tune all the aforementioned ML models. As a representative set, the best-performing LASSO-ML models were selected and their optimal hyperparameters are summarized in Table 3.4.

Table 3.4 Optimal hyperparameters of the LASSO-ML models

ML Model	Hyperparameter	Optimal value
LASSO-GBR	Max depth	5
	Learning rate	0.214801
	Min samples split	8
	Min samples leaf	4
	N estimators	120
LASSO-XGBR	Gamma	0.354712
	Max depth	19
	Min child weight	4
	Max delta step	8
	Subsample	0.324964
	Reg lambda	0.419469
	Reg alpha	0.23643
	Eta	0.184414
	N estimators	190
LASSO-LGBR	Max depth	14
	Min child weight	10
	Subsample	0.184890
	Reg lambda	1
	Reg alpha	1

ML Model	Hyperparameter	Optimal value
LASSO-LGBR	Learning rate	0.174714
	N estimators	218
LASSO-RF	Max depth	10
	Min samples split	2
	Min samples leaf	1
	N estimators	299

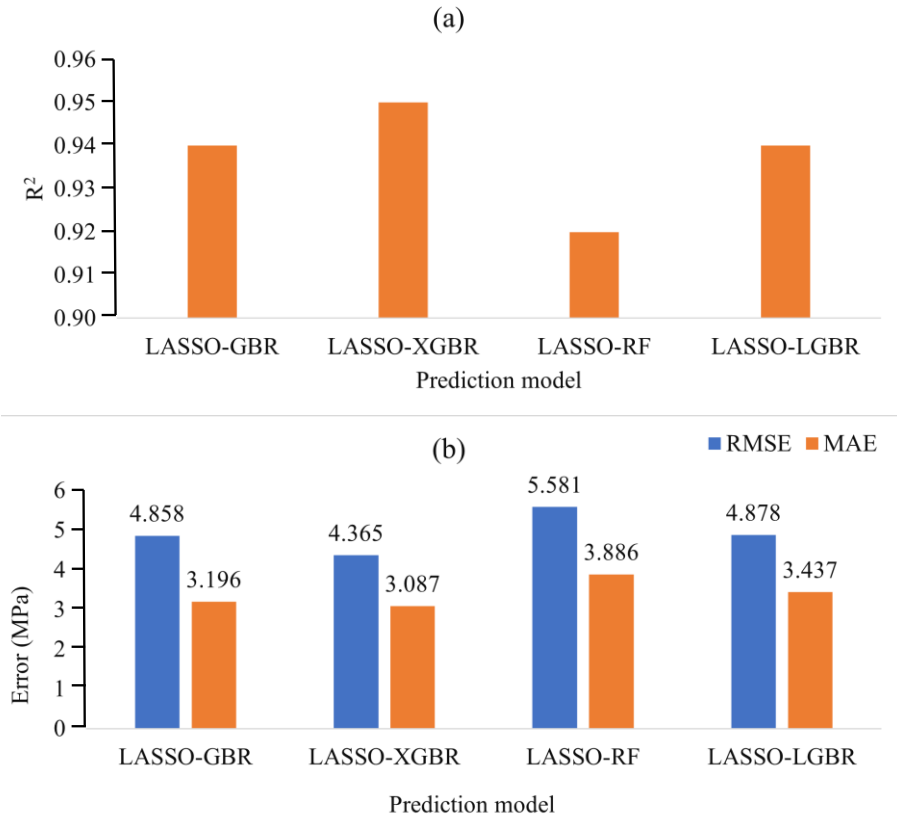

Figure 3.6 Prediction performance of LASSO-ML models in terms of (a) R^2 (b) error metrics

Another noteworthy finding from the results is the superior performance of the LASSO-XGBR model compared to the other LASSO-based models. Figure 3.6 illustrates the performance of each LASSO-ML model on test data in terms of the (a) R^2 and (b) RMSE and MAE. Figure 3.6 (a) shows that the R^2 of the LASSO-XGBR model was 0.01, 0.03, and 0.01 higher than the LASSO-GBR, LASSO-RF, and LASSO-LGBR models, respectively. The superior performance of the LASSO-XGBR was more evident in Figure 3.6 (b) as LASSO-XGBR obtained much lower RMSE and MAE errors of 4.365 MPa and 3.087 MPa, respectively, when compared to LASSO-GBR (4.858 MPa and 3.196 MPa), LASSO-RF (5.581 MPa and 3.886 MPa), and LASSO-LGBR (4.878 MPa and 3.437 MPa). The superiority of the LASSO-XGBR model can be attributed to its capability to overcome overfitting issues that will increase the performance of the model by penalizing complex models through regularization techniques (Zhang et al. 2022b). Several studies reported XGBR as the most effective model for the prediction of UCS in various cementitious materials. For example, an XGBR model reportedly achieved an R^2 value of 0.96 on test data, while outperforming LGBR and RF models that only achieved R^2 values of 0.93 and 0.91, respectively, when predicting the UCS of fly ash slag-based alkali-activated material (Shah et al. 2022). In addition, the superiority of the XGBR model (i.e., R^2 of 0.85 and RMSE of 7.478 MPa) over the GBR model (i.e., R^2 of 0.83 and RMSE of 7.828 MPa) has also been reported when forecasting the UCS of concrete made with recycled concrete aggregates (Tran et al. 2022). The LASSO-XGBR model was selected as the best ML model in this study due to its superior performance. Its prediction results served as the basis for discussions in Sections 3.3.3 and 3.3.4.

3.3.3. Importance of input features

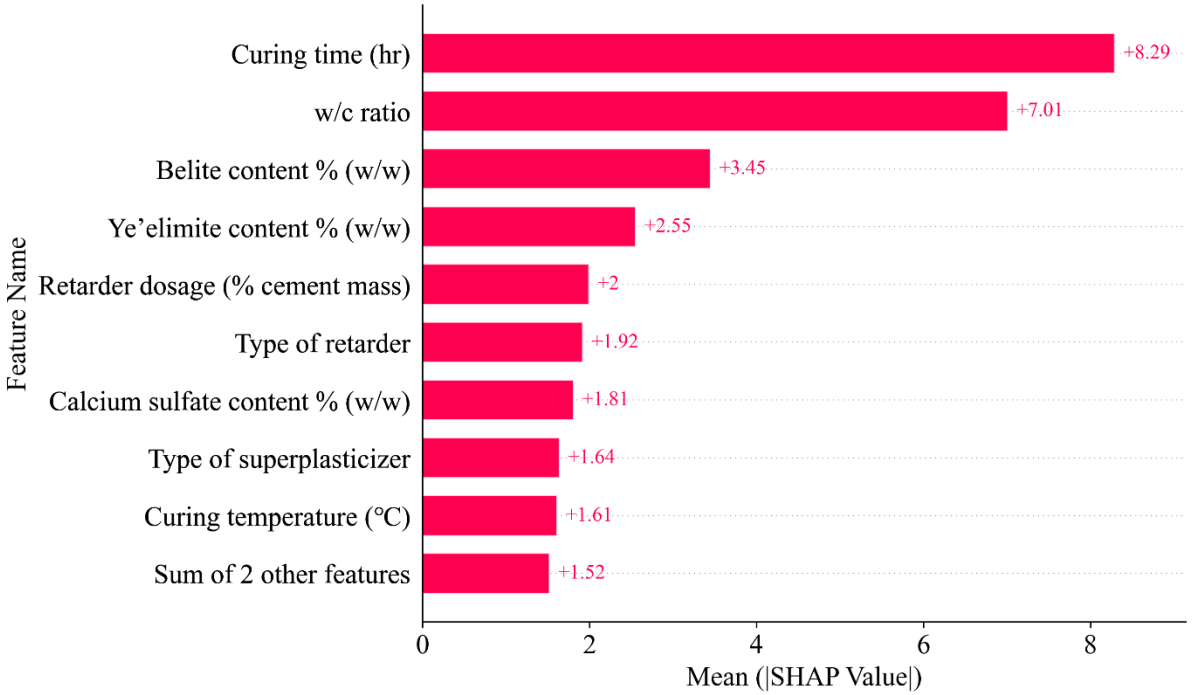

Figure 3.7 SHAP feature importance

Figure 3.7 shows the SHAP feature importance of different input parameters based on the prediction results from the LASSO-XGBR model. A higher mean absolute SHAP score indicates a greater influence of an input feature on the UCS. According to Figure 3.7, curing time was the most important input feature for the model with a score of 8.29. This can be explained by the significant influence of curing time on the number of hydration products formed, which directly impacts the strength of the cement (Tao et al. 2023). This result is in agreement with many other feature ranking results of ensemble models built to predict the UCS of similar cementitious materials: fly ash-based geopolymer (Dong et al. 2023), cement-based grouting material (Zhao et al. 2023) and calcium-based geopolymer (Huo et al. 2022).

The w/c ratio emerged as the second most significant factor, with a score of 7.01. This finding can be explained by the strong correlation between water content and total porosity of CSA cements, that affect the UCS (Ke et al. 2021). Generally, the porosity of cement paste increases significantly with the increase of w/c ratio, ultimately causing a notable decrease in the UCS of cement-based materials (Burris and Kurtis 2022). Interestingly, Ke et al. (2021) also reported a more pronounced impact of the w/c ratio on the porosity of CSA cement compared to that on OPC cement, when both were evaluated under the same w/c ratio. In their study, when the same w/c ratio was used, the total porosity of the CSA cement paste was 1.13 times higher than that of the OPC. Furthermore, when compared to the studies on alkali-activated material (Shah et al. 2022) and geopolymers (Huo et al. 2022), the feature importance of the w/c ratio was lower than that observed in this study. Therefore, the addition of water to CSA cement mixtures should be exercised with great caution, particularly when compared to other analogous materials.

The belite and ye'elimite contents were ranked as the third and fourth most influential input features with scores of 3.45 and 2.55, respectively. The high SHAP values of these two features were observed because ye'elimite and belite are the main two composites in CSA cement, which account for about 70 to 80% of the mass of CSA cement (Tao et al. 2023). Ye'elimite and belite are also the most important composites in CSA cement, as they hydrate with water at early ages and later ages, dominating strength development at early ages and later ages, respectively (Huang et al. 2022a). In contrast, calcium sulfate content had a lesser effect on the model with a lower ranking score of 1.81. This can be ascribed to the capability of ye'elimite to react with free water to produce monosulfoaluminate in the absence of calcium sulfate, contributing to the strength development of CSA cement mixtures (Huang et al. 2020).

Retarder dosage and type of retarder were ranked closely with scores of 2 and 1.92, respectively. These findings suggest that both the dosage of retarder and the specific retarding mechanism it employs across different retarder types equally impact the strength development of CSA cement. Some of these mechanisms are, suppressing the precipitation of ettringite, binding calcium ions which reduce the rate of hydration reaction, and formation of ulexite in the presence of borax to cover ye'elimite surface which hinders the growth of ettringite (Tao et al. 2023). In contrast, the impact of the type of superplasticizer was much lower, as it obtained a score of 1.64. Consistently, the experimental results revealed that the effect of retarders is much more pronounced when compared to superplasticizers. Retarders were seen to affect both early and later age strengths significantly whereas only the early age strength was slightly affected by superplasticizers (Zhang et al. 2016). This agreement between experimental and data-driven approach further attest to the reliability of the presented model.

The curing temperature was ranked seventh, with a relatively lower score of 1.61 when compared with the other features. This can be attributed to the ability of CSA cement to develop strengths rapidly, irrespective of the curing temperature (Huang et al. 2021). The type of test and a/c ratio were ranked as the features with the lowest influence on the model. This observation can be attributed to two plausible explanations. First, the type of test feature was only used to represent the universal standard without including the factors which add experimental variability (i.e., loading rate, specimen shape, size, specimen preparation methods) as separate input features in the model. Second, the range of a/c ratio values used in this study was limited, which reduced the variability in results.

3.3.4. Relationships between input features and UCS

The SHAP summary plot (Figure 3.8) allows for a detailed qualitative analysis of how each input feature affects the output of the LASSO-XGBR model. The y-axis and x-axis represent the input features and their corresponding SHAP values (i.e., difference between the average value of all predictions and the prediction for a specific feature in a selected sample), respectively. Each point in the Figure 3.8 represents a sample in the collected database and the color of the point depicts the value of the selected input feature in that sample. In the color bar, the red color symbolizes larger values while the smaller values are represented in blue color. In addition, the position of a particular point in the x-axis is linked to the outcome of the target variable (i.e., UCS of the CSA cement). The vertical line at a value of zero SHAP value corresponds to the average value of the UCS predictions by the model. Consequently, a negative SHAP value suggests that the feature value contributes to a prediction that is lower than the average, while a positive SHAP value expresses the opposite.

In addition to the SHAP summary plot, the individual feature dependence plots depicted in Figure 3.9 were used to analyze the relationships quantitatively. The horizontal red dashed line represents the average UCS prediction whereas red circles indicate specific locations where a noticeable change in trend is observed (for numerical input features). It is important to note that the features: type of test and a/c ratio were excluded from this extended analysis as their collective influence (i.e., a score of 1.52) was even lower than the individual influence of the lowest ranked feature (i.e., a score of 1.61), as shown in Figure 3.7. The detailed discussion in Sections 3.3.4.1, 3.3.4.3, and 3.3.4.2 are based on Figure 3.8 and Figure 3.9.

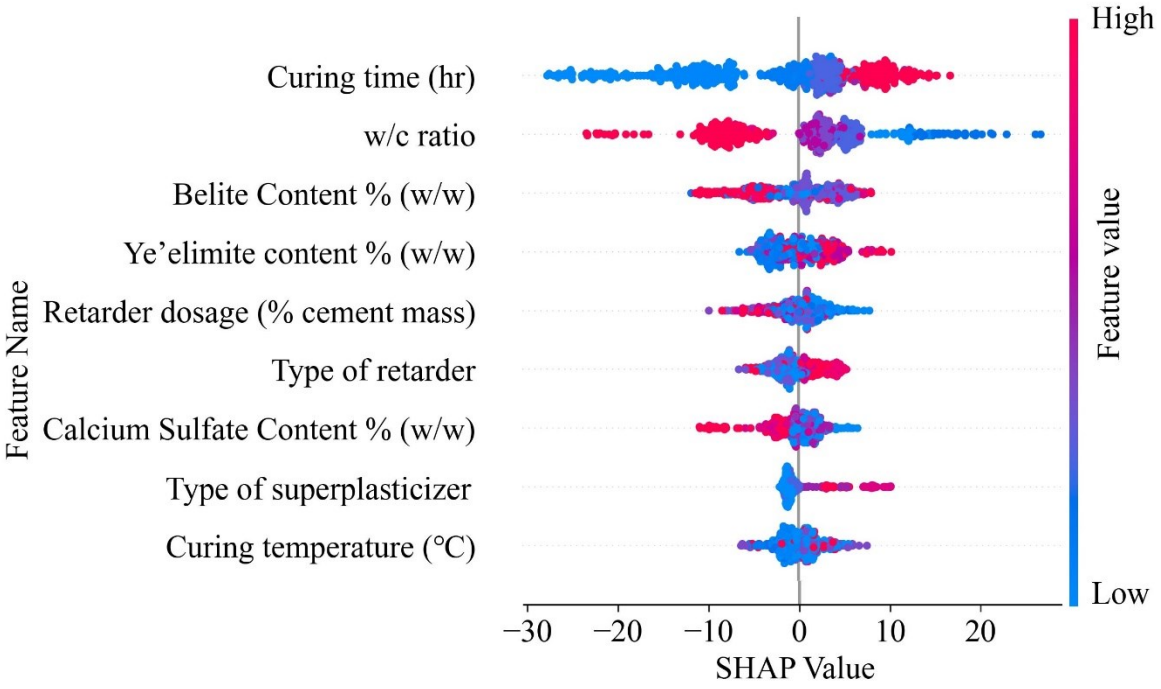

Figure 3.8 SHAP summary plot

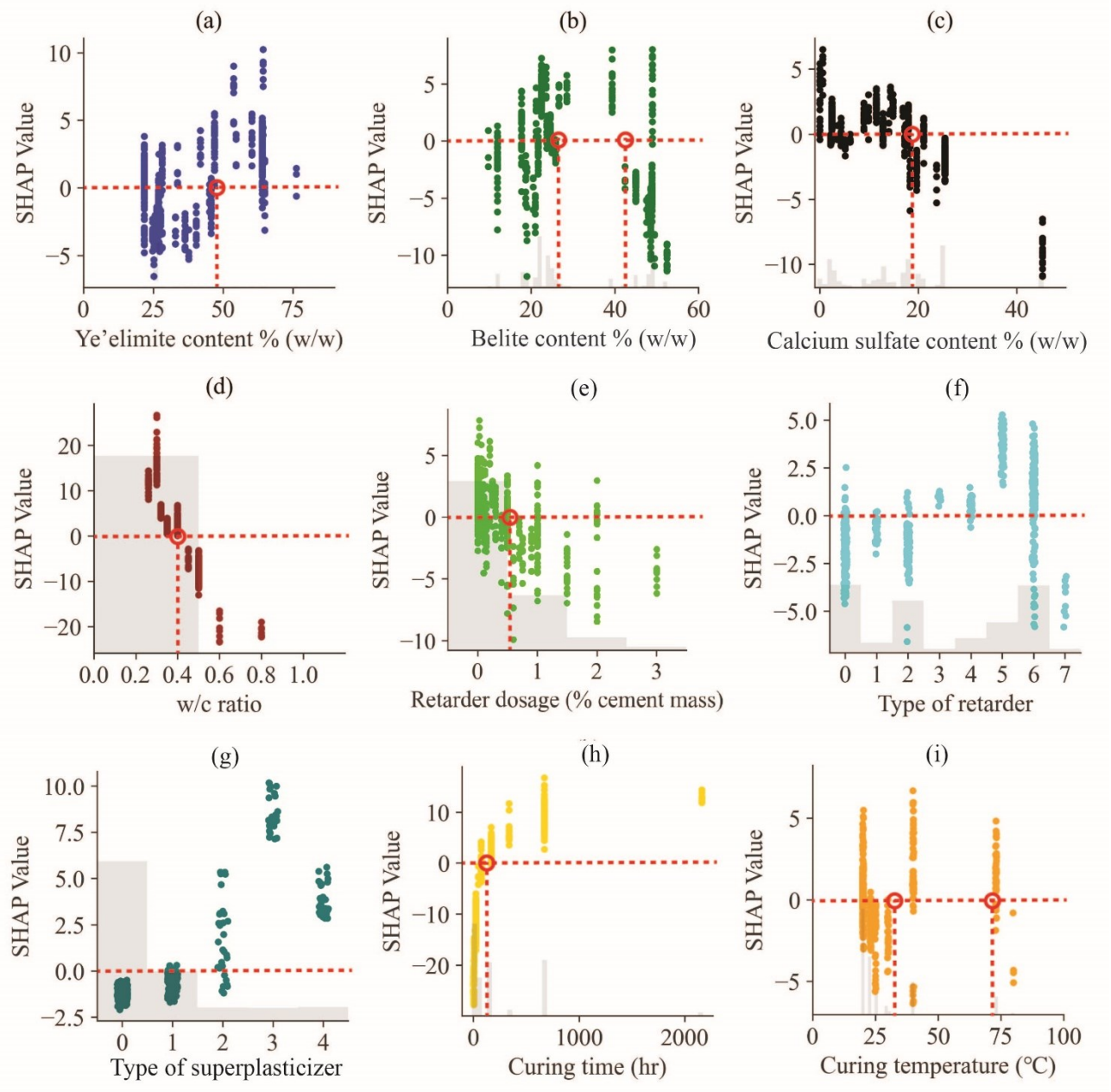

Figure 3.9 SHAP individual feature dependence plots (a) ye'elimite content (b) belite content (c) calcium sulfate content (d) w/c ratio (e) retarder dosage (f) type of retarder (1-7 represent molasses, sodium gluconate, a mixture of citric acid and borax, tartaric acid, borax, citric acid, and vitamin-C, respectively) (g) type of superplasticizer (1-4 represent polycarboxylate acid, β-

naphthalenelfonic acid, aminosulfonic acid, and powder naphthalene, respectively) (h) curing time (i) curing temperature

3.3.4.1. The effect of mineral composition

The findings depicted in Figure 3.9 shows that the presence of excessively high or low belite contents in CSA cement adversely affects the resulting strengths. Conversely, higher ye'elimite contents contribute to strengths higher than the average, while lower ye'elimite content leads to lower strengths. Above observations can be attributed to the less reactivity of belite when compared with ye'elimite (Huang et al. 2020). Notably, the hydration reactions can be slowed down under exceedingly high belite and insufficient ye'elimite contents, particularly at early ages, thus impeding the strength development. However, it is important to note that a sufficient amount of belite is still necessary to ensure continued strength development of CSA cement at later stages (Tao et al. 2023). In addition, the results show that CSA cement with excessive amounts of calcium sulfate produces mixtures with strengths lower than the average. This phenomenon can be explained by the deficiency of ye'elimite in CSA cement with excessive calcium sulfate. Figure 3.9 (a), (b), and (c) follows the same trends observed in Figure 3.8. It shows that CSA cement with mineral composition: ye'elimite content exceeding 50%, belite content ranging from 26% to 42%, and calcium sulfate content below 18% achieve UCS values higher than the average. However, the practical application of such CSA cement with very high ye'elimite content would be limited due to the high price of raw materials, particularly bauxite (Pimraksa and Chindaprasirt 2018).

3.3.4.2. The effect of curing conditions

According to the SHAP summary plot results, the UCS of CSA cement can be improved by increasing the curing time, as higher curing times corresponded to higher SHAP values. Although it can be seen that a majority of samples subjected to shorter curing times have UCS values that

are lower than the average, another significant portion of such samples could be found to have strengths that exceed the average. This can be attributed to the ability of CSA cement mixtures to attain a very high percentage of the ultimate strength at very early stages such as 24 h. For example, Burris and Kurtis (2022) reported that over 75% of the ultimate strength could be achieved within 24 h in the tested CSA cement. Results depicted in Figure 3.9 (h) are consistent as the observed positive SHAP values plateaued after 176 hr (i.e., 7 days) of curing time. In addition, higher than the average UCS values are exhibited in samples cured for longer periods. This can be attributed to the ability of CSA cement to develop strength over time as the available belite usually reacts at later stages to produce more hydration products (Huang et al. 2022a).

The relationship between curing temperature and the UCS of the CSA cement is plotted in Figure 3.9 (i). It shows that the SHAP values of different temperatures are in a small range of -6 to 7. This means the temperatures does not make a great influence on the UCS of CSA cement-based mixtures. The potential reason for this observation might be that CSA cement can react fast with water at different temperatures (Huang et al. 2019; Wang et al. 2017).

3.3.4.3. The effect of material proportioning features and admixtures

The w/c ratio showed a negative correlation with the UCS, as samples with higher w/c ratios contributed to lower SHAP values that reduce the UCS of the samples. This can be ascribed to the increased formation of pores in CSA mixtures with excessive water contents, upon drying (Ke et al. 2021). According to Figure 3.9 (d), w/c ratios greater than 0.4 lead to a CSA cement mixture with a strength lower than the average.

In addition, Figure 3.8 depicts that higher retarder dosages correspond to UCS values lower than the average. In contrast, CSA mixtures achieved strengths higher than the average in the absence

of any retarder addition (i.e., a dosage of 0%). These observations can be mainly ascribed to the retarding effect on the hydration reaction and strength development at early ages and the changes in morphology and microstructure of hydration products in cement pastes when higher dosages of retarders are used (Huang et al. 2022a). Figure 3.9 (e) shows that the usage of retarder dosages of over 0.6% produces CSA cement mixtures with strengths lower than the average.

Figure 3.9 (f) provides some insightful observations regarding the influence of different retarders on the USC of CSA cement-based samples. Figure 3.9 (f) shows that the SHAP values of molasses (#1), sodium gluconate (#2), and Vitamin C (#7) are mostly lower than 0, meaning that these retarders have a higher chance to degrade the mechanical strength of CSA cement-based mixtures. When selecting a retarder for CSA cement, it would be wise not to select these retarders. Comparatively, the SHAP values of a mixture of citric acid and borax (#3), tartaric acid (#4), and borax (#5) are mostly higher than 0. This observation indicates that the retarders (#3 to #5) have the least detrimental effect on strength and selecting them instead has a higher chance of improving the mechanical performance of CSA cement-based mixtures. However, it is important to note that the evaluation of retarders should not be solely based on their influence on UCS. For example, Huang et al. (2022b) reported that borax only extended the setting time of a CSA cement from five minutes to 11.5 minutes at a dosage of 2% of cement mass, which means borax may not an effective retarder for some CSA cement. Therefore, when selecting a retarder, the influence of retarders on setting times should also be taken into consideration, as setting time extension is the primary purpose of the addition of a retarder.

Figure 3.9 (g) presents the SHAP values of different superplasticizers. It shows that the SHAP values of different superplasticizers are in a range from -2.5 to 10, which means addition of superplasticizers does not pose an obvious negative effect on the UCS of CSA cement-based

mixtures. This is because the w/c ratio is reduced when superplasticizers are added as an admixture, promising a lower porosity and a higher UCS (Ke and Zhang 2020; Zhang et al. 2016). Figure 3.9 (g) also show that the SHAP values of β-naphthalenelfonic acid (#2), aminosulfonic acid (#3), and powder naphthalene (#4) are higher than polycarboxylate acid (#1). This can be explained by the slight retarding effect of superplasticizers, which is more prominent in (#1), than in (#2 to #4) (Zhang et al. 2016). Although the influence on UCS is an important factor when selecting a superplasticizer, the ability of a superplasticizer to improve the workability of CSA cement is the dominant factor deciding its suitability for a particular application (Tambara Júnior et al. 2023).

3.4. Conclusions

This study is the first to employ ensemble machine learning (ML) methods to forecast the unconfined compressive strength (UCS) of calcium sulfoaluminate (CSA) cement mixtures. Additionally, the SHapely Additive exPlanations (SHAP) analysis allowed for interpreting the relationships between input features and UCS. The following conclusions are drawn from this study.

1) LASSO was the best feature selection method that could consistently improve the performance of all ML algorithms for predicting the UCS of CSA cement-based mixtures. From the LASSO-based models, the LASSO-XGBR model was selected as the best model as it outperformed the others with the highest R^2 of 0.95 and lowest errors (e.g., an MAE of 3.087 MPa).

2) The overall feature importance ranking based on mean absolute SHAP value can be presented as: curing time (8.29) > w/c ratio (7.01) > belite content (3.45) > ye'elimite content (2.55) >

retarder dosage (2) > type of retarder (1.92) > calcium sulfate content (1.81) > type of superplasticizer (1.64) > curing temperature (1.61). The overall feature importance ranking will assist engineers to make educated decisions about the prioritization of input features to achieve a desired strength of a CSA cement mixture.

3) Higher ye'elimite content contributed to UCS values higher than the average, whereas the presence of higher calcium sulfate content reduced the strengths below the average in CSA cement mixtures. Regardless of whether the curing temperature was increased or decreased, it had a minimal impact on the UCS. Mixture of citric acid and borax, tartaric acid, and borax were identified as the retarders that exhibited the least detrimental effects on the UCS. Compared with retarders, superplasticizers barely had a negative effect on the UCS. This information will assist engineers to make well-informed decisions about the appropriate levels and types of input features necessary to attain a desired strength of a CSA cement mixture.

4) In summary, this study developed an accurate ML model for predicting the UCS of CSA cement mixtures. This work may serve as the basis for the efficient design and development of CSA cement mixtures, as it paves the way for rapid UCS predictions and meaningful interpretations.

Chapter 4. Conclusions and key contributions

4.1. Conclusions

This work is the first to develop machine learning (ML) techniques for predicting the unconfined compressive strength (UCS) of alkali-activated cemented paste backfill (AAS-based CPB) and calcium sulfoaluminate cement (CSA)-based mixtures. The following conclusions are drawn from this study.

(1) Non-linear ensemble boosting ML models outperformed the other single learning ML models. The least absolute shrinkage and selection operator-based extreme gradient boosting (LASSO-XGBR) model achieved the best accuracy of 95% for predicting the UCS of CSA cement mixtures, with the least errors of 4.365 MPa and 3.087 MPa for root mean squared error (RMSE) and mean absolute error (MAE), respectively. In addition, the gradient boosting regression (GBR) was the best model for predicting the UCS of AAS-based CPB, with the highest recorded accuracy of 96.7% and the lowest errors of 0.237 MPa and 0.162 MPa for RMSE and MAE, respectively.

(2) The LASSO feature selection method consistently improved the accuracies and reduced the computational times of all the ML models employed to predict the UCS of CSA cement mixtures. The LASSO-XGBR model was 4.69 s faster than the base XGBR model. In addition, the error values were 0.173 MPa and 0.133 MPa lower than the base XGBR model in the LASSO-XGBR model for RMSE and MAE, respectively.

(3) The curing time, water-to-cement (w/c) ratio, belite content, ye'elimite content, retarder dosage and type of retarder were the most influential input features for the UCS prediction model in CSA cement mixtures. Likewise, curing time, w/c ratio, liquid-to-solid ratio, silicate modulus

of the activator and Na_2O content of the binder could be identified as the features with the highest influence on the UCS of AAS-based CPB mixtures.

(4) According to the Shapely-Additive exPlanations (SHAP), the ye'elimite content is positively correlated with the UCS of CSA cement, whereas the calcium sulfate content is negatively correlated. In addition, the SHAP results revealed that the samples cured for longer curing times contributed to higher UCS values. Conversely, increased w/c ratios and retarder dosages showed a negative impact on the UCS.

4.2. Key contributions

The findings of this work will be beneficial for the efficient development of sustainable cementitious materials for application in the mining industry. The key contributions of this study are listed as follows:

(1) For the first time, meaningful and diversified datasets representing experimental studies performed worldwide, in relation to the AAS-based CPB and CSA cement-based mixtures were assembled from the literature. These datasets will enhance the knowledge of the engineering community by facilitating the options of results validation, comparison and identification of patterns.

(2) This study is the first to apply ML methods for AAS-based CPB and CSA cement-based mixtures, which allowed rapid and accurate predictions of the UCS. The models comprise multiple input features that enable the opportunity to explore different scenarios by manipulating input features, without the need for conducting resource-intensive physical experiments.

(3) Previously unexplored territory of feature importance ranking for both AAS-based CPB and CSA cement-based mixtures, was investigated in this work. This new information will assist

engineers in making well-informed decisions regarding the manipulation of input features by enabling them to prioritize specific features to achieve the desired strength of the mixtures.

(4) Overall, this work may promote the production and application of sustainable AAS-based CPB and CSA cement-based mixtures by guiding their mixture designs with accurate and rapid UCS predictions and an improved understanding of the complex relationships. The findings of this study will ultimately contribute to the sustainability goal of net zero emissions in the mining industry through increased usage of these mixtures for mining applications due to their ML-based efficient development.

Chapter 5. Limitations and future work

The 307 groups of data collected in the first investigation (Chapter 2) from the literature review were limited to nine different experimental schemes. To further generalize the prediction model, more data will be collected from the continuously updated literature in future work. In addition, out of the nine studies used for data extraction, only two studies (Jiang et al. 2019; Jiang et al. 2022a) could be found to have considered the curing temperature as a design parameter. Consequently, curing temperature was not selected as an input parameter in the prediction model due to the limited data availability. However, according to the studies of Jiang et al. (2019) and Jiang et al. (2022a), curing temperature has a pronounced effect on the UCS, coupled with the alkali-activator concentration and type of the activator. In addition, the influence of the same coupled effect on the rheological properties of AAS-based CPB has also been investigated and proved (Jiang et al. 2022b). Therefore, more data must be collected from future studies which would consider curing temperature in experimental designs. Then, curing temperature could be added as an input parameter in the future to improve the prediction model. Pore fluid chemistry properties (i.e., concentration of different ions and pH level) have also been identified as crucial parameters which define the strength development of AAS-based CPB (Jiang et al. 2022a; Jiang et al. 2022b). However, due to the limited data availability, pore fluid chemistry parameters were not considered input parameters in this study. The models could be further improved in the future with the addition of these parameters and relevant data. Likewise, in the second investigation (Chapter 3), the dataset was only limited to 723 data points. However, for generalization purposes of the models, more data will be collected from regularly updated literature in the future. Specifically, to observe more distinct relationships between curing temperature, a/c ratio, and UCS

of CSA cement-based mixtures, it would be necessary to collect a larger number of data points with a broader range of values for these features.

It is also important to note that the UCS values utilized in this study represent average values obtained after conducting multiple tests, typically a minimum of three iterations, to ensure accuracy and reliability. While this approach is common practice in experimental research, it introduces a layer of variability into the dataset. As part of future improvements, the error associated with the averaged UCS values can be incorporated to the datasets as an additional input feature. This approach can potentially lead to more robust models capable of accounting for variability and providing more accurate predictions.

Moreover, this study was limited to applying the sequential-model-based optimization method and random search method to tune the hyperparameters of ML models. However, various other hyperparameter tuning methods, namely, genetic algorithm (GA) (Qi et al. 2018a), particle swarm optimization (PSO) (Qi et al. 2018b), whale optimization algorithm (WOA) (Xi et al. 2023) have been used to improve the performance of ML models. Therefore, a comparative study between these methods would be beneficial to identify the best-suited optimization method.

In addition, although UCS is an essential characteristic measure of any CSA cement, other properties such as setting time, workability, and density should also be considered for a practical application (Tao et al. 2023). Similarly, for AAS-based CPB, the nonlinear relationships between other critical characteristic parameters and their influencing variables are still not clear, such as workability (Ercikdi et al. 2013), yield stress (Kou et al. 2020) and Young's modulus (Kou et al. 2020). Therefore, more efforts will be needed to investigate the relationships between these properties and input features using data-driven methods in the future.

Mixture design optimization (Sadrossadat et al. 2020) work can also be carried out on the prediction models using different optimization methods (i.e., PSO, GA and BO) to obtain optimum values of input parameters which will maximize the UCS of these cementitious mixtures. As the mining industry embraces sustainable cementitious materials like AAS-based CPB and CSA cement, it is essential to conduct a cost-benefit analysis to assess economic feasibility of their application. Challenges related to sourcing materials, as well as logistical concerns (i.e., transportation and storage) must be addressed. More complex ML models could be introduced for these optimization problems by considering the performance of cements, overall cost (i.e., direct, indirect and fixed costs), availability of material and the percentage of CO_2 reduction. Finally, the cost-benefit analysis will help mining companies make informed decisions, optimize operations, and align with the industry's sustainability goals, contributing to both environmental and economic benefits.

References

Adel, H., Palizban, S.M.M., Sharifi, S.S., Ilchi Ghazaan, M. & Habibnejad Korayem, A. 2022. Predicting mechanical properties of carbon nanotube-reinforced cementitious nanocomposites using interpretable ensemble learning models. Construction and Building Materials, **354**, 129209, doi: https://doi.org/10.1016/j.conbuildmat.2022.129209.

Arachchilage, C.B., Fan, C., Zhao, J., Huang, G. & Liu, W.V. 2023. A machine learning model to predict unconfined compressive strength of alkali-activated slag-based cemented paste backfill. Journal of Rock Mechanics and Geotechnical Engineering.

Arcila, S. & Beland, F. 2023. Cement Reduction in Cemented Paste Backfill by using Admixtures. *CIM MTL23*, Palais des Congrès de Montréal.

ASTM, A. C39/C39M-18 2018. Standard Test Method for Compressive Strength of Concrete.
Bahl, A., Hellack, B., Balas, M., Dinischiotu, A., Wiemann, M., Brinkmann, J., Luch, A., Renard, B.Y. & Haase, A. 2019. Recursive feature elimination in random forest classification supports nanomaterial grouping. NanoImpact, **15**, 100179, doi: https://doi.org/10.1016/j.impact.2019.100179.

Baturynska, I. & Martinsen, K. 2021. Prediction of geometry deviations in additive manufactured parts: comparison of linear regression with machine learning algorithms. Journal of Intelligent Manufacturing, **32**, 179-200, doi: 10.1007/s10845-020-01567-0.

Benzaazoua, M., Belem, T. & Bussière, B. 2002. Chemical factors that influence the performance of mine sulphidic paste backfill. Cement and Concrete Research, **32**, 1133-1144, doi: https://doi.org/10.1016/S0008-8846(02)00752-4.

Benzaazoua, M., Fall, M. & Belem, T. 2004. A contribution to understanding the hardening process of cemented pastefill. Minerals Engineering, **17**, 141-152, doi: https://doi.org/10.1016/j.mineng.2003.10.022.

Bloss, M.L. 2014. An operational perspective of mine backfill. *In*: Potvin, Y. & Grice, T. (eds.) *Mine Fill 2014: Eleventh International Symposium on Mining with Backfill*. Australian Centre for Geomechanics, Perth, 15-30.

Bonetto, R. & Latzko, V. 2020. Chapter 8 - Machine learning. *In*: Fitzek, F.H.P., Granelli, F. & Seeling, P. (eds.) *Computing in Communication Networks*. Academic Press, 135-167.

Boser, B.E., Guyon, I.M. & Vapnik, V.N. 1992. A training algorithm for optimal margin classifiers. *Proceedings of the fifth annual workshop on Computational learning theory*. Association for Computing Machinery, Pittsburgh, Pennsylvania, USA, 144–152.

Bouckaert, S., Pales, A.F., McGlade, C., Remme, U., Wanner, B., Varro, L., D'Ambrosio, D. & Spencer, T. 2021. *Net zero by 2050: A roadmap for the global energy sector.* International Energy Agency.

Breiman, L. 2001. Random Forests. Machine Learning, **45**, 5-32, doi: https://doi.org/10.1023/A:1010933404324.

Brescia-Norambuena, L., González, M., Avudaiappan, S., Saavedra Flores, E.I. & Grasley, Z. 2021. Improving concrete underground mining pavements performance through the synergic effect of silica fume, nanosilica, and polypropylene fibers. Construction and Building Materials, **285**, 122895, doi: https://doi.org/10.1016/j.conbuildmat.2021.122895.

Burris, L.E. & Kurtis, K.E. 2018. Influence of set retarding admixtures on calcium sulfoaluminate cement hydration and property development. Cement and Concrete Research, **104**, 105-113, doi: https://doi.org/10.1016/j.cemconres.2017.11.005.

Burris, L.E. & Kurtis, K.E. 2022. Water-to-cement ratio of calcium sulfoaluminate belite cements: Hydration, setting time, and strength development. Cement, **8**, 100032, doi: https://doi.org/10.1016/j.cement.2022.100032.

Cao, S., Xue, G., Yilmaz, E., Yin, Z. & Yang, F. 2021. Utilizing concrete pillars as an environmental mining practice in underground mines. Journal of Cleaner Production, **278**, 123433, doi: https://doi.org/10.1016/j.jclepro.2020.123433.

Chen, I.A. & Juenger, M.C.G. 2011. Synthesis and hydration of calcium sulfoaluminate-belite cements with varied phase compositions. Journal of Materials Science, **46**, 2568-2577, doi: https://doi.org/10.1007/s10853-010-5109-9.

Chen, L., Sun, Z., Liu, G., Ma, G. & Liu, X. 2022. Spraying characteristics of mining wet shotcrete. Construction and Building Materials, **316**, 125888, doi: https://doi.org/10.1016/j.conbuildmat.2021.125888.

Chen, M., Guo, X., Zheng, Y., Li, L., Yan, Z., Zhao, P., Lu, L. & Cheng, X. 2018. Effect of Tartaric Acid on the Printable, Rheological and Mechanical Properties of 3D Printing Sulphoaluminate Cement Paste. Materials, **11**, doi: https://doi.org/10.3390/ma11122417.

Chen, P., Zhang, L., Wang, J., Lou, X., Huang, L. & Xu, Y. 2021. Exploring vitamin-C as a retarder for calcium sulfoaluminate cement. Construction and Building Materials, **312**, 125334, doi: https://doi.org/10.1016/j.conbuildmat.2021.125334.

Chen, T. & Guestrin, C. 2016. XGBoost: A Scalable Tree Boosting System. *Proceedings of the 22nd ACM SIGKDD International Conference on Knowledge Discovery and Data Mining*. Association for Computing Machinery, San Francisco, California, USA, 785–794.

Chou, J.-S. & Pham, A.-D. 2013. Enhanced artificial intelligence for ensemble approach to predicting high performance concrete compressive strength. Construction and Building Materials, **49**, 554-563, doi: https://doi.org/10.1016/j.conbuildmat.2013.08.078.

Choudhary, D., Keshari, J. & Khan, I.A. 2021. Prediction of Compressive Strength of Ultra-High-Performance Concrete Using Machine Learning Algorithms—SFS and ANN. *In*: Gao, X.-Z.,

Tiwari, S., Trivedi, M.C. & Mishra, K.K. (eds.) *Advances in Computational Intelligence and Communication Technology*. Springer Singapore, Singapore, 17-27.

Cihangir, F. & Akyol, Y. 2018. Mechanical, hydrological and microstructural assessment of the durability of cemented paste backfill containing alkali-activated slag. International Journal of Mining, Reclamation and Environment, **32**, 123-143, doi: 10.1080/17480930.2016.1242183.

Cihangir, F. & Akyol, Y. 2020. Effect of Desliming of Tailings on the Fresh and Hardened Properties of Paste Backfill Made from Alkali-Activated Slag. Advances in Materials Science and Engineering, **2020**, 4536257, doi: 10.1155/2020/4536257.

Cihangir, F., Ercikdi, B., Kesimal, A., Deveci, H. & Erdemir, F. 2015. Paste backfill of high-sulphide mill tailings using alkali-activated blast furnace slag: Effect of activator nature, concentration and slag properties. Minerals Engineering, **83**, 117-127, doi: https://doi.org/10.1016/j.mineng.2015.08.022.

Cihangir, F., Ercikdi, B., Kesimal, A., Ocak, S. & Akyol, Y. 2018. Effect of sodium-silicate activated slag at different silicate modulus on the strength and microstructural properties of full and coarse sulphidic tailings paste backfill. Construction and Building Materials, **185**, 555-566, doi: https://doi.org/10.1016/j.conbuildmat.2018.07.105.

Cihangir, F., Ercikdi, B., Kesimal, A., Turan, A. & Deveci, H. 2012. Utilisation of alkali-activated blast furnace slag in paste backfill of high-sulphide mill tailings: Effect of binder type and dosage. Minerals Engineering, **30**, 33-43, doi: https://doi.org/10.1016/j.mineng.2012.01.009.

Coppola, L., Bellezze, T., Belli, A., Bignozzi, M.C., Bolzoni, F., Brenna, A., Cabrini, M., Candamano, S., Cappai, M., Caputo, D., Carsana, M., Casnedi, L., Cioffi, R., Cocco, O., Coffetti, D., Colangelo, F., Coppola, B., Corinaldesi, V., Crea, F., Crotti, E., Daniele, V., De Gisi, S., Delogu, F., Diamanti, M.V., Di Maio, L., Di Mundo, R., Di Palma, L., Donnini, J., Farina, I., Ferone, C., Frontera, P., Gastaldi, M., Giosuè, C., Incarnato, L., Liguori, B., Lollini, F., Lorenzi, S., Manzi, S., Marino, O., Marroccoli, M., Mascolo, M.C., Mavilia, L., Mazzoli, A., Medici, F., Meloni, P., Merlonetti, G., Mobili, A., Notarnicola, M., Ormellese, M., Pastore, T., Pedeferri, M.P., Petrella, A., Pia, G., Redaelli, E., Roviello, G., Scarfato, P., Scoccia, G., Taglieri, G., Telesca, A., Tittarelli, F., Todaro, F., Vilardi, G. & Yang, F. 2018. Binders alternative to Portland cement and waste management for sustainable construction—part 1. Journal of Applied Biomaterials & Functional Materials, **16**, 186-202, doi: 10.1177/2280800018782845.

Dahish, H.A., Alfawzan, M.S., Tayeh, B.A., Abusogi, M.A. & Bakri, M. 2023. Effect of inclusion of natural pozzolan and silica fume in cement - based mortars on the compressive strength utilizing artificial neural networks and support vector machine. Case Studies in Construction Materials, **18**, e02153, doi: https://doi.org/10.1016/j.cscm.2023.e02153.

Dong, W., Huang, Y., Cui, A. & Ma, G. 2023. Mix design optimization for fly ash-based geopolymer with mechanical, environmental, and economic objectives using soft computing technology. Journal of Building Engineering, **72**, 106577, doi: https://doi.org/10.1016/j.jobe.2023.106577.

Đurđevac Ignjatović, L., Krstić, V., Radonjanin, V., Jovanović, V., Malešev, M., Ignjatović, D. & Đurđevac, V. 2022. Application of Cement Paste in Mining Works, Environmental Protection, and the Sustainable Development Goals in the Mining Industry. *Sustainability*.

Duxson, P., Provis, J.L., Lukey, G.C., Mallicoat, S.W., Kriven, W.M. & van Deventer, J.S.J. 2005. Understanding the relationship between geopolymer composition, microstructure and mechanical properties. Colloids and Surfaces A: Physicochemical and Engineering Aspects, **269**, 47-58, doi: https://doi.org/10.1016/j.colsurfa.2005.06.060.

Edgar, T.W. & Manz, D.O. 2017. Chapter 6 - Machine Learning. *In*: Edgar, T.W. & Manz, D.O. (eds.) *Research Methods for Cyber Security*. Syngress, 153-173.

Ekanayake, I.U., Meddage, D.P.P. & Rathnayake, U. 2022. A novel approach to explain the black-box nature of machine learning in compressive strength predictions of concrete using Shapley additive explanations (SHAP). Case Studies in Construction Materials, **16**, e01059, doi: https://doi.org/10.1016/j.cscm.2022.e01059.

El Naqa, I. & Murphy, M.J. 2015. What Is Machine Learning? *In*: El Naqa, I., Li, R. & Murphy, M.J. (eds.) *Machine Learning in Radiation Oncology: Theory and Applications*. Springer International Publishing, Cham, 3-11.

Ercikdi, B., Baki, H. & İzki, M. 2013. Effect of desliming of sulphide-rich mill tailings on the long-term strength of cemented paste backfill. Journal of Environmental Management, **115**, 5-13, doi: https://doi.org/10.1016/j.jenvman.2012.11.014.

Ercikdi, B., Cihangir, F., Kesimal, A., Deveci, H. & Alp, İ. 2009. Utilization of industrial waste products as pozzolanic material in cemented paste backfill of high sulphide mill tailings. Journal of Hazardous Materials, **168**, 848-856, doi: https://doi.org/10.1016/j.jhazmat.2009.02.100.

Erdal, H.I. 2013. Two-level and hybrid ensembles of decision trees for high performance concrete compressive strength prediction. Engineering Applications of Artificial Intelligence, **26**, 1689-1697, doi: https://doi.org/10.1016/j.engappai.2013.03.014.

Eyo, E.U. & Abbey, S.J. 2021. Machine learning regression and classification algorithms utilised for strength prediction of OPC/by-product materials improved soils. Construction and Building Materials, **284**, 122817, doi: https://doi.org/10.1016/j.conbuildmat.2021.122817.

Fan, C., Zhang, N., Jiang, B. & Liu, W.V. 2022. Preprocessing Large Datasets Using Gaussian Mixture Modelling to Improve Prediction Accuracy of Truck Productivity at Mine Sites. Archives of Mining Sciences, **vol. 67**, 661-680, doi: https://doi.org/10.24425/ams.2022.143680.

Fan, C., Zhang, N., Jiang, B. & Liu, W.V. 2023a. Prediction of truck productivity at mine sites using tree-based ensemble models combined with Gaussian mixture modelling. International Journal of Mining, Reclamation and Environment, **37**, 66-86, doi: https://doi.org/10.1080/17480930.2022.2142425.

Fan, C., Zhang, N., Jiang, B. & Liu, W.V. 2023b. Using deep neural networks coupled with principal component analysis for ore production forecasting at open-pit mine sites. Journal of Rock Mechanics and Geotechnical Engineering.

Fan, C., Zhang, N., Jiang, B. & Liu, W.V. 2023c. Weighted ensembles of artificial neural networks based on Gaussian mixture modeling for truck productivity prediction at open-pit mines. Mining, Metallurgy & Exploration, **40**, 583-598, doi: https://doi.org/10.1007/s42461-023-00747-9.

Feng, D.-C., Wang, W.-J., Mangalathu, S. & Taciroglu, E. 2021. Interpretable XGBoost-SHAP Machine-Learning Model for Shear Strength Prediction of Squat RC Walls. Journal of Structural Engineering, **147**, 04021173, doi: https://doi.org/10.1061/(ASCE)ST.1943-541X.0003115.
Friedman, J.H. 2001. Greedy function approximation: A gradient boosting machine. The Annals of Statistics, **29**, 1189-1232, 1144.

García Maté, M., Londono-Zuluaga, D., De la Torre, A., Losilla, E.R., Cabeza, A., Aranda, M. & Santacruz, I. 2016. Tailored setting times with high compressive strengths in bassanite calcium sulfoaluminate eco-cements. Cement and Concrete Composites, **72**, doi: https://doi.org/10.1016/j.cemconcomp.2016.05.021.

Hastie, T., Tibshirani, R. & Friedman, J. 2009. Ensemble Learning. *In*: Hastie, T., Tibshirani, R. & Friedman, J. (eds.) *The Elements of Statistical Learning: Data Mining, Inference, and Prediction*. Springer New York, New York, NY, 605-624.

Head, T., MechCoder, G.L. & Shcherbatyi, I. 2018. scikit-optimize/scikit-optimize: v0. 5.2. Version v0, **5**.

Hewitt, D., Allard, S. & Radziszewski, P. 2009. Pipe lining abrasion testing for paste backfill operations. Minerals Engineering, **22**, 1088-1090, doi: https://doi.org/10.1016/j.mineng.2009.03.010.

Hu, Y., Li, K., Zhang, B. & Han, B. 2022. Strength investigation of the cemented paste backfill in alpine regions using lab experiments and machine learning. Construction and Building Materials, **323**, 126583, doi: https://doi.org/10.1016/j.conbuildmat.2022.126583.

Hu, Y., Li, W., Ma, S. & Shen, X. 2017. Influence of borax and citric acid on the hydration of calcium sulfoaluminate cement. Chemical Papers, **71**, 1909-1919, doi: https://doi.org/10.1007/s11696-017-0185-9.

Huang, G., Gupta, R. & Liu, W.V. 2022a. Effects of sodium gluconate on hydration reaction, setting, workability, and strength development of calcium sulfoaluminate belite cement mixtures. Journal of Sustainable Cement-Based Materials, **11**, 273-285, doi: https://doi.org/10.1080/21650373.2021.1936269.

Huang, G., Pudasainee, D., Gupta, R. & Liu, W.V. 2020. Utilization and performance evaluation of molasses as a retarder and plasticizer for calcium sulfoaluminate cement-based mortar.

Construction and Building Materials, **243**, 118201, doi: https://doi.org/10.1016/j.conbuildmat.2020.118201.

Huang, G., Pudasainee, D., Gupta, R. & Liu, W.V. 2021. Thermal properties of calcium sulfoaluminate cement-based mortars incorporated with expanded perlite cured at cold temperatures. Construction and Building Materials, **274**, 122082, doi: https://doi.org/10.1016/j.conbuildmat.2020.122082.

Huang, G., Pudasainee, D., Gupta, R. & Victor Liu, W. 2019. Hydration reaction and strength development of calcium sulfoaluminate cement-based mortar cured at cold temperatures. Construction and Building Materials, **224**, 493-503, doi: https://doi.org/10.1016/j.conbuildmat.2019.07.085.

Huang, G., Zhao, J., Gupta, R. & Liu, W.V. 2022b. Influence of tartaric acid dosage on the early-age and long-term properties of calcium sulfoaluminate belite cement composites. Construction and Building Materials, **356**, 129257, doi: https://doi.org/10.1016/j.conbuildmat.2022.129257.

Huo, W., Zhu, Z., Sun, H., Ma, B. & Yang, L. 2022. Development of machine learning models for the prediction of the compressive strength of calcium-based geopolymers. Journal of Cleaner Production, **380**, 135159, doi: https://doi.org/10.1016/j.jclepro.2022.135159.

ISO. 2009. Cement-Test Methods-Determination of Strength. ISO: Geneva, Switzerland.
ISO. 2021. Test method of cement mortar strength (ISO method).

Jerome, H.F. 2001. Greedy function approximation: A gradient boosting machine. The Annals of Statistics, **29**, 1189-1232, doi: 10.1214/aos/1013203451.

Jiang, H., Han, J., Li, Y., Yilmaz, E., Sun, Q. & Liu, J. 2020. Relationship between ultrasonic pulse velocity and uniaxial compressive strength for cemented paste backfill with alkali-activated slag. Nondestructive Testing and Evaluation, **35**, 359-377, doi: 10.1080/10589759.2019.1679140.
Jiang, H., Qi, Z., Yilmaz, E., Han, J., Qiu, J. & Dong, C. 2019. Effectiveness of alkali-activated slag as alternative binder on workability and early age compressive strength of cemented paste backfills. Construction and Building Materials, **218**, 689-700, doi: https://doi.org/10.1016/j.conbuildmat.2019.05.162.

Jiang, H., Ren, L., Gu, X., Zheng, J. & Cui, L. 2022a. Synergistic effect of activator nature and curing temperature on time-dependent rheological behavior of cemented paste backfill containing alkali-activated slag. Environmental Science and Pollution Research, doi: 10.1007/s11356-022-23053-1.

Jiang, H., Ren, L., Zhang, Q., Zheng, J. & Cui, L. 2022b. Strength and microstructural evolution of alkali-activated slag-based cemented paste backfill: Coupled effects of activator composition and temperature. Powder Technology, **401**, 117322, doi: https://doi.org/10.1016/j.powtec.2022.117322.

Jing, H., Xu, M., Gao, M., Li, M. & Dai, S. 2022. Effect of Compounding Retarder and PCE on the Early Properties and Hydration of High-Belite Sulphoaluminate Cement. Applied Sciences, **12**, doi: https://doi.org/10.3390/app122110731.

Juszczak, P., Tax, D.M.J. & Duin, R.P.W. 2002. Feature scaling in support vector data description. Kazemi, R. 2023. Artificial intelligence techniques in advanced concrete technology: A comprehensive survey on 10 years research trend. Engineering Reports, **n/a**, e12676, doi: https://doi.org/10.1002/eng2.12676.

Ke, G., Meng, Q., Finley, T., Wang, T., Chen, W., Ma, W., Ye, Q. & Liu, T.-Y. 2017. LightGBM: A Highly Efficient Gradient Boosting Decision Tree. *NIPS*.

Ke, G. & Zhang, J. 2020. Effects of Retarding Admixture, Superplasticizer and Supplementary Cementitious Material on the Rheology and Mechanical Properties of High Strength Calcium Sulfoaluminate Cement Paste. Journal of Advanced Concrete Technology, **18**, 17-26, doi: https://doi.org/10.3151/jact.18.17.

Ke, G., Zhang, J., Liu, Y. & Xie, S. 2021. Pore characteristics of calcium sulfoaluminate cement paste with impact of supplementary cementitious materials and water to binder ratio. Powder Technology, **387**, 146-155, doi: https://doi.org/10.1016/j.powtec.2021.04.027.

Keaton, J.R. 2018. Coefficient of Uniformity. *In*: Bobrowsky, P.T. & Marker, B. (eds.) *Encyclopedia of Engineering Geology*. Springer International Publishing, Cham, 158-159.

Kesimal, A., Yilmaz, E., Ercikdi, B., Alp, I. & Deveci, H. 2005. Effect of properties of tailings and binder on the short-and long-term strength and stability of cemented paste backfill. Materials Letters, **59**, 3703-3709, doi: https://doi.org/10.1016/j.matlet.2005.06.042.

Khan, K., Ahmad, W., Amin, M.N., Rafiq, M.I., Abu Arab, A.M., Alabdullah, I.A., Alabduljabbar, H. & Mohamed, A. 2023. Evaluating the effectiveness of waste glass powder for the compressive strength improvement of cement mortar using experimental and machine learning methods. Heliyon, **9**, e16288, doi: https://doi.org/10.1016/j.heliyon.2023.e16288.

Kou, Y., Jiang, H., Ren, L., Yilmaz, E. & Li, Y. 2020. Rheological Properties of Cemented Paste Backfill with Alkali-Activated Slag. Minerals, **10**, 288.

Kwak, S., Kim, J., Ding, H., Xu, X., Chen, R., Guo, J. & Fu, H. 2022. Machine learning prediction of the mechanical properties of γ-TiAl alloys produced using random forest regression model. Journal of Materials Research and Technology, **18**, 520-530, doi: https://doi.org/10.1016/j.jmrt.2022.02.108.

Lacoste, A., Larochelle, H., Laviolette, F. & Marchand, M. 2014. Sequential model-based ensemble optimization. arXiv preprint arXiv:1402.0796.

Li, F., Zhang, L., Chen, B., Gao, D., Cheng, Y., Zhang, X., Yang, Y., Gao, K., Huang, Z. & Peng, J. 2018a. A Light Gradient Boosting Machine for Remainning Useful Life Estimation of Aircraft

Engines. *2018 21st International Conference on Intelligent Transportation Systems (ITSC)*, 3562-3567.

Li, G., Zhang, J., Song, Z., Shi, C. & Zhang, A. 2018b. Improvement of workability and early strength of calcium sulphoaluminate cement at various temperature by chemical admixtures. Construction and Building Materials, **160**, 427-439, doi: https://doi.org/10.1016/j.conbuildmat.2017.11.076.

Li, J., Cheng, K., Wang, S., Morstatter, F., Trevino, R.P., Tang, J. & Liu, H. 2017. Feature Selection: A Data Perspective. ACM Comput. Surv., **50**, 94, doi: https://doi.org/10.1145/3136625.
Li, Y., Li, H., jin, C. & Shen, J. 2022. The study of effect of carbon nanotubes on the compressive strength of cement-based materials based on machine learning. Construction and Building Materials, **358**, 129435, doi: https://doi.org/10.1016/j.conbuildmat.2022.129435.

Liang, M., Chang, Z., Wan, Z., Gan, Y., Schlangen, E. & Šavija, B. 2022. Interpretable Ensemble-Machine-Learning models for predicting creep behavior of concrete. Cement and Concrete Composites, **125**, 104295, doi: https://doi.org/10.1016/j.cemconcomp.2021.104295.

Liang, W., Luo, S., Zhao, G. & Wu, H. 2020. Predicting Hard Rock Pillar Stability Using GBDT, XGBoost, and LightGBM Algorithms. Mathematics, **8**, doi: 10.3390/math8050765.
Liu, J., Li, G., Yang, S. & Huang, J. 2020. Prediction Models for Evaluating the Strength of Cemented Paste Backfill: A Comparative Study. Minerals, **10**, 1041.

Liu, X., Tang, H., Ding, Y. & Yan, D. 2022. Investigating the performance of machine learning models combined with different feature selection methods to estimate the energy consumption of buildings. Energy and Buildings, **273**, 112408, doi: https://doi.org/10.1016/j.enbuild.2022.112408.

Lu, X., Zhou, W., Ding, X., Shi, X., Luan, B. & Li, M. 2019. Ensemble Learning Regression for Estimating Unconfined Compressive Strength of Cemented Paste Backfill. IEEE Access, **7**, 72125-72133, doi: 10.1109/ACCESS.2019.2918177.

Lundberg, S.M., Erion, G., Chen, H., DeGrave, A., Prutkin, J.M., Nair, B., Katz, R., Himmelfarb, J., Bansal, N. & Lee, S.-I. 2020. From local explanations to global understanding with explainable AI for trees. Nature Machine Intelligence, **2**, 56-67, doi: 10.1038/s42256-019-0138-9.

Lundberg, S.M. & Lee, S.-I. 2017. A unified approach to interpreting model predictions. *Proceedings of the 31st International Conference on Neural Information Processing Systems*. Curran Associates Inc., Long Beach, California, USA, 4768–4777.

Min, C., Xiong, S., Shi, Y., Liu, Z. & Lu, X. 2023. Early-age compressive strength prediction of cemented phosphogypsum backfill using lab experiments and ensemble learning models. Case Studies in Construction Materials, **18**, e02107, doi: https://doi.org/10.1016/j.cscm.2023.e02107.

Minaz Hossain, M., Nasir Uddin, M. & Abu Sayed Hossain, M. 2023. Prediction of compressive strength ultra-high steel fiber reinforced concrete (UHSFRC) using artificial neural networks (ANNs). Materials Today: Proceedings, doi: https://doi.org/10.1016/j.matpr.2023.02.409.

Mitchell, T.M. 2007. Machine learning. McGraw-hill New York.

Mohamed, O., Kewalramani, M., Ati, M. & Hawat, W.A. 2021. Application of ANN for prediction of chloride penetration resistance and concrete compressive strength. Materialia, **17**, 101123, doi: https://doi.org/10.1016/j.mtla.2021.101123.

Mohan, M.K., Rahul, A.V., De Schutter, G. & Van Tittelboom, K. 2021. Early age hydration, rheology and pumping characteristics of CSA cement-based 3D printable concrete. Construction and Building Materials, **275**, 122136, doi: https://doi.org/10.1016/j.conbuildmat.2020.122136.

Moreira , d.A.M.V. & Silva, F.d.A. 2020. The use of the Barcelona test as quality control of fiber reinforced shotcrete for underground mining. Construction and Building Materials, **262**, 120719, doi: https://doi.org/10.1016/j.conbuildmat.2020.120719.

Morin, V., Termkhajornkit, P., Huet, B. & Pham, G. 2017. Impact of quantity of anhydrite, water to binder ratio, fineness on kinetics and phase assemblage of belite-ye'elimite-ferrite cement. Cement and Concrete Research, **99**, 8-17, doi: https://doi.org/10.1016/j.cemconres.2017.04.014.

Naqi, A. & Jang, J.G. 2019. Recent Progress in Green Cement Technology Utilizing Low-Carbon Emission Fuels and Raw Materials: A Review. *Sustainability*.

Nazari, A. & Sanjayan, J.G. 2015. Modelling of compressive strength of geopolymer paste, mortar and concrete by optimized support vector machine. Ceramics International, **41**, 12164-12177, doi: https://doi.org/10.1016/j.ceramint.2015.06.037.

Nguyen, H., Kinnunen, P., Gijbels, K., Carvelli, V., Sreenivasan, H., Kantola, A.M., Telkki, V.-V., Schroeyers, W. & Illikainen, M. 2019. Ettringite-based binder from ladle slag and gypsum – The effect of citric acid on fresh and hardened state properties. Cement and Concrete Research, **123**, 105800, doi: https://doi.org/10.1016/j.cemconres.2019.105800.

Nguyen, N.-H., Tong, K.T., Lee, S., Karamanli, A. & Vo, T.P. 2022. Prediction compressive strength of cement-based mortar containing metakaolin using explainable Categorical Gradient Boosting model. Engineering Structures, **269**, 114768, doi: https://doi.org/10.1016/j.engstruct.2022.114768.

Noorani, I. & Mehrdoust, F. 2022. Parameter estimation of uncertain differential equation by implementing an optimized artificial neural network. Chaos, Solitons & Fractals, **165**, 112769, doi: https://doi.org/10.1016/j.chaos.2022.112769.

Otchere, D.A., Ganat, T.O.A., Ojero, J.O., Tackie-Otoo, B.N. & Taki, M.Y. 2022. Application of gradient boosting regression model for the evaluation of feature selection techniques in improving

reservoir characterisation predictions. Journal of Petroleum Science and Engineering, **208**, 109244, doi: https://doi.org/10.1016/j.petrol.2021.109244.

Pacheco-Torgal, F. 2015. 1 - Introduction to Handbook of Alkali-activated Cements, Mortars and Concretes. *In*: Pacheco-Torgal, F., Labrincha, J.A., Leonelli, C., Palomo, A. & Chindaprasirt, P. (eds.) *Handbook of Alkali-Activated Cements, Mortars and Concretes*. Woodhead Publishing, Oxford, 1-16.

Pacheco-Torgal, F., Castro-Gomes, J. & Jalali, S. 2008. Alkali-activated binders: A review: Part 1. Historical background, terminology, reaction mechanisms and hydration products. Construction and Building Materials, **22**, 1305-1314, doi: https://doi.org/10.1016/j.conbuildmat.2007.10.015.

Papadakis, V.G., Antiohos, S. & Tsimas, S. 2002. Supplementary cementing materials in concrete: Part II: A fundamental estimation of the efficiency factor. Cement and Concrete Research, **32**, 1533-1538, doi: https://doi.org/10.1016/S0008-8846(02)00829-3.

Pimraksa, K. & Chindaprasirt, P. 2018. 14 - Sulfoaluminate cement-based concrete. *In*: Pacheco-Torgal, F., Melchers, R.E., Shi, X., Belie, N.D., Tittelboom, K.V. & Sáez, A. (eds.) *Eco-Efficient Repair and Rehabilitation of Concrete Infrastructures*. Woodhead Publishing, 355-385.

Pisner, D.A. & Schnyer, D.M. 2020. Chapter 6 - Support vector machine. *In*: Mechelli, A. & Vieira, S. (eds.) *Machine Learning*. Academic Press, 101-121.

Qi, C., Chen, Q., Dong, X., Zhang, Q. & Yaseen, Z.M. 2020a. Pressure drops of fresh cemented paste backfills through coupled test loop experiments and machine learning techniques. Powder Technology, **361**, 748-758, doi: https://doi.org/10.1016/j.powtec.2019.11.046.

Qi, C., Chen, Q., Fourie, A., Tang, X., Zhang, Q., Dong, X. & Feng, Y. 2019a. Constitutive modelling of cemented paste backfill: A data-mining approach. Construction and Building Materials, **197**, 262-270, doi: https://doi.org/10.1016/j.conbuildmat.2018.11.142.

Qi, C., Chen, Q., Fourie, A. & Zhang, Q. 2018a. An intelligent modelling framework for mechanical properties of cemented paste backfill. Minerals Engineering, **123**, 16-27, doi: https://doi.org/10.1016/j.mineng.2018.04.010.

Qi, C., Chen, Q. & Sonny Kim, S. 2020b. Integrated and intelligent design framework for cemented paste backfill: A combination of robust machine learning modelling and multi-objective optimization. Minerals Engineering, **155**, 106422, doi: https://doi.org/10.1016/j.mineng.2020.106422.

Qi, C. & Fourie, A. 2019. Cemented paste backfill for mineral tailings management: Review and future perspectives. Minerals Engineering, **144**, 106025, doi: https://doi.org/10.1016/j.mineng.2019.106025.

Qi, C., Fourie, A. & Chen, Q. 2018b. Neural network and particle swarm optimization for predicting the unconfined compressive strength of cemented paste backfill. Construction and Building Materials, **159**, 473-478, doi: https://doi.org/10.1016/j.conbuildmat.2017.11.006.

Qi, C., Fourie, A., Chen, Q. & Zhang, Q. 2018c. A strength prediction model using artificial intelligence for recycling waste tailings as cemented paste backfill. Journal of Cleaner Production, **183**, 566-578, doi: https://doi.org/10.1016/j.jclepro.2018.02.154.

Qi, C., Ly, H.-B., Minh Le, L., Yang, X., Guo, L. & Thai Pham, B. 2021. Improved strength prediction of cemented paste backfill using a novel model based on adaptive neuro fuzzy inference system and artificial bee colony. Construction and Building Materials, **284**, 122857, doi: https://doi.org/10.1016/j.conbuildmat.2021.122857.

Qi, C., Tang, X., Dong, X., Chen, Q., Fourie, A. & Liu, E. 2019b. Towards Intelligent Mining for Backfill: A genetic programming-based method for strength forecasting of cemented paste backfill. Minerals Engineering, **133**, 69-79, doi: https://doi.org/10.1016/j.mineng.2019.01.004.

Qiu, J., Guo, Z., Li, L., Zhang, S., Zhao, Y. & Ma, Z. 2020. A Hybrid Artificial Intelligence Model for Predicting the Strength of Foam-Cemented Paste Backfill. IEEE Access, **8**, 84569-84583, doi: 10.1109/ACCESS.2020.2992595.

Rahman, J., Ahmed, K.S., Khan, N.I., Islam, K. & Mangalathu, S. 2021. Data-driven shear strength prediction of steel fiber reinforced concrete beams using machine learning approach. Engineering Structures, **233**, 111743, doi: https://doi.org/10.1016/j.engstruct.2020.111743.

Rashad, A.M. 2013. A comprehensive overview about the influence of different additives on the properties of alkali-activated slag – A guide for Civil Engineer. Construction and Building Materials, **47**, 29-55, doi: https://doi.org/10.1016/j.conbuildmat.2013.04.011.

Rashid, M., Kamruzzaman, J., Imam, T., Wibowo, S. & Gordon, S. 2022. A tree-based stacking ensemble technique with feature selection for network intrusion detection. Applied Intelligence, **52**, 9768-9781, doi: https://doi.org/10.1007/s10489-021-02968-1.

Rungchet, A., Chindaprasirt, P., Wansom, S. & Pimraksa, K. 2016. Hydrothermal synthesis of calcium sulfoaluminate–belite cement from industrial waste materials. Journal of Cleaner Production, **115**, 273-283, doi: https://doi.org/10.1016/j.jclepro.2015.12.068.

Russell, S.J. 2010. Artificial intelligence a modern approach. Pearson Education, Inc.

Sadrossadat, E., Basarir, H., Luo, G., Karrech, A., Durham, R., Fourie, A. & Elchalakani, M. 2020. Multi-objective mixture design of cemented paste backfill using particle swarm optimisation algorithm. Minerals Engineering, **153**, 106385, doi: https://doi.org/10.1016/j.mineng.2020.106385.

Sajda, P. 2002. Neural Networks. *In*: Ramachandran, V.S. (ed.) *Encyclopedia of the Human Brain*. Academic Press, New York, 373-383.

Shah, S.F.A., Chen, B., Zahid, M. & Ahmad, M.R. 2022. Compressive strength prediction of one-part alkali activated material enabled by interpretable machine learning. Construction and Building Materials, **360**, 129534, doi: https://doi.org/10.1016/j.conbuildmat.2022.129534.

Shen, J., Li, Y., Lin, H., Li, H., Lv, J., Feng, S. & Ci, J. 2022. Prediction of compressive strength of alkali-activated construction demolition waste geopolymers using ensemble machine learning. Construction and Building Materials, **360**, 129600, doi: https://doi.org/10.1016/j.conbuildmat.2022.129600.

Shen, Y., Zhang, W., Zhu, H., Li, J. & Shi, S. 2023. Effect of borax on calcium sulfoaluminate cement properties. Ceramics-Silikáty **67**, 10-19, doi: https://doi.org/10.13168/cs.2022.0055.

Shenbagam, V.K. & Chaunsali, P. 2022. Influence of calcium hydroxide and calcium sulfate on early-age properties of non-expansive calcium sulfoaluminate belite cement. Cement and Concrete Composites, **128**, 104444, doi: https://doi.org/10.1016/j.cemconcomp.2022.104444.

Shi, C. & Fernández-Jiménez, A. 2006. Stabilization/solidification of hazardous and radioactive wastes with alkali-activated cements. Journal of Hazardous Materials, **137**, 1656-1663, doi: https://doi.org/10.1016/j.jhazmat.2006.05.008.

Shi, C., Jiménez, A.F. & Palomo, A. 2011. New cements for the 21st century: The pursuit of an alternative to Portland cement. Cement and Concrete Research, **41**, 750-763, doi: https://doi.org/10.1016/j.cemconres.2011.03.016.

Skocek, J., Maciej, Z., Bullerjahn, F. & Ben Haha, M. 2015. Effect of retarders on the early performance of CSA-type cement.

Sun, Q., Li, T. & Liang, B. 2020a. Preparation of a New Type of Cemented Paste Backfill with an Alkali-Activated Silica Fume and Slag Composite Binder. Materials (Basel, Switzerland), **13**, 372, doi: 10.3390/ma13020372.

Sun, Y., Li, G., Zhang, J., Sun, J. & Xu, J. 2020b. Development of an Ensemble Intelligent Model for Assessing the Strength of Cemented Paste Backfill. Advances in Civil Engineering, **2020**, 1643529, doi: 10.1155/2020/1643529.

Tambara Júnior, L.U.D., dos Santos Lima, G.T., Silvestro, L., Ruviaro, A.S., Gleize, P.J.P. & de Azevedo, A.R.G. 2023. Influence of polycarboxylate superplasticizer and calcium sulfoaluminate cement on the rheology, hydration kinetics, and porosity of Portland cement pastes. Journal of Building Engineering, **68**, 106120, doi: https://doi.org/10.1016/j.jobe.2023.106120.

Tao, Y., Rahul, A.V., Mohan, M.K., De Schutter, G. & Van Tittelboom, K. 2023. Recent progress and technical challenges in using calcium sulfoaluminate (CSA) cement. Cement and Concrete Composites, **137**, 104908, doi: https://doi.org/10.1016/j.cemconcomp.2022.104908.

Tariq, A. & Yanful, E.K. 2013. A review of binders used in cemented paste tailings for underground and surface disposal practices. Journal of Environmental Management, **131**, 138-149, doi: https://doi.org/10.1016/j.jenvman.2013.09.039.

Tian, X., Xu, W., Song, S., Rao, F. & Xia, L. 2020. Effects of curing temperature on the compressive strength and microstructure of copper tailing-based geopolymers. Chemosphere, **253**, 126754, doi: https://doi.org/10.1016/j.chemosphere.2020.126754.

Tibshirani, R. 2011. Regression shrinkage and selection via the lasso: a retrospective. Journal of the Royal Statistical Society: Series B (Statistical Methodology), **73**, 273-282, doi: https://doi.org/10.1111/j.1467-9868.2011.00771.x.

Tinoco, J., Gomes Correia, A. & Cortez, P. 2014. Support vector machines applied to uniaxial compressive strength prediction of jet grouting columns. Computers and Geotechnics, **55**, 132-140, doi: https://doi.org/10.1016/j.compgeo.2013.08.010.

Tran, V.Q., Dang, V.Q. & Ho, L.S. 2022. Evaluating compressive strength of concrete made with recycled concrete aggregates using machine learning approach. Construction and Building Materials, **323**, 126578, doi: https://doi.org/10.1016/j.conbuildmat.2022.126578.

Walker, R. & Pavía, S. 2011. Physical properties and reactivity of pozzolans, and their influence on the properties of lime–pozzolan pastes. Materials and Structures, **44**, 1139-1150, doi: 10.1617/s11527-010-9689-2.

Wang, P., Li, N. & Xu, L. 2017. Hydration evolution and compressive strength of calcium sulphoaluminate cement constantly cured over the temperature range of 0 to 80°C. Cement and Concrete Research, **100**, 203-213, doi: https://doi.org/10.1016/j.cemconres.2017.05.025.

Weil, M., Dombrowski, K. & Buchwald, A. 2009. 10 - Life-cycle analysis of geopolymers. *In*: Provis, J.L. & van Deventer, J.S.J. (eds.) *Geopolymers*. Woodhead Publishing, 194-210.
Woolf, B.P. 2009. Chapter 7 - Machine Learning. *In*: Woolf, B.P. (ed.) *Building Intelligent Interactive Tutors*. Morgan Kaufmann, San Francisco, 221-297.

Wu, L., Hu, C. & Liu, W.V. 2020. Forecasting the deterioration of cement-based mixtures under sulfuric acid attack using support vector regression based on Bayesian optimization. SN Applied Sciences, **2**, 1970, doi: 10.1007/s42452-020-03778-9.

Xi, B., Huang, Z., Al-Obaidi, S. & Ferrara, L. 2023. Predicting ultra high-performance concrete self-healing performance using hybrid models based on metaheuristic optimization techniques. Construction and Building Materials, **381**, 131261, doi: https://doi.org/10.1016/j.conbuildmat.2023.131261.

Xu, H. & Van Deventer, J.S.J. 2000. The geopolymerisation of alumino-silicate minerals. International Journal of Mineral Processing, **59**, 247-266, doi: https://doi.org/10.1016/S0301-7516(99)00074-5.

Xu, L., Liu, S., Li, N., Peng, Y., Wu, K. & Wang, P. 2018. Retardation effect of elevated temperature on the setting of calcium sulfoaluminate cement clinker. Construction and Building Materials, **178**, 112-119, doi: https://doi.org/10.1016/j.conbuildmat.2018.05.061.

Yu, H., Wu, L., Liu, W. & Pourrahimian, Y. 2018. Effects of fibers on expansive shotcrete mixtures consisting of calcium sulfoaluminate cement, ordinary Portland cement, and calcium sulfate. Journal of Rock Mechanics and Geotechnical Engineering, **10**, doi: https://doi.org/10.1016/j.jrmge.2017.12.001.

Yu, Z., Shi, X.-z., Chen, X., Zhou, J., Qi, C.-c., Chen, Q.-s. & Rao, D.-j. 2021. Artificial intelligence model for studying unconfined compressive performance of fiber-reinforced cemented paste backfill. Transactions of Nonferrous Metals Society of China, **31**, 1087-1102, doi: https://doi.org/10.1016/S1003-6326(21)65563-2.

Zajac, M., Skocek, J., Stabler, C., Bullerjahn, F. & Haha, M.B. 2019. Hydration and performance evolution of belite–ye'elimite–ferrite cement. Advances in Cement Research, **31**, 124-137, doi: https://doi.org/10.1680/jadcr.18.00110.

Zhang, G., Li, G. & Li, Y. 2016. Effects of superplasticizers and retarders on the fluidity and strength of sulphoaluminate cement. Construction and Building Materials, **126**, 44-54, doi: https://doi.org/10.1016/j.conbuildmat.2016.09.019.

Zhang, J., Niu, W., Yang, Y., Hou, D. & Dong, B. 2022a. Machine learning prediction models for compressive strength of calcined sludge-cement composites. Construction and Building Materials, **346**, 128442, doi: https://doi.org/10.1016/j.conbuildmat.2022.128442.

Zhang, M., Zhang, C., Zhang, J., Wang, L. & Wang, F. 2023. Effect of composition and curing on alkali activated fly ash-slag binders: Machine learning prediction with a random forest-genetic algorithm hybrid model. Construction and Building Materials, **366**, 129940, doi: https://doi.org/10.1016/j.conbuildmat.2022.129940.

Zhang, S., Ren, F., Zhao, Y., Qiu, J. & Guo, Z. 2021. The effect of stone waste on the properties of cemented paste backfill using alkali-activated slag as binder. Construction and Building Materials, **283**, 122686, doi: https://doi.org/10.1016/j.conbuildmat.2021.122686.

Zhang, W., Wu, C., Tang, L., Gu, X. & Wang, L. 2022b. Efficient time-variant reliability analysis of Bazimen landslide in the Three Gorges Reservoir Area using XGBoost and LightGBM algorithms. Gondwana Research, doi: https://doi.org/10.1016/j.gr.2022.10.004.

Zhao, W., Feng, S., Liu, J. & Sun, B. 2023. An explainable intelligent algorithm for the multiple performance prediction of cement-based grouting materials. Construction and Building Materials, **366**, 130146, doi: https://doi.org/10.1016/j.conbuildmat.2022.130146.

Zorlu, K., Gokceoglu, C., Ocakoglu, F., Nefeslioglu, H.A. & Acikalin, S. 2008. Prediction of uniaxial compressive strength of sandstones using petrography-based models. Engineering Geology, **96**, 141-158, doi: https://doi.org/10.1016/j.enggeo.2007.10.009.

Zou, D., Zhang, Z. & Wang, D. 2020. Influence of citric acid and sodium gluconate on hydration of calcium sulfoaluminate cement at various temperatures. Construction and Building Materials, **263**, 120247, doi: https://doi.org/10.1016/j.conbuildmat.2020.120247.